ABSTRACT

RADIATION OF SPHERICAL AND CYLINDRICAL ANTENNAS IN INCOMPRESSIBLE AND COMPRESSIBLE PLASMAS

By

Cheng-Chi Lin

The interaction of an antenna with a plasma becomes one of the most interesting and important topics in science and engineering, since the communication between a space vehicle and a ground station has become involved with the ionosphere or an ionized gas. The performance of an antenna in an ionized gas or plasma is entirely different from its performance in free space. The purposes of this study are to investigate theoretically and experimentally the radiation of a spherical antenna and a cylindrical antenna when immersed in a plasma and to detect the existence of an electroacoustic or a longitudinal plasma wave excited by the antenna.

In the theoretical analysis, spherical and cylindrical dipole antennas are used as the radiating sources. The surrounding plasma is assumed to be a weakly ionized gas type and is treated either as a lossy, cold (incompressible) plasma or as a lossy, hot (compressible) plasma. Two rather different physical models and two different sets of basic equations are adapted for these two kinds of plasmas. When the antennas is immersed in a lossy, cold plasma, the plasma

is characterized as a lossy medium with equivalent permittivity and conductivity. For this case, Maxwell's equations are adequate to treat the problem. When the antenna is placed in a lossy, hot plasma, the plasma is regarded as a one-component electron fluid with the motion of positive ions neglected. The basic equations for this case are Maxwell's equations and the linearized moment equations which are derived from the Boltzmann equation assuming that the perturbation of the plasma due to the source being small.

The spherical antenna imbedded in a lossy, cold plasma of finite extent is studied first and then extended to the case of lossy, hot plasma of finite extent. These two problems are solved directly from the basic equations mentioned above and the radiated field in the far-zone of antenna is obtained explicitly as a function of the antenna dimensions and the plasma parameters.

The cylindrical dipole antenna immersed in a lossy, cold plasma of infinite extent is examined next. King-Middleton's theory and King's modified method are employed to determine the approximate current distribution on the antenna and after that the input impedance of the antenna is determined as a function of the antenna dimensions and the plasma parameters. This problem is not extended to the hot-plasma case because of its complexity in the mathematical development. Finally, an existing theory of a cylindrical dipole antenna immersed in a lossless, hot plasma is briefly reviewed. Extensive numerical results were obtained and compared with the experimental results.

In order to conduct an extensive and accurate experimental study on the interaction of an antenna with a hot plasma, a great deal of time and effort was exerted to produce a large volume of stable, high-density plasma. In our experiment, the hot plasma was provided by a mercury arc discharge which was created in three different plasma tubes. A novel method of placing a spot fixer in the mercury pool was used to stabilize the plasma. The spherical and cylindrical antennas were used as the radiating sources and they were fed through a large ground plane. The radiation fields from both antennas and the input impedance of the cylindrical antenna are measured as a function of the plasma parameters. The hetrodyne receiving system was used for the antenna radiation measurement while the standard SWR method was adopted for the antenna impedance measurement.

It is shown both theoretically and experimentally that the radiation from a plasma-coated spherical antenna can be enhanced if the antenna is operated at a frequency much lower than the plasma frequency and the dimensions of the antenna and the plasma layer are appropriately chosen. This phenomenon may prove useful for overcoming the blackout problem suffered by a reentry vehicle, or may offer a novel method of low-loss tuning of a small antenna.

The experimental results on the input impedance and the radiation pattern of the cylindrical antenna tend to indicate that in addition to the usual electromagnetic wave an electroacoustic or a longitudinal plasma wave can be excited by the antenna in the hot plasma.

RADIATION OF SPHERICAL AND CYLINDRICAL ANTENNAS IN INCOMPRESSIBLE AND COMPRESSIBLE PLASMAS

By

Cheng-Chi Lin

A THESIS

Submitted to
Michigan State University
in partial fulfillment of the requirements
for the degree of

DOCTOR OF PHILOSOPHY

Department of Electrical Engineering and Systems Science

1969

G61174
3-18-70

To my parents

Mr. & Mrs. Chia-Chung Lin

ACKNOWLEDGMENTS

The author is sincerely grateful to his major professor Dr. K. M. Chen for his guidance and encouragement in the course of this research.

He also wishes to thank the members of his guidance committee, Dr. G. Kemeny, Dr. B. Ho, Dr. J. Asmussen Jr. and Dr. C. Y. Lo, for reading the dissertation and valuable suggestions. The help extended by Mr. J. W. Hoffman of the Division of Engineering Research is also appreciated.

Finally, the author wishes to express a special thank to his wife, Lee-Ching, for her encouragement, understanding and patience.

The research reported in this dissertation was supported by the National Science Foundation under Grant GK-1026.

TABLE OF CONTENTS

		Page
	ACKNOWLEDGMENTS.	iii
	LIST OF FIGURES.	vii
1.	INTRODUCTION	1
2.	RADIATION FROM A SPHERICAL ANTENNA IMBEDDED IN A LOSSY, COLD PLASMA OF FINITE EXTENT . . .	6
	2.1 Introduction	6
	2.2 Geometry and Statement of the Problem	8
	2.3 Solutions to Maxwell's Equations in the Plasma Region.	10
	2.4 Solutions to Maxwell's Equations in the Free-Space Region.	17
	2.5 Boundary Conditions for Calculating the Radiation Fields	18
	2.6 Numerical Results.	21
3.	RADIATION FROM A SPHERICAL ANTENNA IMBEDDED IN A LOSSY, HOT PLASMA OF FINITE EXTENT	33
	3.1 Introduction	33
	3.2 Geometry and Statement of the Problem	34
	3.3 Fields in Dielectric Region (Plasma-Sheath Region)	36
	3.4 Fields in Hot-Plasma Region	37
	3.5 Fields in Free-Space Region	47
	3.6 Matching of Boundary Conditions at Interfaces . . .	48
	3.7 Radiated Field in Free-Space Region.	54
	3.8 Numerical Results.	56

Page

4. EXPERIMENTAL INVESTIGATION ON THE RADIATION FROM A SPHERICAL ANTENNA IN A HOT PLASMA . . . 77

4.1 Introduction 77
4.2 Experimental Setup 78
4.3 Experimental Results and Comparison with Theories 81
4.4 Discussion 82

5. RADIATION OF A CYLINDRICAL ANTENNA IMMERSED IN A LOSSY, COLD PLASMA OF INFINITE EXTENT . . . 88

5.1 Introduction 88
5.2 Geometry and Statement of the Problem 90
5.3 Basic Equations 92
5.4 Boundary Conditions 95
5.5 Integral Equation for the Current 96
5.6 Approximate Solution of the Integral Equation 99
5.7 Input Impedance of the Cylindrical Antenna 106
5.8 Numerical Results 108

6. EXPERIMENTAL INVESTIGATION ON THE RADIATION OF A CYLINDRICAL ANTENNA IN A HOT PLASMA . . . 115

6.1 Introduction 115
6.2 Experimental Setups 116
6.2.1 Construction of a Large Volume of Stable, High-Density Plasma 116
6.2.2 Experimental Setup for the Measurement of Antenna Impedance in a Hot Plasma . . . 117
6.2.3 Experimental Setup for the Measurement of Antenna Radiation Through a Hot Plasma . 120
6.3 Review of a Lossless, Hot-Plasma Theory 123
6.4 Experimental Results and Comparison with Theories 127
6.4.1 Comparison of Experiment With a Lossless, Hot-Plasma Theory on Antenna Input Impedance 128
6.4.2 Comparison of Experiment With a Lossy, Cold-Plasma Theory on Antenna Input Impedance 130

Page

6.4.3 Experimental Results on Antenna Radiation Fields 132
6.5 Discussion 133

REFERENCES 146

LIST OF FIGURES

Figure		Page
2.1	A spherical antenna covered by a lossy, cold plasma layer.	9
2.2	Theoretical radiation of a spherical antenna (a = 0.635 cm) in a cold plasma ($\nu/2\pi$ = 0.03 GHz) driven at various frequencies as a function of plasma density.	26
2.3	Theoretical radiation of a spherical antenna (a = 0.635 cm) in a cold plasma ($\nu/2\pi$ = 0.003 GHz) driven at various frequencies as a function of plasma density.	27
2.4	Theoretical radiation of a spherical antenna (a = 0.635 cm) in a cold plasma ($\nu/2\pi$ = 0.12 GHz) driven at various frequencies as a function of plasma density.	28
2.5	Effect of the electron collision frequency on the enhancement of antenna radiation.	29
2.6	Effect of the thickness (d) of plasma layer on the enhancement of antenna radiation.	30
2.7	Effect of the spherical antenna size on the enhancement of antenna radiation with a fixed thickness of plasma layer (d = 5.08 cm)	31
2.8	Effect of the spherical antenna size on the enhancement of antenna radiation with a fixed radius of plasma layer (b = 7.62 cm)	32
3.1	A spherical antenna covered by a lossy, hot plasma layer.	35

Figure		Page

3.2 Theoretical radiation of a spherical antenna ($a = 2.54$ cm) in a lossy, hot plasma ($\nu/2\pi = 0.12$ GHz, $v_o/c_o = 0.01$) driven at various frequencies as a function of plasma density. 63

3.3 Theoretical radiation of a spherical antenna ($a = 2.54$ cm) in a lossy, hot plasma ($\nu/2\pi = 0.12$ GHz, $v_o/c_o = 0.01$) driven at various frequencies as a function of plasma density. 64

3.4 Theoretical radiation of a spherical antenna ($a = 2.54$ cm) in a lossy, hot plasma ($\nu/2\pi = 0.12$ GHz, $v_o/c_o = 0.01$) driven at various frequencies as a function of plasma density. 65

3.5 Theoretical radiation of a spherical antenna ($a = 1.27$ cm) in a lossy, hot plasma ($\nu/2\pi = 0.12$ GHz, $v_o/c_o = 0.01$) driven at various frequencies as a function of plasma density. 66

3.6 Theoretical radiation of a spherical antenna ($a = 1.27$ cm) in a lossy, hot plasma ($\nu/2\pi = 0.12$ GHz, $v_o/c_o = 0.01$) driven at various frequencies as a function of plasma density. 67

3.7 Theoretical radiation of a spherical antenna ($a = 1.27$ cm) in a lossy, hot plasma ($\nu/2\pi = 0.12$ GHz, $v_o/c_o = 0.01$) driven at various frequencies as a function of plasma density. 68

3.8 Theoretical radiation of a spherical antenna ($a = 2.54$ cm) in a lossy, hot plasma ($\nu/2\pi = 0.03$ GHz, $v_o/c_o = 0.01$) driven at 0.4 GHz as a function of plasma density 69

3.9 Theoretical radiation of a spherical antenna ($a = 3.81$ cm) in a lossy, hot plasma ($\nu/2\pi = 0.03$ GHz, $v_o/c_o = 0.01$) driven at 0.4 GHz as a function of plasma density 70

3.10 Theoretical radiation of a spherical antenna ($a = 5.08$ cm) in a lossy, hot plasma ($\nu/2\pi = 0.03$ GHz, $v_o/c_o = 0.01$) driven at 0.4 GHz as a function of plasma density 71

Figure		Page
3.11	Theoretical radiation of a spherical antenna ($a = 6.35$ cm) in a lossy, hot plasma ($\nu/2\pi = 0.03$ GHz, $v_o/c_o = 0.01$) driven at 0.4 GHz as a function of plasma density.	72
3.12	Theoretical radiation of a spherical antenna ($a = 2.54$ cm) in a lossy, hot plasma ($\nu/2\pi = 0.003$ GHz, $v_o/c_o = 0.01$) driven at 0.4 GHz as a function of plasma density.	73
3.13	Theoretical radiation of a spherical antenna ($a = 3.81$ cm) in a lossy, hot plasma ($\nu/2\pi = 0.003$ GHz, $v_o/c_o = 0.01$) driven at 0.4 GHz as a function of plasma density.	74
3.14	Theoretical radiation of a spherical antenna ($a = 5.08$ cm) in a lossy, hot plasma ($\nu/2\pi = 0.003$ GHz, $v_o/c_o = 0.01$) driven at 0.4 GHz as a function of plasma density.	75
3.15	Theoretical radiation of a spherical antenna ($a = 6.35$ cm) in a lossy, hot plasma ($\nu/2\pi = 0.003$ GHz, $v_o/c_o = 0.01$) driven at 0.4 GHz as a function of plasma density.	76
4.1	Experimental setup for the radiation measurement of spherical antenna.	79
4.2	A hemi-spherical plasma tube (3-inch radius) under operation inside of a microwave anechoic chamber	80
4.3	Experimental setup outside of a microwave anechoic chamber	80
4.4	Experimental and theoretical radiation of a spherical antenna ($a = 2.54$ cm) in a plasma driven at various frequencies as a function of plasma density	84
4.5	Experimental and theoretical radiation of a spherical antenna ($a = 1.27$ cm) in a plasma driven at various frequencies as a function of plasma density.	85

Figure		Page

4.6 Experimental and theoretical radiation of a spherical antenna ($a = 2.54$ cm) in a hot plasma driven at various frequencies as a function of plasma density. 86

4.7 Experimental and theoretical radiation of a spherical antenna ($a = 1.27$ cm) in a hot plasma driven at various frequencies as a function of plasma density. 87

5.1 A cylindrical antenna immersed in an infinite, lossy and cold plasma 91

5.2 Theoretical input impedance of a monopole ($h/\lambda_o = 0.313$, $a/\lambda_o = 0.008$) in a cold plasma as a function of plasma density 111

5.3 Theoretical input impedance of a monopole ($h/\lambda_o = 0.282$, $a/\lambda_o = 0.0072$) in a cold plasma as a function of plasma density 112

5.4 Theoretical input impedance of a monopole ($h/\lambda_o = 0.213$, $a/\lambda_o = 0.008$) in a cold plasma as a function of plasma density 113

5.5 Theoretical input impedance of a monopole ($h/\lambda_o = 0.192$, $a/\lambda_o = 0.0072$) in a cold plasma as a function of plasma density 114

6.1 Experimental setup for the impedance measurement of cylindrical antenna 118

6.2 A cylindrical plasma tube (14-inch diameter by 18-inch length) under operation and the surrounding experimental setup 119

6.3 Experimental setup for the radiation measurement of cylindrical antenna 121

6.4 A cylindrical plasma tube (6-inch diameter by 12-inch length) under operation inside of a microwave anechoic chamber 122

Figure | Page

6.5 Experimental and theoretical input impedance of a monopole ($h/\lambda_o = 0.313$, $a/\lambda_o = 0.008$) in a hot plasma as a function of plasma density. . . . 135

6.6 Experimental and theoretical input impedance of a monopole ($h/\lambda_o = 0.282$, $a/\lambda_o = 0.0072$) in a hot plasma as a function of plasma density. . . . 136

6.7 Experimental and theoretical input impedance of a monopole ($h/\lambda_o = 0.213$, $a/\lambda_o = 0.008$) in a hot plasma as a function of plasma density. . . . 137

6.8 Experimental and theoretical input impedance of a monopole ($h/\lambda_o = 0.192$, $a/\lambda_o = 0.0072$) in a hot plasma as a function of plasma density. . . . 138

6.9 Experimental and theoretical input impedance of a monopole ($h/\lambda_o = 0.313$, $a/\lambda_o = 0.008$) in a plasma as a function of plasma density. 139

6.10 Experimental and theoretical input impedance of a monopole ($h/\lambda_o = 0.282$, $a/\lambda_o = 0.0072$) in a plasma as a function of plasma density. 140

6.11 Experimental and theoretical input impedance of a monopole ($h/\lambda_o = 0.213$, $a/\lambda_o = 0.008$) in a plasma as a function of plasma density. 141

6.12 Experimental and theoretical input impedance of a monopole ($h/\lambda_o = 0.192$, $a/\lambda_o = 0.0072$) in a plasma as a function of plasma density 142

6.13 Experimental radiation patterns of a monopole ($h/\lambda_o = 0.6$, $a/\lambda_o = 0.008$) surrounded by a hot plasma of various densities 143

6.14 Experimental radiation patterns of a monopole ($h/\lambda_o = 0.66$, $a/\lambda_o = 0.008$) surrounded by a hot plasma of various densities 144

6.15 Experimental radiation patterns of a monopole ($h/\lambda_o = 0.233$, $a/\lambda_o = 0.008$) surrounded by a hot plasma of various densities 145

CHAPTER 1

INTRODUCTION

The research described in this dissertation deals with the radiation of spherical and cylindrical antennas imbedded in incompressible and compressible plasmas. The first part of the dissertation studies the radiation from a spherical antenna when it is covered by a finite layer of plasma. This study is motivated by a newly discovered phenomenon that the antenna radiation can be enhanced if the antenna frequency is lower than the plasma frequency of the coating plasma layer. The second part of the dissertation investigates the interaction of a cylindrical antenna with a plasma. One of the main objectives of this investigation is to detect the excitation of an electroacoustic wave by an antenna and the effect of this wave on the characteristics of the antenna. Additional introductions on these studies are given below.

It is well known that when an antenna is covered by a layer of plasma with a plasma frequency higher than the antenna frequency, the antenna radiation is reduced drastically. The conventional approach to overcome this blackout phenomenon is to raise the antenna frequency to exceed the plasma frequency of the plasma volume. This approach is usually hampered by the practical limitation of available high-frequency sources. In the first part of this dissertation, a new phenomenon on the enhanced radiation from a plasma-coated spherical antenna is studied. It is shown both theoretically and experimentally that the radiation from a spherical antenna covered by a spherical layer of plasma can be enhanced if the antenna frequency is adjusted to be much lower than the plasma frequency of the plasma layer and the dimensions of the antenna and the plasma layer are properly chosen.

The phenomenon of the enhanced radiation from a small antenna covered by a plasma layer was reported first by Messiaen and Vandenplas[1] in 1967. These authors also predicted a series of resonance peaks on the antenna radiation and a significant effect of the plasma sheath on the radiation. Chen and Lin[2, 3] studied the same phenomenon on a cylindrical antenna of various lengths covered by a finite volume of lossy, hot plasma. Instead of finding a series of resonance peaks, they observed a strong enhancement on the antenna radiation over a wide band of antenna frequencies which are much lower than the plasma frequency of the plasma volume. They also found a negligible effect on the antenna radiation due to the plasma sheath or the DC potential of the antenna. Although the phenomena of enhanced radiation observed by Messiaen and Vandenplas and by Chen and Lin are similar, the detailed results are different. The effects of the dimensions of the antenna and the plasma layer on the phenomenon of enhanced radiation have not been investigated before. In this study the phenomenon of enhanced radiation is examined more carefully by conducting both theoretical and experimental studies on a plasma-coated spherical antenna. The spherical geometry is adopted to make the theoretical study tractable. In the experiment an imaged hemisphere on a ground plane was used as an antenna and a mercury arc discharge was used as the coating plasma. In the theoretical models, the spherical antenna is first assumed to be covered by a lossy, cold plasma layer with the plasma sheath on the antenna surface ignored. The study is then extended to a lossy, hot plasma layer with the plasma sheath included. The theoretical results based on these models are in satisfactory agreement with the experimental observation.

When an antenna on a reentry vehicle is covered by a plasma layer and suffers blackout, a possible scheme of overcoming this problem will be to reduce the antenna frequency to a value which is much lower than the plasma frequency and in the range for the enhanced radiation. Another potential application of this phenomenon is the low-loss tuning of a small antenna. Theoretically, the plasma can be made lossless so that this tuning scheme may prove to be more effective than any conventional impedance tuning.

The second part of the dissertation investigates the interaction of a cylindrical antenna with a plasma. When an electromagnetic radiating source is immersed in a hot plasma, an electroacoustic or a longitudinal plasma wave may be excited in addition to the usual electromagnetic wave. Numerous theoretical papers have been published on the subject. Cohen[4] was the first one to show the possible excitation of an electroacoustic wave by a radiating source in a hot plasma. Hessel and Shamoys[5] and Fejer[6] studied the electroacoustic wave excited by a small source. Chen[7] investigated the effect of an electroacoustic wave on the radiation of a cylindrical antenna. Wait[8] examined the electroacoustic wave excited by a slotted-sphere antenna. There are many other theoretical papers which are not mentioned here.

In contrast with the abundance of theoretical papers, extremely few experimental studies have been published. The relevant experimental studies are the observation of electroacoustic wave by Whale[9] in a rocket flight, Schmitt's[10] observation of Tonks-Dattner's resonance excited by an antenna, and the experiments on a cylindrical antenna in a hot plasma conducted by Jassby and Bachyski[11] and by Chen, Jackson and Lin[12,13]. Nevertheless, to our best knowledge, no extensive experimental study has been conducted to study the electroacoustic wave excited by an antenna in a hot plasma.

In this part of study an extensive experimental investigation was conducted to: (1) detect the existence of an electroacoustic wave in a hot plasma, and (2) study the effect of this electroacoustic wave on the circuit and the radiation properties of an antenna. Two approaches: (1) to measure the antenna input impedance as a function of the plasma parameters, and (2) to measure the antenna radiation field as a function of the plasma parameters, have been used to detect the electroacoustic wave. In our experiment, the hot plasma was provided by a mercury arc discharge which was created in two plasma tubes. The cylindrical monopole antennas were used as the radiating sources.

A simple theory on a cylindrical antenna immersed in a lossy, cold plasma of infinite extent is developed. The antenna input impedance is obtained as a function of the antenna dimensions and plasma parameters. The significant finding of this theoretical study is the observation of a peak resistance and a change of reactance from capactiviet to inductive when the antenna frequency approaches to the plasma frequency. The comparison between this theory and the experiment indicates that the effect of the electron collision frequency on the antenna input impedance is significant in the neighborhood of plasma frequency.

The experimental results are also compared with another set of theoretical results obtained by Chen[7]. The agreements on the antenna input resistance and the observation of peak radiation near the axial direction of the antenna tend to indicate the existence of an electroacoustic wave excited by the antenna and its significant effect on the characteristics of the antenna.

CHAPTER 2

RADIATION FROM A SPHERICAL ANTENNA IMBEDDED IN A LOSSY, COLD PLASMA OF FINITE EXTENT

2.1 Introduction

The radiation of a spherical antenna when surrounded by a layer of lossy, cold plasma is studied in this chapter. This study is motivated by a newly discovered phenomenon which indicates that the radiation from an antenna can be enhanced if the plasma frequency of the plasma is considerably higher than the antenna frequency and the dimensions of the antenna and the plasma layer are appropriately chosen.

When an antenna is covered by a layer of plasma with a plasma frequency higher than the antenna frequency, the antenna radiation is reduced drastically, a phenomenon known as the blackout. The conventional approach to overcome this blackout phenomenon is to raise the antenna frequency to exceed the plasma frequency of the plasma. This approach is usually hampered by the practical limitation of available high frequency sources. The new phenomenon on the enhanced radiation from a plasma-coated antenna to be studied in this chapter may serve as a solution to the blackout problem encountered by a reentry antenna.

The phenomenon of the enhanced radiation from a small antenna covered by a plasma layer was reported first by Messiaen and Vandenplas[1] in 1967. These authors also predicted a series of resonance peaks on the antenna radiation and a significant effect of the plasma sheath on the radiation. Chen and Lin[2, 3] have investigated the same phenomenon on a cylindrical antenna of various lengths covered by a finite volume of lossy, hot plasma. Instead of finding a series of resonance peaks, they observed a strong enhancement on the antenna radiation over a wide band of antenna frequencies which are much lower than the plasma frequency of the plasma volume. They also found a negligible effect on the antenna radiation due to the plasma sheath or DC potential of the antenna. Although the phenomena of enhanced radiation observed by Messiaen and Vandenplas and Chen and Lin are similar, the detailed results are different. Neither the effects of the dimensions of antenna nor the size of the plasma layer on the phenomenon of enhanced radiation have been investigated before. This unusual phenomenon of enhanced radiation to be studied in this chapter may be attributed to the coating of antenna with a dielectric of negative permittivity which is the simple model of an overdense plasma.

In our study, the spherical geometry is adopted for the sake of making the theoretical study tractable. In this theoretical model, the spherical antenna is assumed to be covered by an uniform, lossy and cold plasma and the plasma sheath on the antenna surface is ignored.

Based on the finding of our study in this chapter, it appears feasible that when an antenna on a reentry vehicle is covered by a plasma layer and suffers a blackout, a possible scheme of overcoming this problem will be to reduce the antenna frequency to a value which is much lower than the plasma frequency and in the range for the enhanced radiation. Another potential application of this phenomenon is the low-loss tuning of a small antenna. Since only a lossless plasma with a negative permittivity is needed for this purpose, this tuning scheme may prove to be more efficient than any conventional impedance tuning.

2.2 Geometry and Statement of the Problem

The geometry of the problem is shown in Fig. 2.1. A spherical antenna of radius a is covered by a spherical layer of uniform lossy plasma with a thickness of b-a. The antenna surface is perfectly conducting except for a narrow equatorial gap between $\pi/2 - \theta_1 \leq \theta \leq \pi/2 + \theta_1$. Across this gap a voltage of amplitude V and frequency ω is applied. The spherical coordinates (γ, θ, ϕ) are adopted and the rotational symmetry is assumed. The

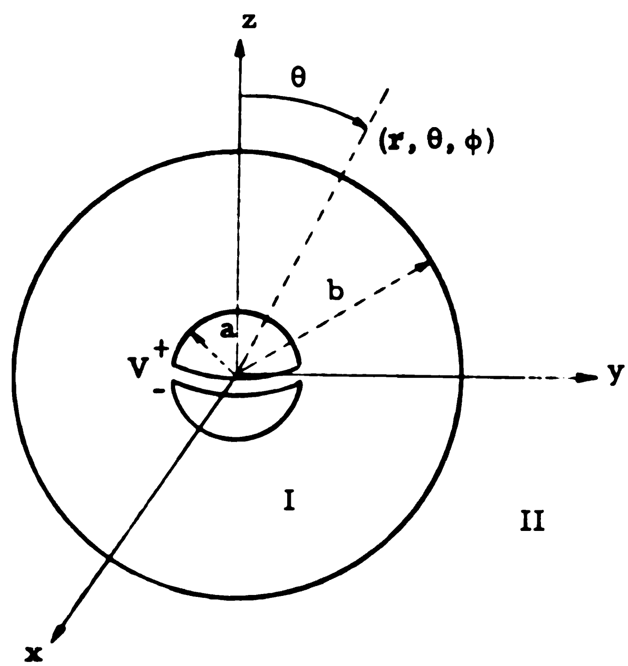

Region I: cold plasma $(\mu_o, \epsilon, \sigma)$

Region II: free space (μ_o, ϵ_o)

Fig. 2.1 A spherical antenna covered by a lossy, cold plasma layer.

plasma is assumed to be a weakly ionized gas and can be considered as a lossy medium with a permittivity of $\epsilon = \epsilon_o(1 - \frac{\omega_p^2}{\omega^2+\nu^2})$, a conductivity of $\sigma = \frac{n_o e^2}{m_e} \frac{\nu}{\omega^2+\nu^2}$, and a permeability of $\mu = \mu_o$ where ω and ω_p are the antenna and plasma frequencies, e and m_e are the charge and mass of electrons. n_o is the density of plasma, ν is the collision frequency of electrons with neutral particles, and ϵ_o and μ_o are the permittivity and permeability of free space. The total space excluding the antenna is divided into two regions. Region I is the plasma layer and the rest of the free space is Region II.

The assumption of infinitesimal driving gap is made to simplify the problem because only the radiated fields of the antenna are to be sought in this study. If the input impedance of the antenna is also to be determined, the assumption of a finite driving gap is needed to avoid the divergence of some series appeared in the mathematical expressions.

2.3 Solutions to Maxwell's Equations in the Plasma Region

The basic equations which govern the system are Maxwell's equations. Maxwell's equations in Region I (plasma layer, $a \leq r \leq b$) are

$$\begin{cases} \nabla \times \vec{E}_1 = -j\omega\mu_o\vec{H}_1 & (2.1) \\ \nabla \times \vec{H}_1 = j\omega\xi\vec{E}_1 & (2.2) \end{cases}$$

where $\vec{E}$ and $\vec{H}$ are the electric and magnetic fields and ξ is the complex permittivity given by

$$\xi = \epsilon(1 - j\frac{\sigma}{\omega\epsilon}) . \tag{2.3}$$

The suppressed time dependence is exp(jωt).

From the symmetry of the antenna it can be seen that there is no variation in the ϕ direction and the magnetic field has only a ϕ component. Thus, Eqs. (2.1) and (2.2) can be easily reduced to three scalar equations such as

$$\frac{\partial}{\partial r}(r E_{1\theta}) - \frac{\partial E_{1r}}{\partial \theta} = - j\omega \mu_o r H_{1\phi} \tag{2.4}$$

$$\frac{1}{r \sin\theta} \frac{\partial}{\partial\theta}(\sin\theta H_{1\phi}) = j\omega\xi E_{1r} \tag{2.5}$$

$$-\frac{\partial}{\partial r}(r H_{1\phi}) = j\omega\xi r E_{1\theta} . \tag{2.6}$$

Differentiating Eqs. (2.5) and (2.6), and substituting them into Eq. (2.4) leads to a partial differential equation,

$$\frac{\partial^2}{\partial r^2}(r H_{1\phi}) + \frac{1}{r^2}\frac{\partial}{\partial\theta}\left[\frac{1}{\sin\theta}\frac{\partial}{\partial\theta}(\sin\theta\, r H_{1\phi})\right] + k^2(rH_{1\phi}) = 0 \tag{2.7}$$

where k is the complex propagation constant given by

$$k^2 = \omega^2\mu_o\xi . \tag{2.8}$$

If we write

$$k = \beta - j\alpha , \tag{2.9}$$

β and α can be expressed as

$$\beta = \frac{\beta_o}{\sqrt{2}}\left\{1 - \frac{\omega_p^2}{\omega^2+\nu^2} + \left[1 - \frac{2\omega_p^2}{\omega^2+\nu^2} + \frac{\omega_p^4}{\omega^2(\omega^2+\nu^2)}\right]^{\frac{1}{2}}\right\}^{\frac{1}{2}} \tag{2.10}$$

$$a = \frac{\beta_o}{\sqrt{2}} \left\{ -1 + \frac{\omega_p^2}{\omega^2 + \nu^2} + \left[1 - \frac{2\omega_p^2}{\omega^2 + \nu^2} + \frac{\omega_p^4}{\omega^2(\omega^2 + \nu^2)} \right]^{\frac{1}{2}} \right\}^{\frac{1}{2}} \qquad (2.11)$$

with

$$\beta_o = \omega \sqrt{\mu_o \epsilon_o} \quad . \qquad (2.12)$$

To solve Eq. (2.7), we use the method of the separation of variables. Since $H_{1\phi}$ is independent of ϕ, we can assume

$$rH_{1\phi} = R(r)\,\Theta(\theta) \qquad (2.13)$$

where R is a function of r alone and Θ is a function of θ only. The substitution of Eq. (2.13) in Eq. (2.7) leads to

$$\frac{r^2}{R} \frac{d^2R}{dr^2} + k^2 r^2 = -\frac{1}{\Theta} \frac{d}{d\theta} \left[\frac{1}{\sin\theta} \frac{d}{d\theta} (\Theta \sin\theta) \right] = n\,(n+1) \qquad (2.14)$$

where n is any integer. Equation (2.14) generates two ordinary differential equations,

$$\frac{d}{d\theta} \left[\frac{1}{\sin\theta} \frac{d}{d\theta} (\Theta \sin\theta) \right] + n(n+1)\Theta = 0 \qquad (2.15)$$

$$\frac{r^2}{R} \frac{d^2R}{dr^2} + k^2 r^2 - n(n+1) = 0 \, . \qquad (2.16)$$

Let us consider Eq. (2.15) first. Making the substitutions,

$$u = \cos\theta \, , \quad \sqrt{1 - u^2} = \sin\theta \, , \quad \frac{d}{d\theta} = -\sqrt{1-u^2} \frac{d}{du} \quad ,$$

Eq. (2.15) can be reduced to

$$(1 - u^2) \frac{d^2\Theta}{du^2} - 2u \frac{d\Theta}{du} + \left[n(n+1) - \frac{1}{1-u^2} \right] \Theta = 0 \, . \qquad (2.17)$$

Equation (2.17) is a special form of the associated Legendre's equation,

$$(1 - x^2)\frac{d^2y}{dx^2} - 2x\frac{dy}{dx} + \left[n(n+1) - \frac{m^2}{1 - x^2}\right]y = 0. \tag{2.18}$$

The solution to Eq. (2.18) is

$$y = P_n^m(x)$$

and this function is called an associated Legendre function of the first kind of order n and degree m. These functions are actually related to the ordinary Legendre functions $P_n(x)$ by the relation,

$$P_n^m(x) = (-1)^m(1 - x^2)^{\frac{m}{2}} \frac{d^m P_n(x)}{dx^m}. \tag{2.19}$$

In order to have finite solutions on the interval $-1 \leq x \leq 1$ the parameter n must be zero or a positive integer and that the integer m can take on only the values $-n$, $-(n-1), \ldots, 0, \ldots, (n-1)$, n, i.e., $n \geq |m|$.

Thus a solution to Eq. (2.17) can be obtained as

$$\Theta = P_n^1(u) = P_n^1(\cos\theta) \tag{2.20}$$

where n must be a positive integer and $n \geq 1$.

Note that only one solution for this second-order differential equation (2.17) has been considered. The other solution becomes infinite on the axis, and so it should be excluded from this problem since the axis is included in the geometry.

Other properties of the associated and ordinary Legendre functions that will be useful to us in the later development and numerical calculation are listed as follows:

1. $P_n^1(\cos\theta)$ is zero at $\theta = \pi/2$ if n is even.

2. $P_n^1(\cos\theta)$ is maximum at $\theta = \pi/2$ if n is odd, and the value of this maximum is given by

$$P_n^1(0) = \begin{cases} \dfrac{2}{\sqrt{\pi}} \dfrac{\Gamma(\frac{n}{2}+1)}{\Gamma(\frac{n}{2}+\frac{1}{2})} & \text{for } n = 1, 5, 9 \ldots \\ -\dfrac{2}{\sqrt{\pi}} \dfrac{\Gamma(\frac{n}{2}+1)}{\Gamma(\frac{n}{2}+\frac{1}{2})} & \text{for } n = 3, 7, 11 \ldots \end{cases} \tag{2.21}$$

or

$$\left[P_n^1(0)\right]^2 = \frac{4}{\pi}\left[\frac{\Gamma(\frac{n}{2}+1)}{\Gamma(\frac{n}{2}+\frac{1}{2})}\right]^2 \quad \text{for } n = \text{odd} \tag{2.22}$$

where $\Gamma(x)$ is the Gamma function with argument x.

3. The associated Legendre functions have orthogonality properties,

$$\int_{-1}^{+1} P_n^1(u)\, P_\ell^1(u)\, du = \begin{cases} 0 & \text{for } n \neq \ell \\ \dfrac{2n(n+1)}{2n+1} & \text{for } n = \ell\,. \end{cases} \tag{2.23}$$

4. A recurrence formula for the ordinary Legendre functions is

$$\frac{dP_{n+1}(u)}{du} - u\,\frac{dP_n(u)}{du} - (n+1)\,P_n(u) = 0\,, \tag{2.24}$$

and from (2.19)

$$P_n^1(\cos\theta) = \frac{d}{d\theta} P_n(\cos\theta) . \qquad (2.25)$$

Combining Eqs. (2.24) and (2.25) we obtain an expression,

$$\frac{1}{\sin\theta}\left[\cos\theta\, P_n^1(\cos\theta) - P_{n+1}^1(\cos\theta)\right] = (n+1)P_n(\cos\theta). \qquad (2.26)$$

5. The differentiation formula is

$$\frac{d}{d\theta}\left[P_n^1(\cos\theta)\right] = \frac{1}{\sin\theta}\left[n\, P_{n+1}^1(\cos\theta) - (n+1)\cos\theta\, P_n^1(\cos\theta)\right] . \qquad (2.27)$$

Going back to the differential equation (2.16), we make the substitution,

$$R_1 = \frac{R}{r^{\frac{1}{2}}} . \qquad (2.28)$$

Equation (2.16) then becomes

$$\frac{d^2R_1}{dr^2} + \frac{1}{r}\frac{dR_1}{dr} + \left[k^2 - \frac{(n+\frac{1}{2})^2}{r^2}\right]R_1 = 0 . \qquad (2.29)$$

This is a form of Bessel's equation,

$$\frac{d^2y}{dx^2} + \frac{1}{x}\frac{dy}{dx} + (k^2 - \frac{n^2}{x^2})\, y = 0 . \qquad (2.30)$$

The solution to Eq. (2.29) can then be expressed as

$$R_1 = A_n H_{n+\frac{1}{2}}^{(2)}(kr) + B_n\, H_{n+\frac{1}{2}}^{(1)}(kr) \qquad (2.31)$$

where A_n and B_n are arbitrary constants, $H_{n+\frac{1}{2}}^{(1)}(kr)$ and $H_{n+\frac{1}{2}}^{(2)}(kr)$ are the Hankel functions of the first and second kinds with order

$n+\frac{1}{2}$, which represent the radially inward and outward traveling waves respectively. Combining Eqs. (2.13), (2.20), (2.28) and (2.31) we have

$$H_{1\phi} = \frac{1}{\sqrt{r}} \sum_{n=1}^{\infty} P_n^1(\cos\theta) \left[A_n H_{n+\frac{1}{2}}^{(2)}(kr) + B_n H_{n+\frac{1}{2}}^{(1)}(kr)\right]. \tag{2.32}$$

The other two components of the electric field can be determined easily from Eqs. (2.5) and (2.6).

Substituting Eq. (2.32) into Eq. (2.5) and using Eqs. (2.27) and (2.26) we obtain

$$E_{1r} = \frac{j}{\omega \xi r^{3/2}} \sum_{n=1}^{\infty} n(n+1) P_n(\cos\theta) \left[A_n H_{n+\frac{1}{2}}^{(2)}(kr) + B_n H_{n+\frac{1}{2}}^{(1)}(kr)\right]. \tag{2.33}$$

To derive $E_{1\theta}$, two differentiation formulas of the Hankel functions

$$\frac{d}{dx} H_{n+\frac{1}{2}}^{(1)}(x) = -\frac{n+\frac{1}{2}}{x} H_{n+\frac{1}{2}}^{(1)}(x) + H_{n-\frac{1}{2}}^{(1)}(x) \tag{2.34}$$

$$\frac{d}{dx} H_{n+\frac{1}{2}}^{(2)}(x) = -\frac{n+\frac{1}{2}}{x} H_{n+\frac{1}{2}}^{(2)}(x) + H_{n-\frac{1}{2}}^{(2)}(x) \tag{2.35}$$

are needed.

The substitution of Eq. (2.32) into Eq. (2.6) and the utilization of Eqs. (2.34) and (2.35) lead to

$$E_{1\theta} = \frac{-j}{\omega \xi r^{3/2}} \sum_{n=1}^{\infty} P_n^1(\cos\theta) \left\{A_n \left[nH_{n+\frac{1}{2}}^{(2)}(kr) - kr\, H_{n-\frac{1}{2}}^{(2)}(kr)\right]\right.$$

$$\left. + B_n \left[n\, H_{n+\frac{1}{2}}^{(1)}(kr) - kr\, H_{n-\frac{1}{2}}^{(1)}(kr)\right]\right\}. \tag{2.36}$$

The solutions to Maxwell's equations in this region under rotational symmetry can thus be summarized as

$$H_{1\phi}(r,\theta) = \frac{1}{\sqrt{r}} \sum_{n=1}^{\infty} P_n^1(\cos\theta)\left[A_n H^{(2)}_{n+\frac{1}{2}}(kr) + B_n H^{(1)}_{n+\frac{1}{2}}(kr)\right] \qquad (2.32)$$

$$E_{1r}(r,\theta) = \frac{j}{\omega \xi r^{3/2}} \sum_{n=1}^{\infty} n(n+1) P_n(\cos\theta)\left[A_n H^{(2)}_{n+\frac{1}{2}}(kr) + B_n H^{(1)}_{n+\frac{1}{2}}(kr)\right] \qquad (2.33)$$

$$E_{1\theta}(r,\theta) = \frac{-j}{\omega \xi r^{3/2}} \sum_{n=1}^{\infty} P_n^1(\cos\theta)\left\{A_n\left[nH^{(2)}_{n+\frac{1}{2}}(kr) - krH^{(2)}_{n-\frac{1}{2}}(kr)\right] + B_n\left[nH^{(1)}_{n+\frac{1}{2}}(kr) - kr\,H^{(1)}_{n-\frac{1}{2}}(kr)\right]\right\} \qquad (2.36)$$

and

$$E_{1\phi} = H_{1r} = H_{1\theta} = 0\,. \qquad (2.37)$$

2.4 Solutions to Maxwell's Equations in the Free-Space Region

Maxwell's equations in Region II (free space, $r \geq b$) are

$$\begin{cases} \nabla \times \vec{E}_2 = -j\omega\mu_o \vec{H}_2 & (2.38) \\ \nabla \times \vec{H}_2 = j\omega\epsilon_o \vec{E}_2\,. & (2.39) \end{cases}$$

Since Region II is unbounded, no reflected or inward traveling wave exists in this region. Following the same analysis as in Sec. 2.3, the solutions to Maxwell's equations in this region can be written as

$$H_{2\phi}(r,\theta) = \sqrt{r} \sum_{n=1}^{\infty} C_n P_n^1(\cos\theta)\, H^{(2)}_{n+\frac{1}{2}}(\beta_o r) \qquad (2.40)$$

$$E_{2r}(r,\theta) = \frac{j}{\omega \epsilon_o r^{3/2}} \sum_{n=1}^{\infty} C_n n(n+1) P_n(\cos\theta) H^{(2)}_{n+\frac{1}{2}}(\beta_o r) \qquad (2.41)$$

$$E_{2\theta}(r,\theta) = \frac{-j}{\omega \epsilon_o r^{3/2}} \sum_{n=1}^{\infty} C_n P_n^1(\cos\theta)\left[nH^{(2)}_{n+\frac{1}{2}}(\beta_o r) - \beta_o r\, H^{(2)}_{n-\frac{1}{2}}(\beta_o r)\right] \qquad (2.42)$$

where C_n is an arbitrary constant, n is a positive integer, and β_o is the wave number of free space given by Eq. (2.12).

2.5 Boundary Conditions for Calculating the Radiation Fields

In order to determine the constants A_n, B_n and C_n, the boundary conditions at r = a and r = b are applied.

The voltage applied across the gap is given by

$$V = \int_{\frac{\pi}{2}-\theta_1}^{\frac{\pi}{2}+\theta_1} E_{1\theta}(a,\theta)\, a\, d\theta = \int_0^{\pi} E_{1\theta}(a,\theta)\, a\, d\theta\,, \tag{2.43}$$

because $E_{1\theta}$ is zero on the surface of the conducting sphere except at the gap between $\frac{\pi}{2} - \theta_1 \leq \theta \leq \frac{\pi}{2} + \theta_1$. Since the Legendre polynomials form a complete set of orthogonal functions, any function f(x) on the interval $-1 \leq x \leq 1$ can be expanded in terms of them. The electric field on the surface of the sphere can thus be expanded in a series of Legendre polynomials as

$$E_{1\theta}(a,\theta) = \sum_{n=1}^{\infty} b_n P_n^1(\cos\theta) \tag{2.44}$$

where

$$b_n = \frac{2n+1}{2n(n+1)} \int_0^{\pi} E_{1\theta}(a,\theta) P_n^1(\cos\theta) \sin\theta\, d\theta\,. \tag{2.45}$$

If the gap between the two halves of the sphere is assumed to be small,

$$\left.\begin{array}{l} P_n^1(\cos\theta) \approx P_n^1(0) \\ \sin\theta \approx 1 \end{array}\right\} \quad \begin{array}{l} \frac{\pi}{2} - \theta_1 \leq \theta \leq \frac{\pi}{2} + \theta_1 \\ \theta_1 \text{ is small}\,. \end{array} \tag{2.46}$$

Combining Eqs. (2.43), (2.45) and (2.46), we have

$$b_n = \frac{(2n+1)\, P_n^1(0) V}{2n(n+1)\, a} \quad . \tag{2.47}$$

From Eq. (2.36) we obtain

$$E_{1\theta}(a,\theta) = \frac{-j}{\omega \xi a^{3/2}} \sum_{n=1}^{\infty} P_n^1(\cos\theta) \Big\{ A_n \Big[n H^{(2)}_{n+\frac{1}{2}}(ka) - ka H^{(2)}_{n-\frac{1}{2}}(ka) \Big] + B_n \Big[n H^{(1)}_{n+\frac{1}{2}}(ka) - ka\, H^{(1)}_{n-\frac{1}{2}}(ka) \Big] \Big\} . \tag{2.48}$$

The combination of Eqs. (2.44), (2.47) and (2.48) gives

$$F_1 A_n + F_2 B_n = F_3 V \tag{2.49}$$

where

$$F_1 = n H^{(2)}_{n+\frac{1}{2}}(ka) - ka\, H^{(2)}_{n-\frac{1}{2}}(ka)$$

$$F_2 = n H^{(1)}_{n+\frac{1}{2}}(ka) - ka\, H^{(1)}_{n-\frac{1}{2}}(ka)$$

$$F_3 = j\omega\xi \sqrt{a}\, P_n^1(0) \frac{2n+1}{2n(n+1)} \quad .$$

The continuity of the tangential components of $\vec{E}$ and $\vec{H}$ fields at the plasma-free space interface (r=b) leads to

$$E_{1\theta}(b,\theta) = E_{2\theta}(b,\theta) \tag{2.50}$$

$$H_{1\phi}(b,\theta) = H_{2\phi}(b,\theta) . \tag{2.51}$$

Using Eqs. (2.36), and (2.42), Eq. (2.50) gives

$$F_4 A_n + F_5 B_n - F_6 C_n = 0 \tag{2.52}$$

where

$$F_4 = n H^{(2)}_{n+\frac{1}{2}}(kb) - kb\, H^{(2)}_{n-\frac{1}{2}}(kb)$$

$$F_5 = nH^{(1)}_{n+\frac{1}{2}}(kb) - kbH^{(1)}_{n-\frac{1}{2}}(kb)$$

$$F_6 = \frac{\xi}{\epsilon_o}\left[nH^{(2)}_{n+\frac{1}{2}}(\beta_o b) - \beta_o bH^{(2)}_{n-\frac{1}{2}}(\beta_o b)\right].$$

From Eqs. (2.32) and (2.40), Eq. (2.51) can be expressed as

$$F_7 A_n + F_8 B_n - F_9 C_n = 0 \qquad (2.53)$$

where

$$F_7 = H^{(2)}_{n+\frac{1}{2}}(kb)$$

$$F_8 = H^{(1)}_{n+\frac{1}{2}}(kb)$$

$$F_9 = H^{(2)}_{n+\frac{1}{2}}(\beta_o b).$$

The notations F_i, $i = 1, \ldots, 9$, are used just for convenience. Thus, the constants A_n, B_n and C_n can be solved from Eqs. (2.49), (2.52) and (2.53) as

$$A_n = \frac{VF_3(F_6F_8 - F_5F_9)}{\Delta} \qquad (2.54)$$

$$B_n = \frac{VF_3(F_4F_9 - F_6F_7)}{\Delta} \qquad (2.55)$$

$$C_n = \frac{VF_3(F_4F_8 - F_5F_7)}{\Delta} \qquad (2.56)$$

where

$$\Delta = F_1(F_6F_8 - F_5F_9) + F_2(F_4F_9 - F_6F_7). \qquad (2.57)$$

Up to this point the $\vec{E}$ and $\vec{H}$ fields in Regions I and II are completely determined as functions of r and θ.

The quantity of main interest in this study is the radiated field in the far zone of the antenna. Thus, the field $E_{2\theta}$ at ($r=R$, $\theta=90^o$) can be expressed as

$$E_{2\theta}(R, 90^o) = \frac{-jV}{\omega \epsilon_o R^{3/2}} \sum_{\substack{n=1 \\ (n=odd)}}^{\infty} \frac{F_3(F_4F_8 - F_5F_7)}{\Delta} P_n^1(0) \left[nH^{(2)}_{n+\frac{1}{2}}(\beta_o R) - \beta_o R H^{(2)}_{n-\frac{1}{2}}(\beta_o R) \right] . \qquad (2.58)$$

It can also be rearranged as

$$E_{2\theta}(R, 90^o) = \frac{4\xi\sqrt{a}\, V}{\pi \epsilon_o R^{3/2}} \sum_{\substack{n=1 \\ (n=odd)}}^{\infty} \frac{2n+1}{2n(n+1)} \left[\frac{\Gamma(\frac{n}{2}+1)}{\Gamma(\frac{n}{2}+\frac{1}{2})} \right]^2 \frac{(F_4F_8 - F_5F_7)}{\Delta} \cdot \left[nH^{(2)}_{n+\frac{1}{2}}(\beta_o R) - \beta_o R H^{(2)}_{n-\frac{1}{2}}(\beta_o R) \right] . \qquad (2.59)$$

2.6 Numerical Results

The radiated power from the antenna which is proportional to the square of $E_{\theta 2}(R, 90^o)$ as expressed in Eq. (2.59) has been numerically calculated as a function of the antenna and plasma parameters. Figure 2.2 shows the radiated power from a spherical antenna of 0.635 cm radius driven at various frequencies as a function of the plasma density of the plasma layer. The radius of the spherical plasma layer is 7.62 cm and the electron collision frequency is assumed to be 0.03 GHz. The distance between the radiating and receiving antennas is 0.7 m. In this figure the radiated power at each driven frequency is normalized to its free-space radiated power.

At all antenna driven frequencies we invariably observe that the antenna radiation is reduced as the plasma density is increased and it reaches the cut-off point as the plasma frequency is increased to the neighborhood of the antenna frequency. After the plasma frequency exceeds the antenna frequency, the antenna radiation starts to build up somewhat for higher antenna frequency cases (e.g., 1.8 $\sim$ 1.4 GHz). This trend becomes more outstanding for lower frequency cases. For example, when the antenna frequency is 0.8 GHz, the antenna radiation builds up to the level of free-space radiation after going through the cut-off. If the antenna frequency is further decreased to 0.4 or 0.3 GHz, the antenna radiation can build up to a level about 20 db higher than the free-space radiation after passing the cut-off. The phenomenon of this enhanced radiation is the most interesting finding of this study. Physically it means that if an antenna is operated at a frequency much lower than the plasma frequency of the plasma layer, its radiation will recover from the cut-off and then be enhanced greatly over the free-space radiation level. This phenomenon can be applied directly to solve the blackout phenomenon by simply scaling down the driving frequency of the vehicle antenna when its radiation is cut off by a surrounding plasma layer. The phenomenon of this enhanced radiation probably can be attributed to the tuning effect of the plasma layer on the antenna input impedance. When the antenna frequency is lower than the plasma frequency, the equivalent permittivity of the plasma is negative and the plasma layer may act as an inductor to tune out the large capacitive reactance of the input impedance of a small antenna. This oversimplified explanation is by no means adequate as we can see from more results in other figures.

Figure 2.3 shows the similar phenomenon of Fig. 2.2 for the case of lower electron collision frequency (0.003 GHz). Since the loss of the plasma is lower, the antenna radiation is cut off more drastically and the radiation is enhanced greater for lower antenna frequency cases. Figure 2.4 also shows the similar phenomenon of Fig. 2.2 but for a higher electron collision frequency (0.12 GHz). This figure indicates that a higher loss in plasma makes the cut-off phenomenon less outstanding and the enhancement of radiation slightly lower.

To investigate the effect of the electron collision frequency on the phenomenon of enhanced radiation, the same antenna (0.635 cm radius) with the same plasma layer (7.62 cm radius) driven at 0.3 GHz is considered. The antenna radiation is plotted as a function of ω_p^2/ω^2 for various ν/ω in Fig. 2.5. It is evident that for a lower collision frequency higher enhancement of radiation is obtained at a lower plasma density. If the collision frequency is increased, a lower enhancement of radiation is obtained at a higher plasma density and over a wide range of ω_p^2/ω^2.

The effect of the thickness of plasma layer on the phenomenon of enhanced radiation is shown in Fig. 2.6. The same antenna

(0.635 cm radius) is driven at 0.4 GHz and the electron collision frequency is assumed to be 0.03 GHz. The antenna radiation is plotted as a function of ω_p^2/ω^2 for various values of plasma layer thickness. When the thickness of the plasma layer is the same as the antenna radius (0.635 cm), an enhancement of 15 db is obtained. A maximum enhancement of about 23 db is obtained when the thickness of the plasma layer is about 1 3/4 inches. As the thickness is further increased, the enhancement of radiation decreases. When the thickness of the plasma layer approaches to infinity, the antenna radiation remains zero after passing the cut-off point. This point is expected since the phenomenon of enhanced radiation does not occur if the antenna is placed in a plasma of infinite extent.

The effect of the antenna size on the phenomenon of enhanced radiation is indicated in Fig. 2.7. The antennas of various radii are assumed to be covered by a plasma layer of 2-inch thickness and driven at 0.4 GHz. The electron collision frequency is assumed to be 0.03 GHz. The antenna radiation is plotted as a function of ω_p^2/ω^2. In this figure it is observed that the phenomenon of enhanced radiation becomes less significant if the antenna size is increased. This indicates that for a large antenna, the phenomenon of enhanced radiation may not be observed.

With a fixed radius of 3 inches for the spherical plasma layer, the effect of the antenna size or the thickness of plasma layer on the phenomenon of enhanced radiation is shown in Fig. 2.8. The antennas of various radii are driven at 0.4 GHz. The electron collision frequency is assumed to be 0.03 GHz. The antenna radiation is plotted as a function of ω_p^2/ω^2. In this figure it is also observed that the phenomenon of enhanced radiation become less significant if the antenna size is increased and at the same time the thickness of the plasma layer is decreased. No resonance peaks are observed even when the thickness of the plasma layer is very thin.

It should be noted that in the numerical calculation only the first five terms, i.e., $n = 1, 3, \ldots, 9$, on the right-hand side of Eq. (2.59) are summed up for that series. The numerical results indicate that the $n=1$ term is the dominant term. All the numerical calculations are made by using a CDC 3600 computer.

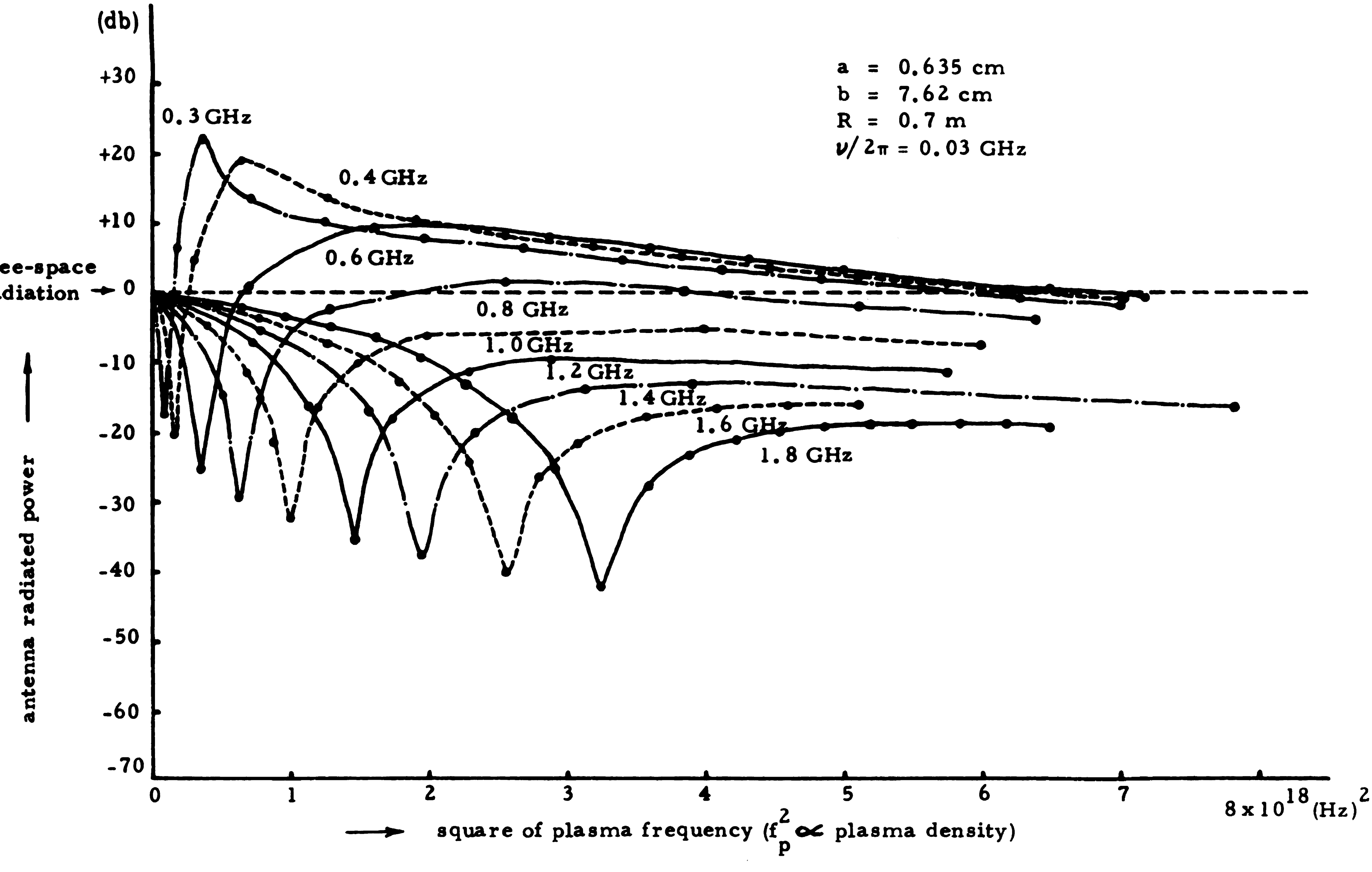

Fig. 2.2 Theoretical radiation of a spherical antenna (a = 0.635 cm) in a cold plasma ($\nu/2\pi$ = 0.03 GHz) driven at various frequencies as a function of plasma density.

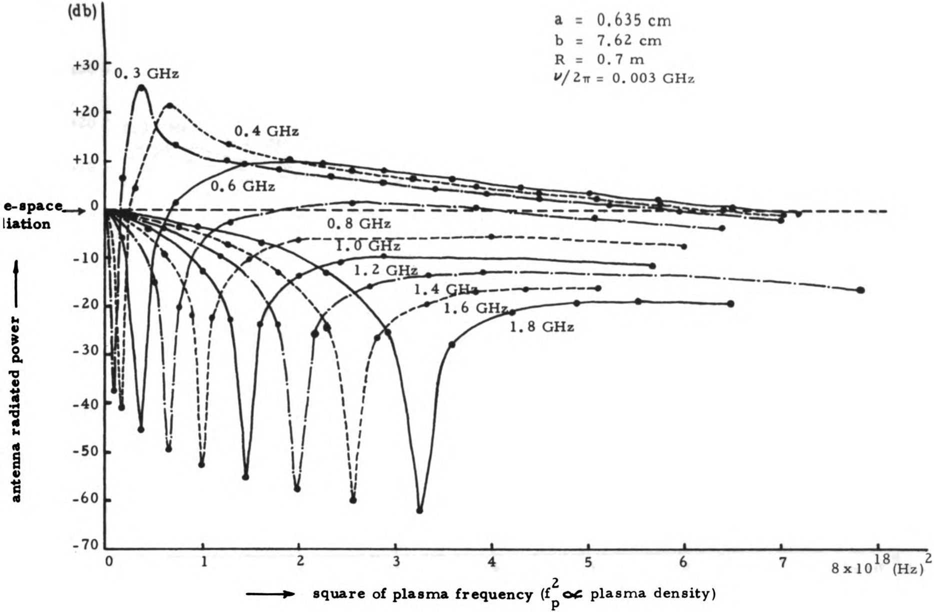

Fig. 2.3 Theoretical radiation of a spherical antenna ($a = 0.635$ cm) in a cold plasma ($\nu/2\pi = 0.003$ GHz) driven at various frequencies as a function of plasma density.

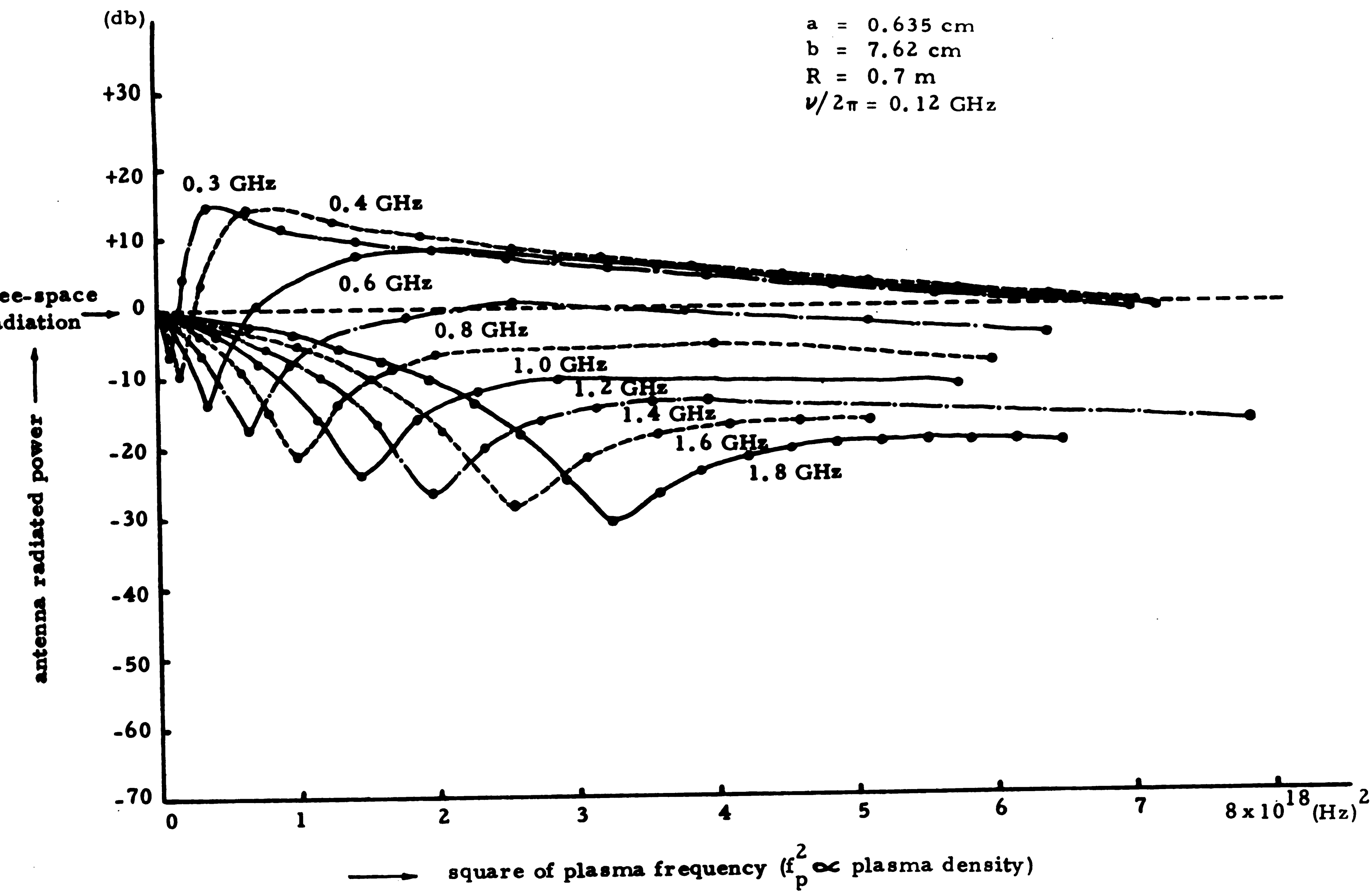

Fig. 2.4 Theoretical radiation of a spherical antenna (a = 0.635 cm) in a cold plasma ($\nu/2\pi$ = 0.12 GHz) driven at various frequencies as a function of plasma density.

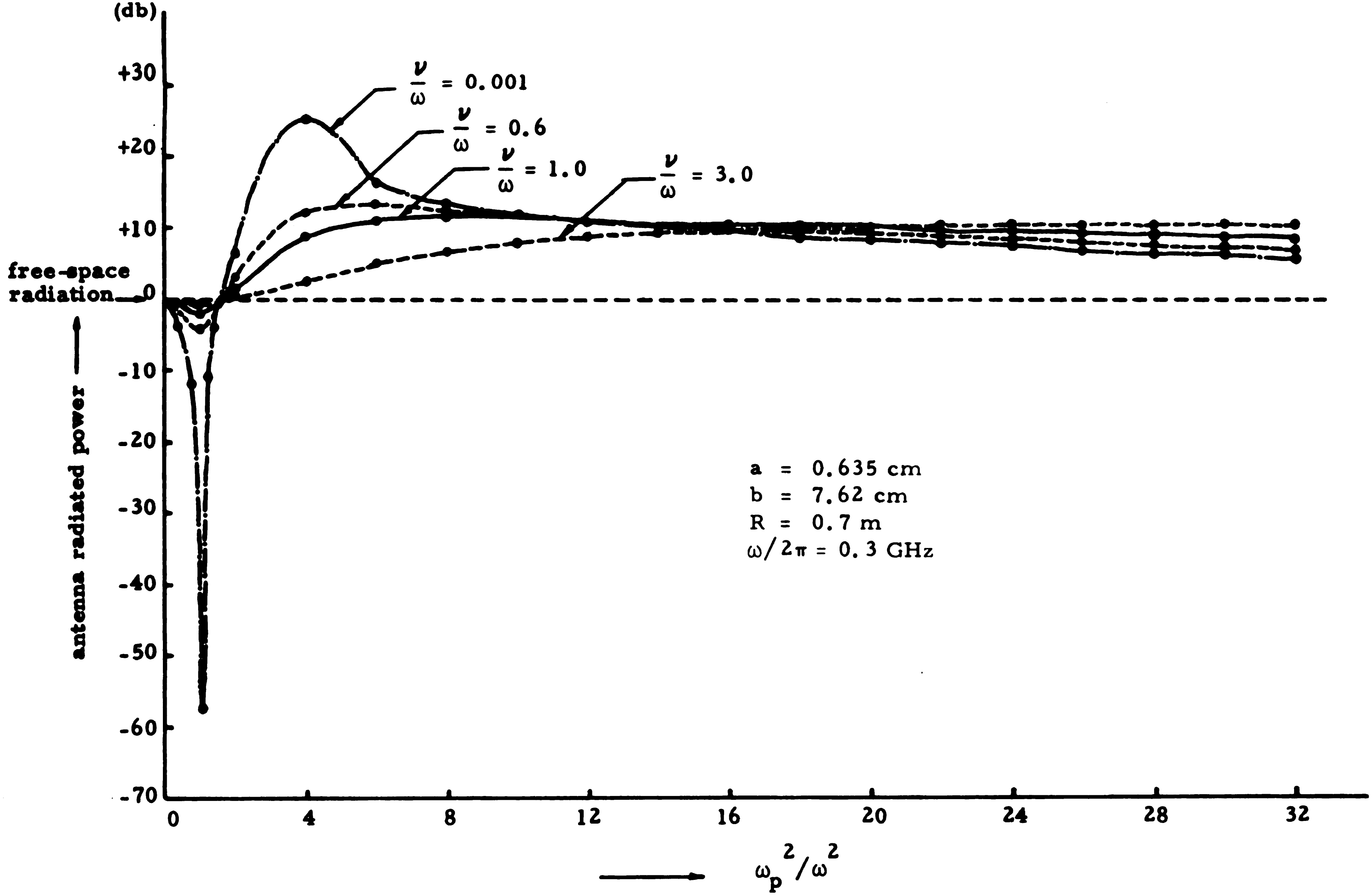

Fig. 2.5 **Effect of the electron collision frequency on the enhancement of antenna radiation.**

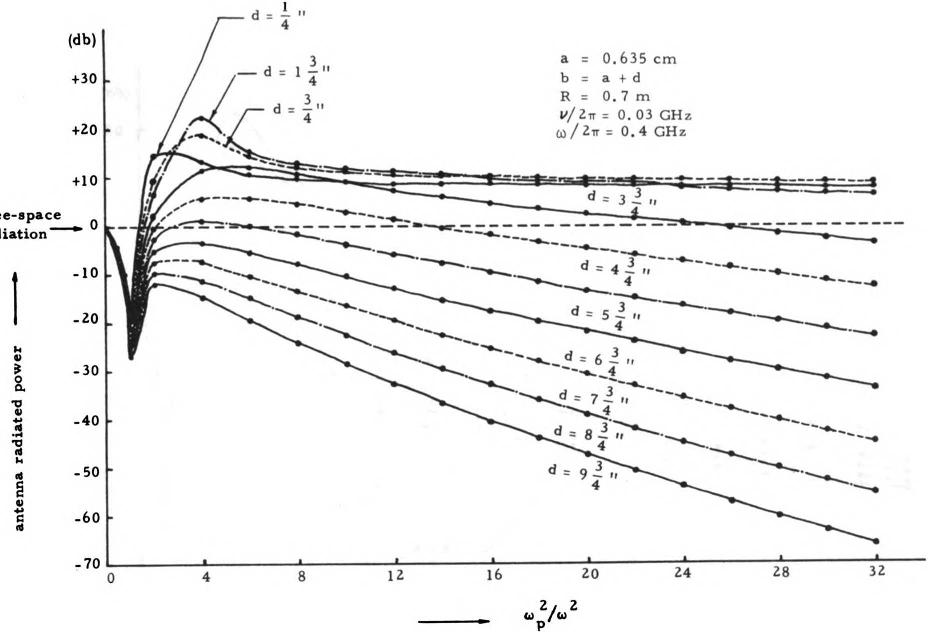

Fig. 2.6 Effect of the thickness (d) of plasma layer on the enhancement of antenna radiation.

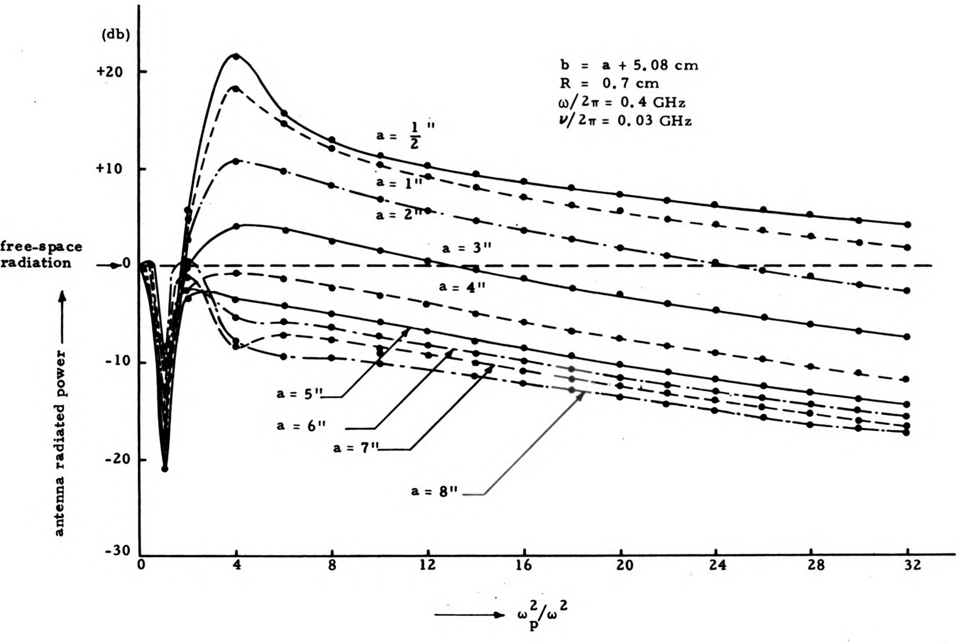

Fig. 2.7 Effect of the spherical antenna size on the enhancement of antenna radiation with a fixed thickness of plasma layer (d = 5.08 cm).

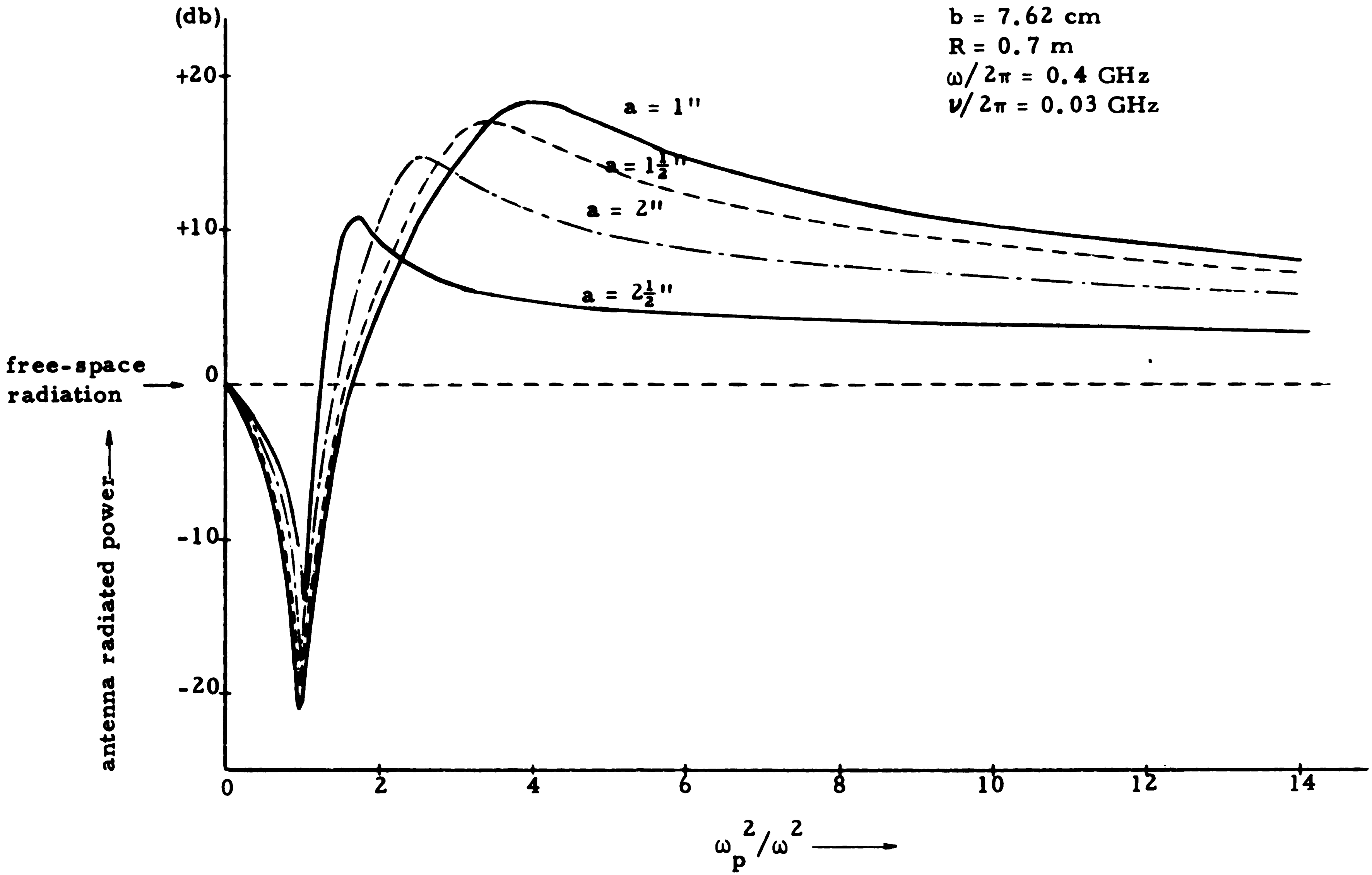

Fig. 2.8 Effect of the spherical antenna size on the enhancement of antenna radiation with a fixed radius of plasma layer (b = 7.62 cm).

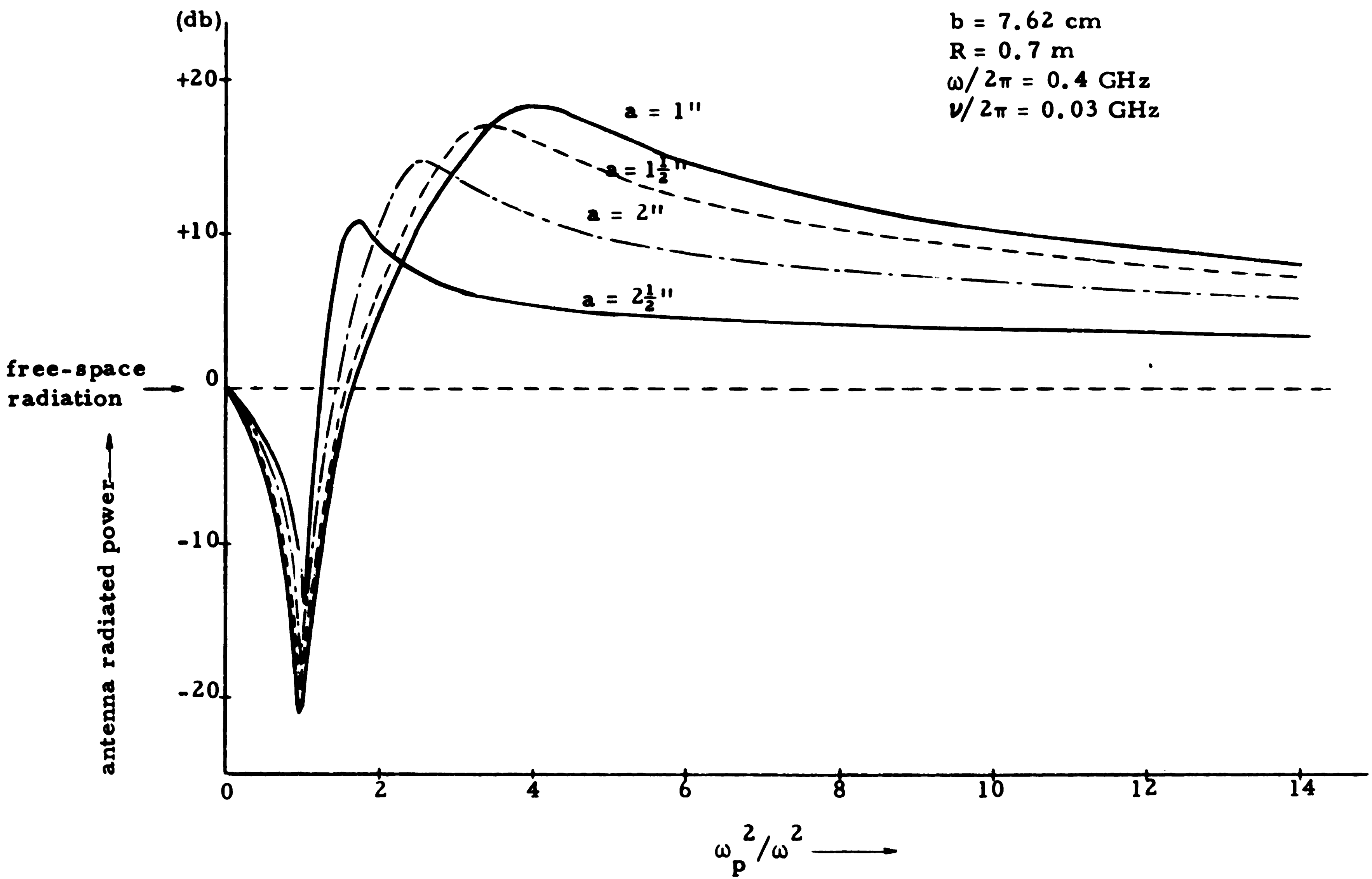

Fig. 2.8 Effect of the spherical antenna size on the enhancement of antenna radiation with a fixed radius of plasma layer (b = 7.62 cm).

CHAPTER 3

RADIATION FROM A SPHERICAL ANTENNA IMBEDDED IN A LOSSY, HOT PLASMA OF FINITE EXTENT

3.1 Introduction

In Chapter 2, a theory for a spherical antenna imbedded in a lossy, cold plasma of finite extent was developed. In this chapter, the surrounding plasma medium is allowed to have the temperature effect and the excitation of an electroacoustic wave within this medium. Another modification to the earlier analysis is to assume the existence of a dielectric coating surrounding the spherical antenna. As an idealized approximation the plasma sheath is regarded as a lossless dielectric coating which is perfectly rigid to the electroacoustic wave. While such a model is highly idealized, it does permit an analysis to be carried out in a relatively tractable manner.

A number of related investigations of the stated problem have been published recently. Wait[8] has studied theoretically a slotted-sphere antenna immersed in a lossy, hot plasma of infinite extent. Messiaen and Vandenplas[1] have investigated theoretically and experimentally on a spherical antenna imbedded in a lossless, cold plasma of finite extent. Both papers assumed the existence of a plasma sheath surrounding the sphere. Since the plasma layer surrounding the antenna of a reentry vehicle and the laboratory-produced plasma are hot, lossy and finite in nature, all these characteristics of the plasma including the plasma sheath are considered in the present study. Because the theoretical model used in the present study is somewhat different from the models used by previous investigators, quite different results are obtained.

Based on this theoretical analysis, a similar enhancement phenomenon on the antenna radiation as discussed in Chapter 1 has also been observed. In addition to this enhancement phenomenon, a series of resonance peaks on the antenna radiation has been found when the plasma layer is thin and the collision frequency of the plasma is low compared with the driving frequency. Also the resonance peaks and the enhancement phenomenon are effected by the thickness of plasma sheath. These two phenomena are carefully examined and extensive numerical results on the antenna radiation are obtained as a function of the antenna dimensions and plasma parameters.

3.2 Geometry and Statement of the Problem

The geometrical configuration is shown in Fig. 3.1 using a spherical coordinate system (r, θ, ϕ). A spherical antenna of radius a is covered by a rigid dielectric sheath whose outer surface

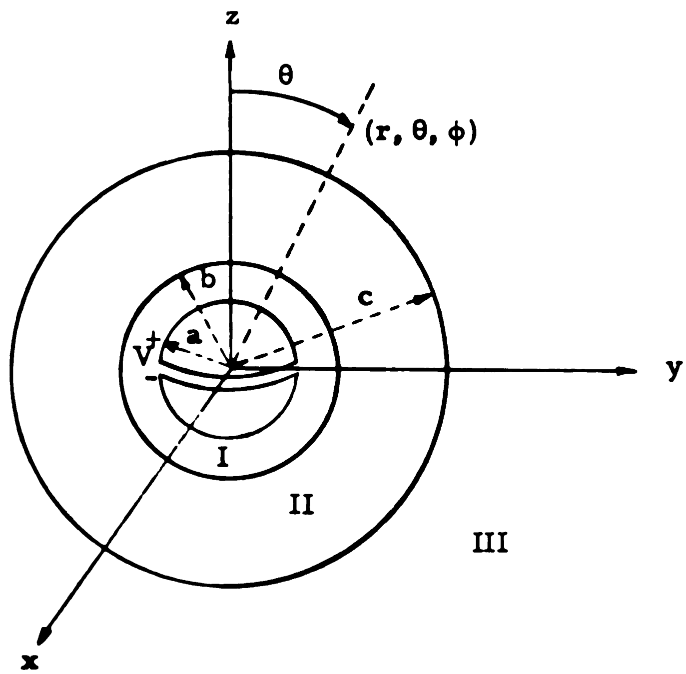

Region I: dielectric coating (μ_o, ϵ_d)

Region II: hot plasma

Region III: free space (μ_o, ϵ_o)

Fig. 3.1 A spherical antenna covered by a lossy, hot plasma layer.

is at r = b. The permittivity of this sheath is ϵ_d and the permeability is μ_o which is taken to be the same as that of the free space. Over the sheath, there is a spherical layer of uniform, lossy and hot plasma with a thickness of (c-b). The plasma is assumed to be a weakly ionized gas type and it can be regarded as a one-component electron fluid.

The spherical antenna is perfectly conducting except for a narrow equatorial gap between $\pi/2 - \theta_1 \leq \theta \leq \pi/2 + \theta_1$. Across this gap the antenna is driven by a constant voltage generator with a voltage of V and an angular frequency of ω. The total space excluding the antenna is divided into three regions. Region I is the dielectric coating (plasma sheath), Region II is the hot plasma layer and the rest of the free space is Region III.

In this study rationalized MKS units are used. The rotational symmetry and the infinitesimal driving gap are assumed. Furthermore, the time dependences for the radiating source and all the fields are assumed to be exp ($j\omega t$).

3.3 Fields in Dielectric Region (Plasma-Sheath Region)

The basic equations which govern Region I (dielectric layer, $a \leq r \leq b$) are Maxwell's equations,

$$\begin{cases} \nabla \times \vec{E}_1 = -j\omega\mu_o \vec{H}_1 & (3.1) \\ \nabla \times \vec{H}_1 = j\omega\epsilon_d \vec{E}_1 & (3.2) \end{cases}$$

where $\vec{E}$ and $\vec{H}$ are the electric and magnetic fields, μ_o is the permeability of free space, and ϵ_d is the permittivity of the dielectric medium. Following the procedures in Sec. 2.3, it is easy to obtain the solutions to Maxwell's equations in this region as

$$H_{1\phi}(r,\theta) = \frac{1}{\sqrt{r}} \sum_{n=1}^{\infty} P_n^1(\cos\theta)[A_n H_{n+\frac{1}{2}}^{(2)}(\beta_d r) + B_n H_{n+\frac{1}{2}}^{(1)}(\beta_d r)] \tag{3.3}$$

$$E_{1r}(r,\theta) = \frac{j}{\omega\epsilon_d r^{3/2}} \sum_{n=1}^{\infty} n(n+1)P_n(\cos\theta)[A_n H_{n+\frac{1}{2}}^{(2)}(\beta_d r) + B_n H_{n+\frac{1}{2}}^{(1)}(\beta_d r)] \tag{3.4}$$

$$E_{1\theta}(r,\theta) = \frac{-j}{\omega\epsilon_d r^{3/2}} \sum_{n=1}^{\infty} P_n^1(\cos\theta)\{A_n[nH_{n+\frac{1}{2}}^{(2)}(\beta_d r) - \beta_d r H_{n-\frac{1}{2}}^{(2)}(\beta_d r)] + B_n[nH_{n+\frac{1}{2}}^{(1)}(\beta_d r) - \beta_d r H_{n-\frac{1}{2}}^{(1)}(\beta_d r)]\} \tag{3.5}$$

and

$$E_{1\phi} = H_{1r} = H_{1\theta} = 0 \tag{3.6}$$

where A_n and B_n are arbitrary constants, n is a positive integer, $H_{n\pm\frac{1}{2}}^{(1)}(\beta_d r)$ and $H_{n\pm\frac{1}{2}}^{(2)}(\beta_d r)$ are the Hankel functions of the first and second kinds with order $n\pm\frac{1}{2}$, $P_n(\cos\theta)$ is the ordinary Legendre function, $P_n^1(\cos\theta)$ is the associated Legendre function of the first kind of order n and degree 1, and β_d is the wave number in this dielectric medium given by $\beta_d = \omega\sqrt{\mu_o\epsilon_d}$.

3.4 Fields in Hot-Plasma Region

In Region II (plasma layer, $b \leq r \leq c$), the plasma medium is regarded as a one-component electron fluid. That is, the ions are neglected in the equation of motion, yet their presence is required to neutralize electrically the plasma. The plasma is also assumed to be a weakly ionized gas having an average number density of electrons n_o which is regarded as constant in the plasma region. The density deviation of the electrons from the mean is denoted as n_1 and their mean induced velocity is $\vec{v}$. The collision frequency of electrons with neutral particles of the gas is ν.

In its unperturbed state the plasma is assumed to be homogeneous and neutral, and perturbation of the plasma due to the source is sufficiently small that the linearized equations are applicable. No static electric or magnetic field is present.

For harmonic time dependence of exp(jωt), the basic equations which govern this region are Maxwell's equations,

$$\nabla \times \vec{E}_2 = -j\omega\mu_o \vec{H}_2 \tag{3.7}$$

$$\nabla \times \vec{H}_2 = -e n_o \vec{v} + j\omega\epsilon_o \vec{E}_2 \tag{3.8}$$

$$\nabla \cdot \vec{E}_2 = -\frac{e n_1}{\epsilon_o} \tag{3.9}$$

$$\nabla \cdot \vec{H}_2 = 0 \tag{3.10}$$

and the linearized continuity and force equations,

$$n_o(\nabla \cdot \vec{v}) + j\omega n_1 = 0 \tag{3.11}$$

$$(\nu + j\omega)\vec{v} = -\frac{e}{m}\vec{E}_2 - \frac{v_o^2}{n_o}\nabla n_1 \tag{3.12}$$

where e and m are the magnitudes of charge and mass of electrons,

μ_o and ϵ_o are the permeability and permittivity of free space, and v_o is the r.m.s. velocity of electrons given by

$$v_o = \sqrt{\frac{3kT}{m}} \tag{3.13}$$

where k is Boltzmann's constant and T is the electron temperature.

It should be noted that the last term in Eq. (3.12) represents the force due to pressure gradient, and Eq. (3.13) is valid on the assumption of adiabatic pressure variation and one-dimensional compression[14]. The above set of equations was used by Chen[7], but in here the source is not included in this region.

In our formulation of the problem, there are four unknown fields $\vec{E}_2$, $\vec{H}_2$, n_1 and $\vec{v}$. We will determine $\vec{H}_2$ and n_1 first and then calculate $\vec{E}_2$ and $\vec{v}$. Taking curl of Eqs. (3.8) and (3.12), we obtain two expressions as

$$\nabla \times \nabla \times \vec{H}_2 = -e n_o \nabla \times \vec{v} + j\omega\epsilon_o \nabla \times \vec{E}_2 \tag{3.14}$$

$$\nabla \times \vec{v} = -\frac{e}{m(\nu + j\omega)} \nabla \times \vec{E}_2 \tag{3.15}$$

The substitution of Eqs. (3.15) and (3.7) in Eq. (3.14) gives

$$\nabla \times \nabla \times \vec{H}_2 = \omega^2 \mu_o \epsilon_o [1 + \frac{\omega_p^2}{j\omega(\nu + j\omega)}] \vec{H}_2 \tag{3.16}$$

where ω_p is the plasma frequency defined as $\omega_p^2 = \frac{n_o e^2}{m\epsilon_o}$. Using a vector identity of

$$\nabla \times \nabla \times \vec{H}_2 = \nabla(\nabla \cdot \vec{H}_2) - \nabla^2 \vec{H}_2 \tag{3.17}$$

and Eq. (3.10), Eq. (3.16) can be reduced to a homogeneous wave equation,

$$(\nabla^2 + k_e^2)\vec{H}_2 = 0 \qquad (3.18)$$

where k_e is the complex propagation constant of the electromagnetic wave given by

$$k_e^2 = \omega^2 \mu_o \xi \qquad (3.19)$$

where ξ is the equivalent complex permittivity defined as

$$\xi = \epsilon_o \left[1 + \frac{\omega_p^2}{j\omega(\nu + j\omega)}\right] = \epsilon_o \left[\left(1 - \frac{\omega_p^2}{\omega^2 + \nu^2}\right) - \frac{j\omega_p^2 \nu}{\omega(\omega^2 + \nu^2)}\right]. \qquad (3.20)$$

If we write

$$k_e = \beta_e - j\alpha_e , \qquad (3.21)$$

β_e and α_e can be expressed as

$$\beta_e = \frac{\beta_o}{\sqrt{2}} \left\{1 - \frac{\omega_p^2}{\omega^2 + \nu^2} + \left[1 - \frac{2\omega_p^2}{\omega^2 + \nu^2} + \frac{\omega_p^4}{\omega^2(\omega^2 + \nu^2)}\right]^{\frac{1}{2}}\right\}^{\frac{1}{2}} \qquad (3.22)$$

$$\alpha_e = \frac{\beta_o}{\sqrt{2}} \left\{-1 + \frac{\omega_p^2}{\omega^2 + \nu^2} + \left[1 - \frac{2\omega_p^2}{\omega^2 + \nu^2} + \frac{\omega_p^4}{\omega^2(\omega^2 + \nu^2)}\right]^{\frac{1}{2}}\right\}^{\frac{1}{2}} . \qquad (3.23)$$

β_e and α_e are the wave number and attenuation constant of the electromagnetic wave in this plasma medium, and β_o is the wave number in free space defined as $\beta_o = \omega\sqrt{\mu_o \epsilon_o}$.

From the symmetry of the antenna it can be seen that there is no variation in the ϕ direction, i.e., $\frac{\partial}{\partial\phi} = 0$ and the magnetic field has only a ϕ component. Thus the Laplacian of the vector magnetic field in spherical coordinates can be expressed(15) as

$$\nabla^2 \vec{H}_2 = \hat{\phi}\left(\nabla^2 H_{2\phi} - \frac{1}{r^2}\csc^2\theta\, H_{2\phi}\right)$$

$$= \hat{\phi}\left[\frac{1}{r^2}\frac{\partial}{\partial r}\left(r^2\frac{\partial H_{2\phi}}{\partial r}\right) + \frac{1}{r^2\sin\theta}\frac{\partial}{\partial\theta}\left(\sin\theta\frac{\partial H_{2\phi}}{\partial\theta}\right) - \frac{1}{r^2}\csc^2\theta\, H_{2\phi}\right] \tag{3.24}$$

where $\hat{\phi}$ is the unit vector in ϕ direction. Two identities can be obtained through differentiation. They are

$$\frac{\partial}{\partial r}\left(r^2\frac{\partial H_{2\phi}}{\partial r}\right) = r\frac{\partial^2}{\partial r^2}(r H_{2\phi}) \tag{3.25}$$

$$\frac{1}{\sin\theta}\frac{\partial}{\partial\theta}\left(\sin\theta\frac{\partial H_{2\phi}}{\partial\theta}\right) - \csc^2\theta\, H_{2\phi} = \frac{\partial}{\partial\theta}\left[\frac{1}{\sin\theta}\frac{\partial}{\partial\theta}(\sin\theta\, H_{2\phi})\right]$$

$$= \frac{\partial^2 H_{2\phi}}{\partial\theta^2} + \cot\theta\frac{\partial H_{2\phi}}{\partial\theta} - \csc^2\theta\, H_{2\phi} \tag{3.26}$$

The substitution of Eqs. (3.24), (3.25) and (3.26) in Eq. (3.18) leads to a partial differential equation,

$$\frac{\partial^2}{\partial r^2}(rH_{2\phi}) + \frac{1}{r^2}\frac{\partial}{\partial\theta}\left[\frac{1}{\sin\theta}\frac{\partial}{\partial\theta}(\sin\theta\, r H_{2\phi})\right] + k_e^2(rH_{2\phi}) = 0 \tag{3.27}$$

which is exactly in the same form as Eq. (2.7). The solution to Eq. (3.27) can then be obtained as

$$H_{2\phi}(r,\theta) = \frac{1}{\sqrt{r}} \sum_{n=1}^{\infty} P_n^1(\cos\theta)\,[\, C_n H_{n+\frac{1}{2}}^{(2)}(k_e r) + D_n H_{n+\frac{1}{2}}^{(1)}(k_e r)\,]. \quad (3.28)$$

The magnetic field is thus determined and n_1 is the next quantity to be determined.

Taking the divergence of Eq. (3.12), we have

$$(\nu + j\omega)\nabla\cdot\vec{v} = -\frac{e}{m}\nabla\cdot\vec{E}_2 - \frac{v_o^2}{n_o}\nabla^2 n_1 . \quad (3.29)$$

From the continuity equation (3.11), it gives

$$\nabla\cdot\vec{v} = -\frac{j\omega n_1}{n_o} . \quad (3.30)$$

Substituting Eqs. (3.30) and (3.9) into Eq. (3.29), we obtain another homogeneous wave equation,

$$(\nabla^2 + k_p^2)n_1 = 0 \quad (3.31)$$

where k_p is the complex propagation constant of the plasma or electroacoustic wave expressed by

$$k_p^2 = \frac{1}{v_o^2}[(\omega^2 - \omega_p^2) - j\omega\nu]. \quad (3.32)$$

If we write

$$k_p = \beta_p - j\alpha_p , \quad (3.33)$$

β_p and α_p can be expressed as

$$\beta_p = \frac{1}{\sqrt{2}\, v_o} \{\omega^2 - \omega_p^2 + [(\omega^2 - \omega_p^2)^2 + \omega^2 \nu^2]^{\frac{1}{2}}\}^{\frac{1}{2}} \tag{3.34}$$

$$\alpha_p = \frac{1}{\sqrt{2}\, v_o} \{-\omega^2 + \omega_p^2 + [(\omega^2 - \omega_p^2)^2 + \omega^2 \nu^2]^{\frac{1}{2}}\}^{\frac{1}{2}} . \tag{3.35}$$

β_p and α_p are the wave number and attenuation constant of the electroacoustic wave in this plasma medium. Due to rotational symmetry, the Laplacian of the scalar field n_1 in spherical coordinates can be expressed as

$$\nabla^2 n_1 = \frac{1}{r^2} \frac{\partial}{\partial r} (r^2 \frac{\partial n_1}{\partial r}) + \frac{1}{r^2 \sin\theta} \frac{\partial}{\partial \theta} (\sin\theta \frac{\partial n_1}{\partial \theta}) . \tag{3.36}$$

Using Eqs. (3.36) and (3.25), Eq. (3.31) can be reduced to a partial differential equation,

$$\frac{\partial^2}{\partial r^2} (rn_1) + \frac{1}{r^2} \frac{1}{\sin\theta} \frac{\partial}{\partial \theta} [\sin\theta \frac{\partial}{\partial \theta} (rn_1)] + k_p^2 (rn_1) = 0 . \tag{3.37}$$

Equation (3.37) is similar to Eq. (2.7) but not identical in form. To solve Eq. (3.37), we employ the method of the separation of variables. Since n_1 is independent of ϕ, we can assume

$$rn_1 = R(r)\Theta(\theta) \tag{3.38}$$

where R is a function of r alone and Θ is a function of θ only. The substitution of Eq. (3.38) in Eq. (3.37) leads to

$$\frac{r^2}{R} \frac{d^2 R}{dr^2} + k_p^2 r^2 = - \frac{1}{\Theta} \frac{1}{\sin\theta} \frac{d}{d\theta} (\sin\theta \frac{d\Theta}{d\theta}) = n(n+1) \tag{3.39}$$

where n is any integer and n(n+1) is the separation constant. Equation (3.39) generates two ordinary differential equations,

$$\frac{1}{\sin\theta}\frac{d}{d\theta}\left(\sin\theta\frac{d\Theta}{d\theta}\right) + n(n+1)\Theta = 0 \tag{3.40}$$

$$\frac{r^2}{R}\frac{d^2R}{dr^2} + k_p^2 r^2 - n(n+1) = 0 \quad . \tag{3.41}$$

Let us consider Eq. (3.40) first. Making the substitutions,

$$u = \cos\theta \,, \quad \sqrt{1-u^2} = \sin\theta \,, \quad \frac{d}{d\theta} = -\sqrt{1-u^2}\frac{d}{du} \,,$$

Eq. (3.40) can be reduced to

$$(1-u^2)\frac{d^2\Theta}{du^2} - 2u\frac{d\Theta}{du} + n(n+1)\Theta = 0. \tag{3.42}$$

Equation (3.42) is a standard form of the ordinary Legendre's equation. A solution to this equation can be obtained as

$$\Theta = P_n(u) = P_n(\cos\theta) \tag{3.43}$$

where n must be a positive integer and $n \geq 0$. Note that only one solution for this second-order differential equation (3.42) has been considered. The other solution becomes infinite on the axis, and so it should be excluded from this problem since the axis is included in the geometry.

Since Eq. (3.41) is exactly in the same form as Eq. (2.16), its solution can be easily written as

$$R = \sqrt{r}\,[E_n H^{(2)}_{n+\frac{1}{2}}(k_p r) + F_n H^{(1)}_{n+\frac{1}{2}}(k_p r)] \tag{3.44}$$

where E_n and F_n are arbitrary constants. Combining Eqs. (3.38), (3.43) and (3.44) we have

$$n_1 = \frac{1}{\sqrt{r}} \sum_{n=0}^{\infty} P_n(\cos\theta)[\,E_n H^{(2)}_{n+\frac{1}{2}}(k_p r) + F_n H^{(1)}_{n+\frac{1}{2}}(k_p r)] \,. \qquad (3.45)$$

Now $\vec{H}_2$ and n_1 have been determined explicitly from Eqs. (3.28) and (3.45). We now aim to express $\vec{E}_2$ and $\vec{v}$ in terms of these two known quantities. From Eq. (3.12) we have

$$\vec{v} = \frac{-e}{m(\nu + j\omega)}\, \vec{E}_2 - \frac{v_o^2}{n_o(\nu + j\omega)}\, \nabla n_1 \,. \qquad (3.46)$$

The substitution of Eq. (3.46) in Eq. (3.8) leads to

$$\vec{E}_2 = \frac{1}{j\omega\xi}\, \nabla \times \vec{H}_2 + \frac{j e v_o^2}{\omega \xi\, (\nu + j\omega)}\, \nabla n_1 \qquad (3.47)$$

where ξ is given in Eq. (3.20). The substitution of Eq. (3.47) in Eq. (3.46) gives

$$\vec{v} = \frac{-e}{m(\nu+j\omega)}\, \frac{1}{j\omega\xi}\, \nabla \times \vec{H}_2 - \frac{v_o^2 \epsilon_o}{n_o \xi(\nu+j\omega)}\, \nabla n_1 \,. \qquad (3.48)$$

Under rotational symmetry two vector differential operations in spherical coordinates can be expressed as

$$\nabla \times \vec{H}_2 = \hat{r}\, \frac{1}{r \sin\theta}\, \frac{\partial}{\partial\theta}\, (\sin\theta\, H_{2\phi}) - \hat{\theta}\, \frac{1}{r}\, \frac{\partial}{\partial r}\, (r H_{2\phi}) \qquad (3.49)$$

$$\nabla n_1 = \hat{r}\, \frac{\partial n_1}{\partial r} + \hat{\theta}\, \frac{1}{r}\, \frac{\partial n_1}{\partial \theta} \qquad (3.50)$$

where $\hat{r}$ and $\hat{\theta}$ are unit vectors in r and θ directions. Combining Eqs. (3.47) to (3.50), we obtain

$$E_{2r} = \frac{1}{j\omega\xi}\,\frac{1}{r\sin\theta}\,\frac{\partial}{\partial\theta}\,(\sin\theta\, H_{2\phi}) + \frac{j\,e\,v_o^2}{\omega\xi(\nu+j\omega)}\,\frac{\partial n_1}{\partial r} \tag{3.51}$$

$$E_{2\theta} = \frac{-1}{j\omega\xi}\,\frac{1}{r}\,\frac{\partial}{\partial r}\,(r\,H_{2\phi}) + \frac{j\,e\,v_o^2}{\omega\xi(\nu+j\omega)}\,\frac{1}{r}\,\frac{\partial n_1}{\partial\theta} \tag{3.52}$$

$$v_r = \frac{-e}{m(\nu+j\omega)}\,\frac{1}{j\omega\xi}\,\frac{1}{r\sin\theta}\,\frac{\partial}{\partial\theta}\,(\sin\theta\, H_{2\phi}) - \frac{v_o^2\epsilon_o}{n_o\xi(\nu+j\omega)}\,\frac{\partial n_1}{\partial r} \tag{3.53}$$

$$v_\theta = \frac{e}{m(\nu+j\omega)}\,\frac{1}{j\omega\xi}\,\frac{1}{r}\,\frac{\partial}{\partial r}\,(r\,H_{2\phi}) - \frac{v_o^2\epsilon_o}{n_o\xi(\nu+j\omega)}\,\frac{1}{r}\,\frac{\partial n_1}{\partial\theta}\;. \tag{3.54}$$

Using Eqs. (2.34), (2.35) and (3.45) we obtain

$$\frac{\partial n_1}{\partial r} = \frac{-1}{r^{3/2}}\sum_{n=0}^{\infty} P_n(\cos\theta)\{E_n[(n+1)H^{(2)}_{n+\frac{1}{2}}(k_p r) - k_p r\,H^{(2)}_{n-\frac{1}{2}}(k_p r)] + F_n[(n+1)H^{(1)}_{n+\frac{1}{2}}(k_p r) - k_p r\,H^{(1)}_{n-\frac{1}{2}}(k_p r)]\}. \tag{3.55}$$

Using Eqs. (2.25) and (3.45) we have

$$\frac{\partial n_1}{\partial\theta} = \frac{1}{\sqrt{r}}\sum_{n=1}^{\infty} P_n^1(\cos\theta)\,[E_n H^{(2)}_{n+\frac{1}{2}}(k_p r) + F_n H^{(1)}_{n+\frac{1}{2}}(k_p r)] \tag{3.56}$$

because for n=0, $P_o^1(\cos\theta) = 0$. It is noted that the first terms on the right-hand side of Eqs. (3.51) to (3.54) can be obtained easily following the same procedures in Sec. 2.3 while the second terms on the right-hand side can be obtained by using Eqs. (3.55) and (3.56). Since we are interested in $E_{2\theta}$ and v_r for the later development, only Eqs. (3.52) and (3.53) are expressed more explicitly as follows:

$$E_{2\theta}(r,\theta) = \frac{-j}{\omega\xi r^{3/2}} \sum_{n=1}^{\infty} P_n^1(\cos\theta)\{C_n[\,nH^{(2)}_{n+\frac{1}{2}}(k_e r) - k_e r H^{(2)}_{n-\frac{1}{2}}(k_e r)]$$

$$+ D_n[\,n H^{(1)}_{n+\frac{1}{2}}(k_e r) - k_e r H^{(1)}_{n-\frac{1}{2}}(k_e r)]\,\}$$

$$+ \frac{j e v_o^2}{\omega\xi(\nu + j\omega) r^{3/2}} \sum_{n=1}^{\infty} P_n^1(\cos\theta)\,[E_n H^{(2)}_{n+\frac{1}{2}}(k_p r) + F_n H^{(1)}_{n+\frac{1}{2}}(k_p r)] \tag{3.57}$$

$$v_r(r,\theta) = \frac{-e}{m(\nu+j\omega)} \frac{j}{\omega\xi r^{3/2}} \sum_{n=1}^{\infty} n(n+1) P_n(\cos\theta)\,[C_n H^{(2)}_{n+\frac{1}{2}}(k_e r)$$

$$+ D_n H^{(1)}_{n+\frac{1}{2}}(k_e r)]$$

$$+ \frac{v_o^2 \epsilon_o}{n_o \xi(\nu + j\omega) r^{3/2}} \sum_{n=0}^{\infty} P_n(\cos\theta)\{E_n[\,(n+1) H^{(2)}_{n+\frac{1}{2}}(k_p r) - k_p r H^{(2)}_{n-\frac{1}{2}}(k_p r)]$$

$$+ F_n[\,(n+1) H^{(1)}_{n+\frac{1}{2}}(k_p r) - k_p r H^{(1)}_{n-\frac{1}{2}}(k_p r)]\,\}\ . \tag{3.58}$$

3.5 Fields in Free-Space Region

The basic equations which govern Region III (free space, $r \geq c$) are Maxwell's equations,

$$\begin{cases} \nabla \times \vec{E}_3 = -j\omega\mu_o \vec{H}_3 & (3.59) \\ \nabla \times \vec{H}_3 = j\omega\epsilon_o \vec{E}_3\ . & (3.60) \end{cases}$$

Since Region III is unbounded, no reflected or inward traveling wave exists in this region. Following the same analysis as in Sec. 2.3, the solutions to Maxwell's equations in this region can be written as

$$H_{3\phi}(r,\theta) = \frac{1}{\sqrt{r}} \sum_{n=1}^{\infty} G_n P_n^1(\cos\theta) H_{n+\frac{1}{2}}^{(2)}(\beta_o r) \tag{3.61}$$

$$E_{3r}(r,\theta) = \frac{j}{\omega\epsilon_o r^{3/2}} \sum_{n=1}^{\infty} G_n n(n+1) P_n(\cos\theta) H_{n+\frac{1}{2}}^{(2)}(\beta_o r) \tag{3.62}$$

$$E_{3\theta}(r,\theta) = \frac{-j}{\omega\epsilon_o r^{3/2}} \sum_{n=1}^{\infty} G_n P_n^1(\cos\theta)\left[n H_{n+\frac{1}{2}}^{(2)}(\beta_o r) - \beta_o r H_{n-\frac{1}{2}}^{(2)}(\beta_o r)\right] \tag{3.63}$$

and

$$E_{3\phi} = H_{3r} = H_{3\theta} = 0 \tag{3.64}$$

where G_n is an arbitrary constant and n is a positive integer.

3.6 Matching of Boundary Conditions at Interfaces

In order to determine the arbitrary constants A_n, B_n, C_n, D_n, E_n, F_n and G_n, the boundary conditions at $r = a$, $r = b$ and $r = c$ are applied.

Following the same procedures of Sec. 2.5 in matching the boundary condition on the antenna surface ($r = a$), we can obtain easily an expression as

$$M_1 A_n + M_2 B_n = M_3 V \tag{3.65}$$

where

$$M_1 = n H_{n+\frac{1}{2}}^{(2)}(\beta_d a) - \beta_d a H_{n-\frac{1}{2}}^{(2)}(\beta_d a)$$

$$M_2 = n H_{n+\frac{1}{2}}^{(1)}(\beta_d a) - \beta_d a\, H_{n-\frac{1}{2}}^{(1)}(\beta_d a)$$

$$M_3 = j\omega\epsilon_d \sqrt{a}\; P_n^1(0) \frac{2n+1}{2n(n+1)} \quad .$$

The continuity of the tangential components of $\vec{E}$ and $\vec{H}$ fields at the dielectric-plasma interface (r = b) is

$$E_{1\theta}(b,\theta) = E_{2\theta}(b,\theta) \tag{3.66}$$

$$H_{1\phi}(b,\theta) = H_{2\phi}(b,\theta)\ . \tag{3.67}$$

Using Eqs. (3.5) and (3.57), Eq. (3.66) gives

$$M_4A_n + M_5B_n + M_6C_n + M_7D_n + M_8E_n + M_9F_n = 0 \tag{3.68}$$

where

$$M_4 = \frac{\xi}{\epsilon_d}\left[nH^{(2)}_{n+\frac{1}{2}}(\beta_d b) - \beta_d b H^{(2)}_{n-\frac{1}{2}}(\beta_d b)\right]$$

$$M_5 = \frac{\xi}{\epsilon_d}\left[nH^{(1)}_{n+\frac{1}{2}}(\beta_d b) - \beta_d b H^{(1)}_{n-\frac{1}{2}}(\beta_d b)\right]$$

$$M_6 = -\left[nH^{(2)}_{n+\frac{1}{2}}(k_e b) - k_e b H^{(2)}_{n-\frac{1}{2}}(k_e b)\right]$$

$$M_7 = -\left[nH^{(1)}_{n+\frac{1}{2}}(k_e b) - k_e b H^{(1)}_{n-\frac{1}{2}}(k_e b)\right]$$

$$M_8 = \frac{e v_o^2}{\nu + j\omega} H^{(2)}_{n+\frac{1}{2}}(k_p b)$$

$$M_9 = \frac{e v_o^2}{\nu + j\omega} H^{(1)}_{n+\frac{1}{2}}(k_p b)\ .$$

From Eqs. (3.3) and (3.28), Eq. (3.67) can be expressed as

$$M_{10}A_n + M_{11}B_n + M_{12}C_n + M_{13}D_n = 0 \tag{3.69}$$

where

$$M_{10} = H^{(2)}_{n+\frac{1}{2}}(\beta_d b)$$

$$M_{11} = H^{(1)}_{n+\frac{1}{2}}(\beta_d b)$$

$$M_{12} = -H^{(2)}_{n+\frac{1}{2}}(k_e b)$$

$$M_{13} = -H^{(1)}_{n+\frac{1}{2}}(k_e b) .$$

The continuity of the tangential components of $\vec{E}$ and $\vec{H}$ fields at the plasma-free space interface (r = c) leads to

$$E_{2\theta}(c, \theta) = E_{3\theta}(c, \theta) \tag{3.70}$$

$$H_{2\phi}(c, \theta) = H_{3\phi}(c, \theta) \tag{3.71}$$

Using Eqs. (3.57) and (3.63), Eq. (3.70) gives

$$M_{14}C_n + M_{15}D_n + M_{16}E_n + M_{17}F_n + M_{18}G_n = 0 \tag{3.72}$$

where

$$M_{14} = -[\, nH^{(2)}_{n+\frac{1}{2}}(k_e c) - k_e c H^{(2)}_{n-\frac{1}{2}}(k_e c)]$$

$$M_{15} = -[\, nH^{(1)}_{n+\frac{1}{2}}(k_e c) - k_e c H^{(1)}_{n-\frac{1}{2}}(k_e c)]$$

$$M_{16} = \frac{ev_o^2}{\nu + j\omega} H^{(2)}_{n+\frac{1}{2}}(k_p c)$$

$$M_{17} = \frac{ev_o^2}{\nu + j\omega} H^{(1)}_{n+\frac{1}{2}}(k_p c)$$

$$M_{18} = \frac{\xi}{\epsilon_o} [\, nH^{(2)}_{n+\frac{1}{2}}(\beta_o c) - \beta_o c H^{(2)}_{n-\frac{1}{2}}(\beta_o c)] .$$

From Eqs. (3.28) and (3.61), Eq. (3.71) can be expressed as

$$M_{19}C_n + M_{20}D_n + M_{21}G_n = 0 \tag{3.73}$$

where

$$M_{19} = H^{(2)}_{n+\frac{1}{2}}(k_e c)$$

$$M_{20} = H^{(1)}_{n+\frac{1}{2}}(k_e c)$$

$$M_{21} = - H^{(2)}_{n+\frac{1}{2}}(\beta_o c) \ .$$

In the present analysis, it is assumed that the normal component of the mean electron velocity vanishes at the interfaces at $r = b$ and $r = c$. These rigid boundary conditions require that

$$v_r(b, \theta) = 0 \tag{3.74}$$

and

$$v_r(c, \theta) = 0 \ . \tag{3.75}$$

Using Eq. (3.58), Eq. (3.74) gives

$$M_{22}C_n + M_{23}D_n + M_{24}E_n + M_{25}F_n = 0 \tag{3.76}$$

where

$$M_{22} = n(n+1)\frac{\omega_p}{\omega} H^{(2)}_{n+\frac{1}{2}}(k_e b)$$

$$M_{23} = n(n+1)\frac{\omega_p}{\omega} H^{(1)}_{n+\frac{1}{2}}(k_e b)$$

$$M_{24} = j e v_o^2 \left[(n+1) H^{(2)}_{n+\frac{1}{2}}(k_p b) - k_p b H^{(2)}_{n-\frac{1}{2}}(k_p b) \right]$$

$$M_{25} = j e v_o^2 \left[(n+1) H^{(1)}_{n+\frac{1}{2}}(k_p b) - k_p b H^{(1)}_{n-\frac{1}{2}}(k_p b) \right] .$$

Similarly from Eqs. (3.58) and (3.75) we obtain

$$M_{26}C_n + M_{27}D_n + M_{28}E_n + M_{29}F_n = 0 \tag{3.77}$$

$$M_{26} = n(n+1)\frac{\omega_p}{\omega}\; H^{(2)}_{n+\frac{1}{2}}(k_e c)$$

$$M_{27} = n(n+1)\frac{\omega_p}{\omega}\; H^{(1)}_{n+\frac{1}{2}}(k_e c)$$

$$M_{28} = j e v_o^2 \left[(n+1) H^{(2)}_{n+\frac{1}{2}}(k_p c) - k_p c H^{(2)}_{n-\frac{1}{2}}(k_p c) \right]$$

$$M_{29} = j e v_o^2 \left[(n+1) H^{(1)}_{n+\frac{1}{2}}(k_p c) - k_p c H^{(1)}_{n-\frac{1}{2}}(k_p c) \right].$$

It should be noted that the summation of the first term on the right-hand side of Eq. (3.58) can be changed from $\sum_{n=1}^{\infty}$ to $\sum_{n=o}^{\infty}$ because the $n = 0$ term makes no contribution to the series. Thus we can equate the two series in Eq. (3.58) to yield Eqs. (3.76) and (3.77) by using the rigid boundary conditions imposed by Eqs. (3.74) and (3.75). Furthermore, the notations for the coefficients M_i, $i = 1, 2, \ldots, 28, 29$, are used merely for convenience.

By matching the boundary conditions on the interfaces, we end up with seven algebraic equations for seven unknowns. For convenience, the matrix representation for these equations is used. Combining these equations, we can form a matrix equation as

$$[M] \begin{bmatrix} A_n \\ B_n \\ C_n \\ D_n \\ E_n \\ F_n \\ G_n \end{bmatrix} = \begin{bmatrix} M_3 V \\ 0 \\ 0 \\ 0 \\ 0 \\ 0 \\ 0 \end{bmatrix} \qquad (3.78)$$

where [M] is the matrix which can be expressed as

$$[M] = \begin{bmatrix} M_1 & M_2 & 0 & 0 & 0 & 0 & 0 \\ M_4 & M_5 & M_6 & M_7 & M_8 & M_9 & 0 \\ M_{10} & M_{11} & M_{12} & M_{13} & 0 & 0 & 0 \\ 0 & 0 & M_{14} & M_{15} & M_{16} & M_{17} & M_{18} \\ 0 & 0 & M_{19} & M_{20} & 0 & 0 & M_{21} \\ 0 & 0 & M_{22} & M_{23} & M_{24} & M_{25} & 0 \\ 0 & 0 & M_{26} & M_{27} & M_{28} & M_{29} & 0 \end{bmatrix} . \tag{3.79}$$

From Eq. (3.78) we obtain the arbitrary constants as

$$\begin{bmatrix} A_n \\ B_n \\ C_n \\ D_n \\ E_n \\ F_n \\ G_n \end{bmatrix} = [M]^{-1} \begin{bmatrix} M_3 V \\ 0 \\ 0 \\ 0 \\ 0 \\ 0 \\ 0 \end{bmatrix} \tag{3.80}$$

where $[M]^{-1}$ is the inverse matrix of [M].

Up to this point all the fields in Regions I, II, and III are completely determined as functions of r and θ.

The determination of the arbitrary constants A_n, B_n, . . ., G_n can be done from Eq. (3.80) by getting the inverse matrix $[M]^{-1}$ through ordinary determinant operation or numerical calculation using a computer.

3.7 Radiated Field in Free-Space Region

Since our main interest in this study is the radiated field in the free-space region, we determine the arbitrary constant G_n only. In order to determine G_n, the ordinary determinant method is employed. From the seven algebraic equations in the last section we can form

$$G_n = \frac{\Delta_2}{\Delta_1} \tag{3.81}$$

where Δ_1 and Δ_2 represent for two determinants as follows:

$$\Delta_1 = \begin{vmatrix} M_1 & M_2 & 0 & 0 & 0 & 0 & 0 \\ M_4 & M_5 & M_6 & M_7 & M_8 & M_9 & 0 \\ M_{10} & M_{11} & M_{12} & M_{13} & 0 & 0 & 0 \\ 0 & 0 & M_{14} & M_{15} & M_{16} & M_{17} & M_{18} \\ 0 & 0 & M_{19} & M_{20} & 0 & 0 & M_{21} \\ 0 & 0 & M_{22} & M_{23} & M_{24} & M_{25} & 0 \\ 0 & 0 & M_{26} & M_{27} & M_{28} & M_{29} & 0 \end{vmatrix}$$

$$\Delta_2 = \begin{vmatrix} M_1 & M_2 & 0 & 0 & 0 & 0 & M_3 V \\ M_4 & M_5 & M_6 & M_7 & M_8 & M_9 & 0 \\ M_{10} & M_{11} & M_{12} & M_{13} & 0 & 0 & 0 \\ 0 & 0 & M_{14} & M_{15} & M_{16} & M_{17} & 0 \\ 0 & 0 & M_{19} & M_{20} & 0 & 0 & 0 \\ 0 & 0 & M_{22} & M_{23} & M_{24} & M_{25} & 0 \\ 0 & 0 & M_{26} & M_{27} & M_{28} & M_{29} & 0 \end{vmatrix} .$$

After some steps of determinant operation, Δ_1 and Δ_2 can be expressed as

$$\Delta_1 = M_{21}(M_2M_{10} - M_1M_{11})\Delta_4 \tag{3.82}$$

$$\Delta_2 = V\,M_3M_{19}(M_5M_{10} - M_4M_{11})\Delta_3 \tag{3.83}$$

where

$$\Delta_3 = (M_{15} - \frac{M_{14}M_{20}}{M_{19}})(M_{24}M_{29} - M_{25}M_{28})$$

$$- (M_{23} - \frac{M_{22}M_{20}}{M_{19}})(M_{16}M_{29} - M_{17}M_{28})$$

$$+ (M_{27} - \frac{M_{26}M_{20}}{M_{19}})(M_{16}M_{25} - M_{17}M_{24})$$

$$\Delta_4 = \left[M_6 - \frac{M_{12}(M_1M_5 - M_4M_2)}{M_1M_{11} - M_{10}M_2}\right]\Delta_5 - \left[M_7 - \frac{M_{13}(M_1M_5 - M_4M_2)}{M_1M_{11} - M_{10}M_2}\right]\Delta_6$$

$$+ M_8\Delta_7 - M_9\Delta_8$$

and

$$\Delta_5 = (M_{15} - \frac{M_{20}M_{18}}{M_{21}})(M_{24}M_{29} - M_{25}M_{28}) - M_{16}(M_{23}M_{29} - M_{25}M_{27})$$

$$+ M_{17}(M_{23}M_{28} - M_{24}M_{27})$$

$$\Delta_6 = (M_{14} - \frac{M_{19}M_{18}}{M_{21}})(M_{24}M_{29} - M_{25}M_{28}) - M_{16}(M_{22}M_{29} - M_{25}M_{26})$$

$$+ M_{17}(M_{22}M_{28} - M_{24}M_{26})$$

$$\Delta_7 = (M_{14} - \frac{M_{19}M_{18}}{M_{21}})(M_{23}M_{29} - M_{25}M_{27}) + M_{17}(M_{22}M_{27} - M_{23}M_{26})$$

$$- (M_{15} - \frac{M_{20}M_{18}}{M_{21}})(M_{22}M_{29} - M_{25}M_{26})$$

$$\Delta_8 = (M_{14} - \frac{M_{19}M_{18}}{M_{21}})(M_{23}M_{28} - M_{24}M_{27}) + M_{16}(M_{22}M_{27} - M_{23}M_{26})$$

$$- (M_{15} - \frac{M_{20}M_{18}}{M_{21}})(M_{22}M_{28} - M_{24}M_{26}) \; .$$

Combining Eqs. (3.81), (3.82) and (3.83) we have

$$G_n = V \frac{M_3 M_{19}(M_5 M_{10} - M_4 M_{11})}{M_{21}(M_2 M_{10} - M_1 M_{11})} \; \frac{\Delta_3}{\Delta_4} \; . \tag{3.84}$$

From Eqs. (3.63) and (3.84) the field $E_{3\theta}$ at $(r = R, \; \theta = 90^o)$ can be expressed as

$$E_{3\theta}(R, 90^o) = \frac{-jv}{\omega \epsilon_o R^{3/2}} \sum_{\substack{n=1 \\ (n=odd)}}^{\infty} \frac{M_3 M_{19}(M_5 M_{10} - M_4 M_{11})}{M_{21}(M_2 M_{10} - M_1 M_{11})} \; \frac{\Delta_3}{\Delta_4} \; P_n^1(0)$$

$$\cdot \left[n H^{(2)}_{n+\frac{1}{2}}(\beta_o R) - \beta_o R H^{(2)}_{n-\frac{1}{2}}(\beta_o R) \right] \; . \tag{3.85}$$

Equation (3.85) can be rearranged as

$$E_{3\theta}(R, 90^o) = \frac{4\epsilon_d \sqrt{a}}{\pi \epsilon_o R^{3/2}} \sum_{\substack{n=1 \\ (n=odd)}}^{\infty} \frac{2n+1}{2n(n+1)} \left[\frac{\Gamma(\frac{n}{2}+1)}{\Gamma(\frac{n}{2}+\frac{1}{2})} \right]^2 \frac{M_{19}(M_5 M_{10} - M_4 M_{11})}{M_{21}(M_2 M_{10} - M_1 M_{11})}$$

$$\cdot \frac{\Delta_3}{\Delta_4} \left[n H^{(2)}_{n+\frac{1}{2}}(\beta_o R) - \beta_o R H^{(2)}_{n-\frac{1}{2}}(\beta_o R) \right] \; . \tag{3.86}$$

3.8 Numerical Results

The radiated power from the antenna in the broadside direction which is proportional to the square of $E_{\theta 3}(R, 90^o)$ as expressed in

Eq. (3.86) has been numerically calculated as a function of the antenna dimensions and plasma parameters. In a realistic situation, the presence of the plasma sheath on the antenna surface is taken into account[8] by the adoption of a concentric dielectric layer which separates the plasma from the metallic surface of the antenna. This adoption can also account for an actual dielectric coating. For a usual plasma sheath, its thickness may be of the order of several Debye lengths. In the present numerical calculation, the plasma sheath is regarded as an electron-free region extending from r = a to r = b. A convenient parameter to describe the thickness of the sheath is the dimensionless quantity s defined by $b - a = \left(\frac{v_o}{\sqrt{3}\omega_p}\right)s$. It is to be noted that $\left(\frac{v_o}{\sqrt{3}\omega_p}\right)$ is of the order of a Debye length in the plasma and, thus, s may be regarded as the "Debye thickness" of the sheath[8]. The permittivity of the sheath can then be assumed to be the same as that of the free space, i.e., $\epsilon_d = \epsilon_o$. Furthermore, in the numerical analysis only the first five terms, i.e., n = 1, 3, ... 9, on the right-hand side of Eq. (3.86) are summed up for that series and for the large arguments, $z > 10$, the asymptotic forms of the Hankel functions of the first and second kinds have been used. The numerical calculation was made by using a CDC 3600 computer.

Figures 3.2 to 3.4 show the radiated power from a spherical antenna of radius 2.54 cm driven at various frequencies as a function of the plasma density of the plasma layer with the Debye thickness s as the running parameter. The radius of the spherical plasma layer is 7 cm (or the thickness of plasma layer is 4.46 cm minus the thickness of plasma sheath) and the distance between the radiating and receiving antennas is 0.915 m. The electron collision frequency is assumed to be 0.12 GHz and the ratio of the r.m.s. electron velocity to the velocity of light in free space, v_o/c_o, is assumed to be 0.01. In these figures the radiated power at each driven frequency is normalized to its free-space radiated power. At all driven frequencies we invariably observe that the antenna radiation is reduced as the plasma density is increased and it reaches the cut-off point as the plasma frequency is increased to the neighborhood of the antenna frequency. After the plasma frequency exceeds the antenna frequency, the antenna radiation starts to build up somewhat for higher antenna frequency cases of 0.8 GHz and 1.2 GHz. This trend becomes more outstanding for lower frequency cases of 0.4 GHz and 0.3 GHz. At 0.4 GHz and 0.3 GHz, the antenna radiation can build up to a level 15 db to 21 db higher than the free-space radiation after passing the cut-off. Physically it means that if an antenna is operated at a frequency much lower than the plasma frequency of the plasma layer, its radiation will recover from the cut-off and then be enhanced greatly over the free-space radiation level. This phenomenon of enhanced radiation is similar to that discussed in Chapter 1 especially when the thickness of the plasma sheath is in the order of one Debye length, i.e., $s = 1$. The effect of the plasma sheath on the antenna radiation can be observed from these figures. When the thickness of the plasma sheath is increased the phenomenon of enhanced radiation after passing the cut-off is more outstanding for both higher and lower frequency cases.

The set of Figs. 3.5 to 3.6 shows the similar phenomenon as the set of Figs. 3.2 to 3.4 but for the case of a smaller antenna (1.27 cm radius). The radius of the plasma layer is again 7 cm. For a smaller antenna, we observe that the antenna radiation is enhanced greater for both higher and lower frequency cases. A strong enhancement of 15 db over free-space radiation for the case of 0.8 GHz in Fig. 3.7 is rather interesting since it tends to indicate that the phenomenon of enhanced radiation can occur even for a higher frequency case if a suitable value is assigned to the plasma parameters.

The effects of the electron collision frequency, the antenna size, the thickness of the plasma layer and the thickness of the plasma sheath on the phenomenon of enhanced radiation can be observed from two sets of figures, Figs. 3.8 to 3.11 and Figs. 3.12 to 3.15. In Figs. 3.8 to 3.11 the radiated powers from spherical antennas of various radii, 2.54 cm, 3.81 cm, 5.08 cm and 6.38 cm, driven at 0.4 GHz are shown as functions of the plasma density of the plasma layer with the Debye thickness s as the running parameter. The radius of the spherical plasma layer is fixed as 7.62 cm and the distance between the radiating and receiving antennas is 0.7 m. The electron collision frequency is assumed to be 0.03 GHz and the ratio of the r.m.s. electron velocity to the velocity of light in free space, v_o/c_o, is assumed to be 0.01. In these figures the radiated power is normalized to its free-space radiated power. For Figs. 3.12 to 3.15 the same set of parameters is used except the electron collision frequency is changed from 0.03 GHz to 0.003 GHz. The main points of observation on the enhanced radiation from the antenna can be summarized as follows:

(1) A higher loss in plasma makes the cut-off phenomenon less outstanding and the enhancement of radiation slightly lower.

(2) For fixed radius of the spherical plasma layer the phenomenon of enhanced radiation becomes less significant as the antenna size is increased and the thickness of plasma layer is reduced.

(3) For fixed antenna size the increase of the thickness of the plasma sheath which is equivalent to the decrease of the thickness of the plasma layer makes the enhanced radiation more outstanding.

(4) Besides the above observations on the general behaviors of the enhanced radiation which are consistent with the phenomena observed in Chapter 1, an interesting finding is made on a series of resonance peaks which occur when the thickness of the plasma layer is thin and the electron collision frequency is low compared with the driving frequency. In Figs. 3.8 and 3.9, the antenna sizes are small with radii 2.54 cm and 3.81 cm and the plasma layers are thick, no resonance peaks are observed. When the antenna size is increased to 5.08 cm radius and the plasma layer becomes rather thin

in Fig. 3.10 the resonance peaks start to show up at $\omega_p^2/\omega^2 = 1.3$. If the antenna size is further increased to 6.35 cm radius, and the plasma layer is further shrunk, more resonance peaks occur at $\omega_p^2/\omega^2 = 0.7$, 1.3 and 1.5. This indicates that if the thickness of the plasma layer is made thin the resonance will occur. Physically, it may be attributed to the electroacoustic resonance in this thin plasma layer. Since the wave length of the electroacoustic wave is rather small, it can set up the standing wave only when the plasma layer is thin. A large plasma layer will make the electroacoustic wave to set up an attenuating traveling wave instead. since the plasma is lossy in nature. In Figs. 3.12 to 3.15, the plasma medium is made less lossy ($\nu/2\pi = 0.003$ GHz). The resonance peaks start to show up for the smaller antenna and thicker plasma layer cases and more resonance peaks occur for the larger antenna and thinner plasma layer cases. This might be due to the fact that since the plasma medium is now less lossy, the electroacoustic wave will suffer less antenuation and even for a larger plasma layer it is still possible to set up the standing wave for the resonance within this layer. There are two other possibilities for producing the resonance peaks. They are: (1) the cavity resonance due to the electromagnetic wave in the spherical plasma layer, and (2) the cavity resonance due to the electromagnetic wave in the plasma sheath region. It is unfortunate that in the present analysis there is no way to identify those resonance peaks with those three different causes. From Fig. 2.8 we found that under the same conditions but a different theory, no resonance peak was observed even when the thickness of the plasma layer was made very thin. This fact tends to indicate that those resonance peaks observed in Figs. 3.10 to 3.15 are due to an electroacoustic wave in the plasma layer or an electromagnetic wave in the plasma sheath region.

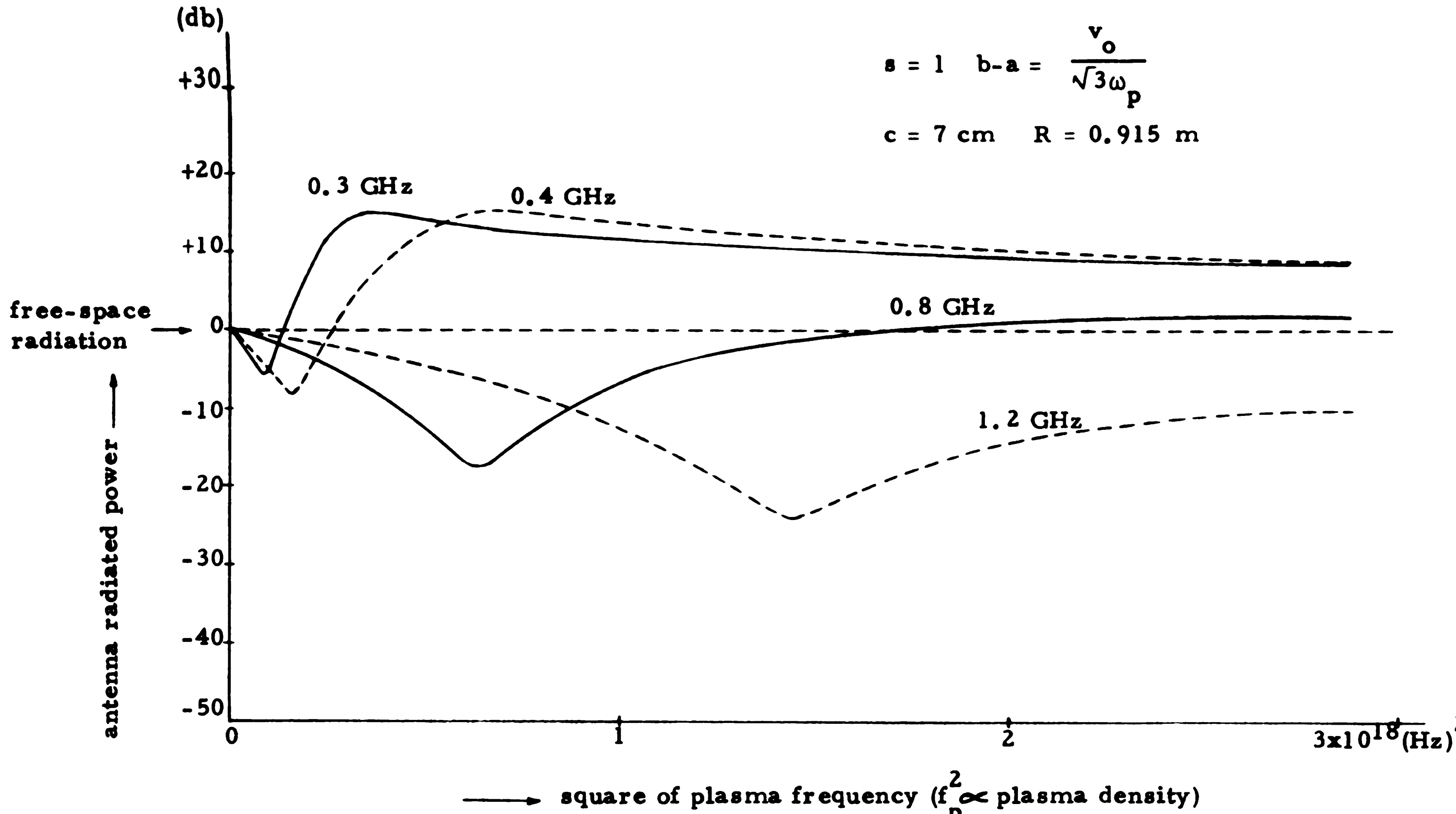

Fig. 3.2 Theoretical radiation of a spherical antenna (a = 2.54 cm) in a lossy, hot plasma ($\nu/2\pi$ = 0.12 GHz, v_o/c_o = 0.01) driven at various frequencies as a function of plasma density.

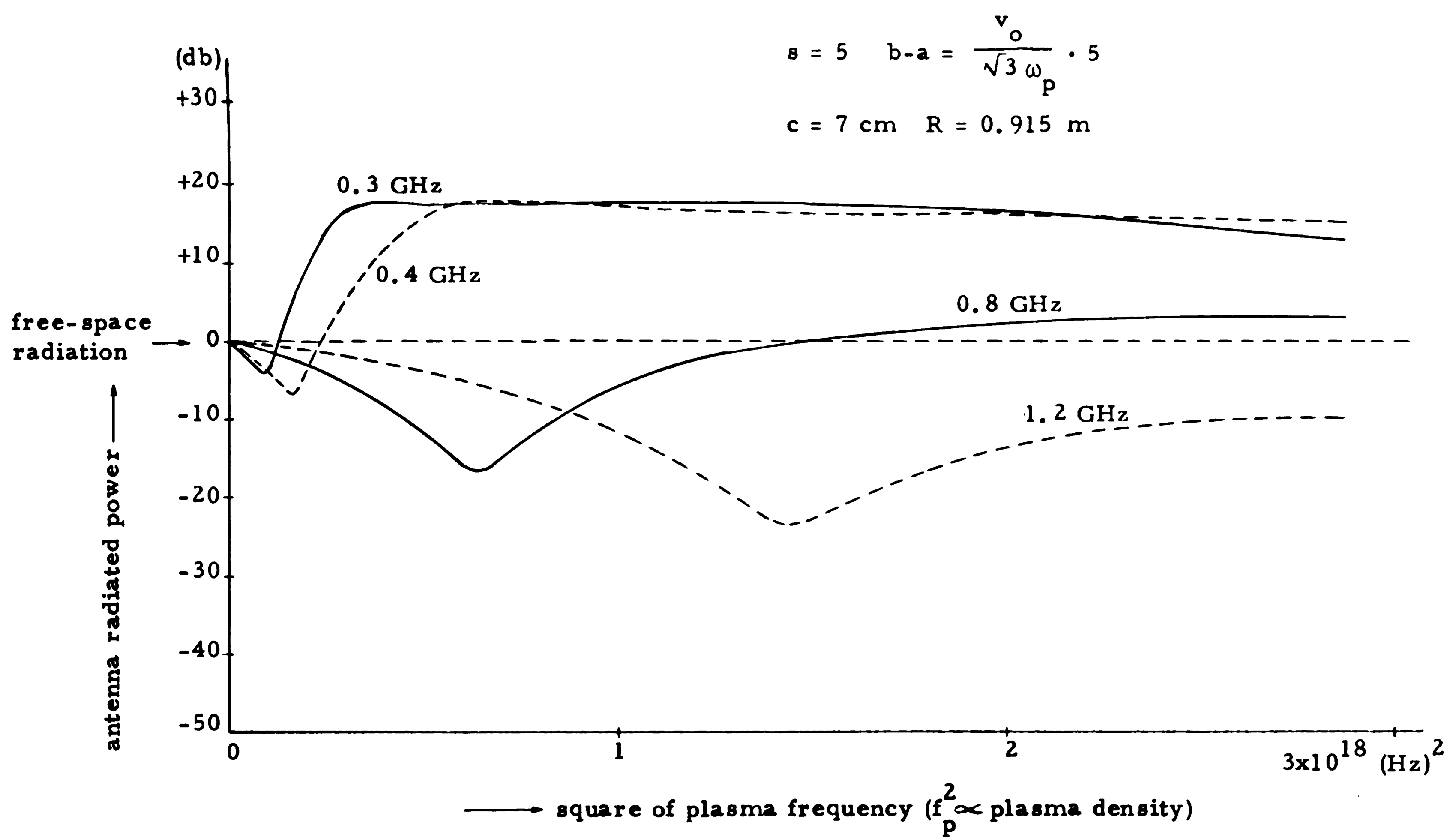

Fig. 3.3 Theoretical radiation of a spherical antenna (a = 2.54 cm) in a lossy, hot plasma ($\nu/2\pi$ = 0.12 GHz, v_o/c_o = 0.01) driven at various frequencies as a function of plasma density.

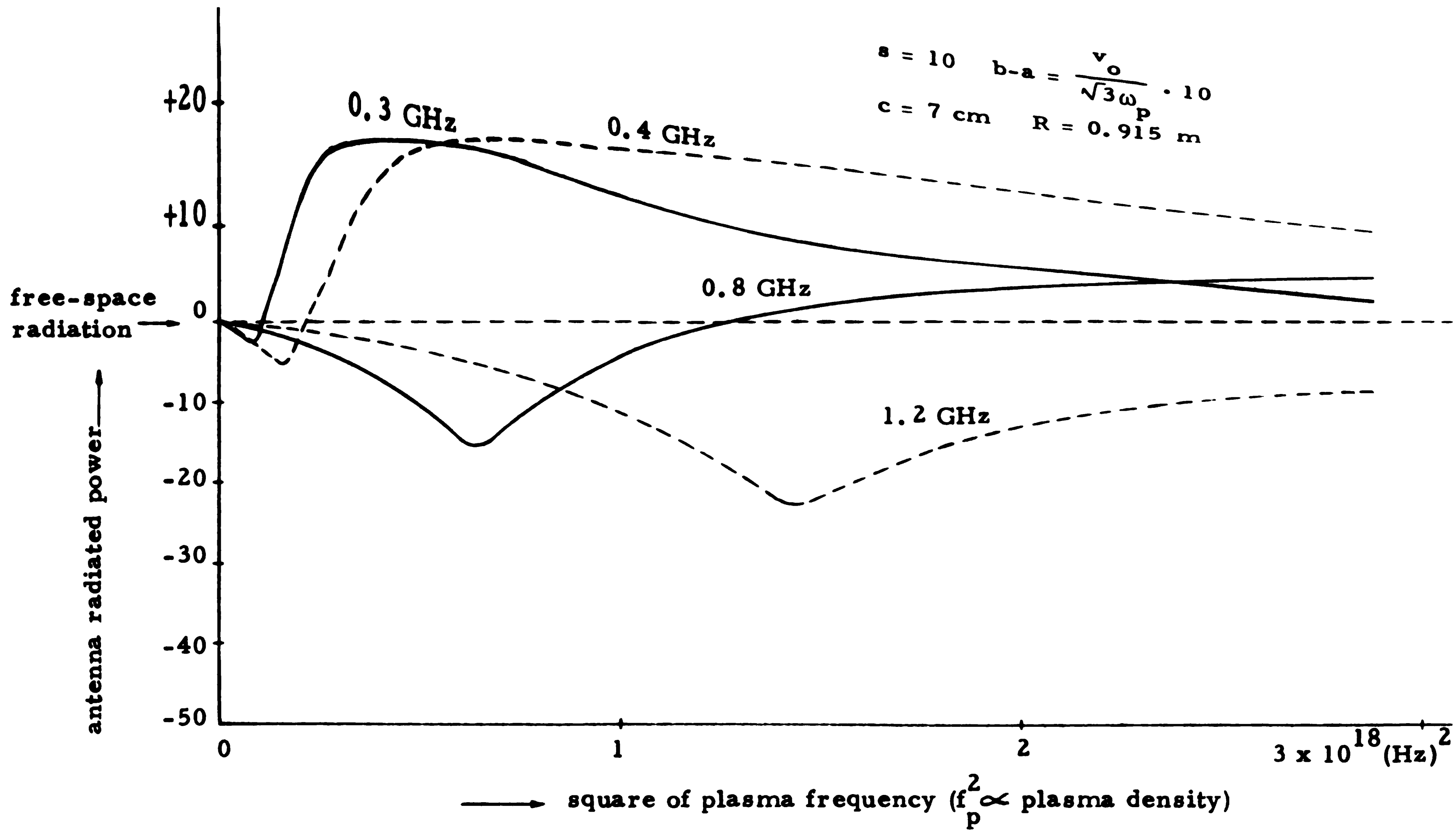

Fig. 3.4 Theoretical radiation of a spherical antenna (a = 2.54 cm) in a lossy, hot plasma ($\nu/2\pi$ = 0.12 GHz, v_o/c_o = 0.01) driven at various frequencies as a function of plasma density.

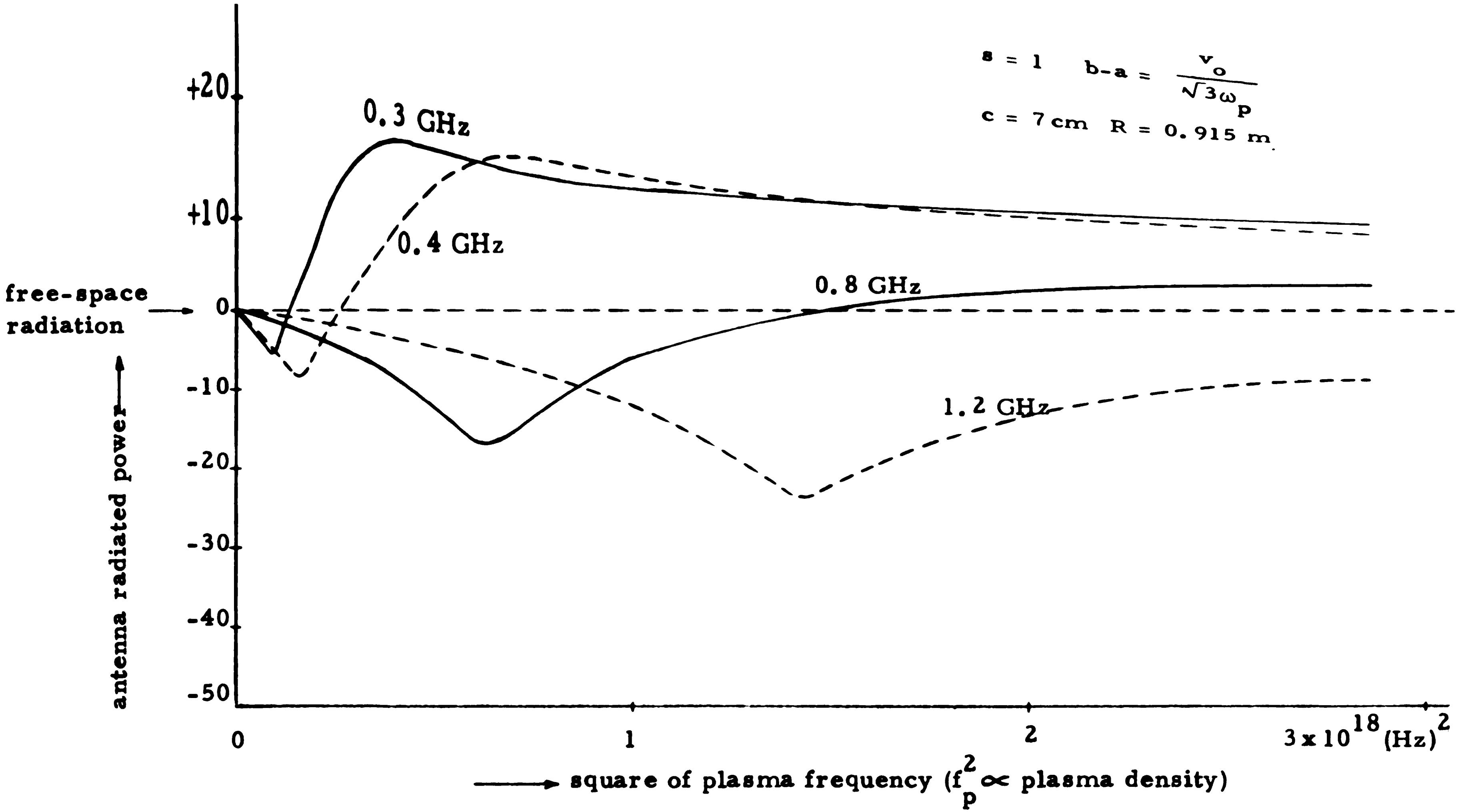

Fig. 3.5 Theoretical radiation of a spherical antenna (a = 1.27 cm) in a lossy, hot plasma ($\nu/2\pi$ = 0.12 GHz, v_o/c_o = 0.01) driven at various frequencies as a function of plasma density.

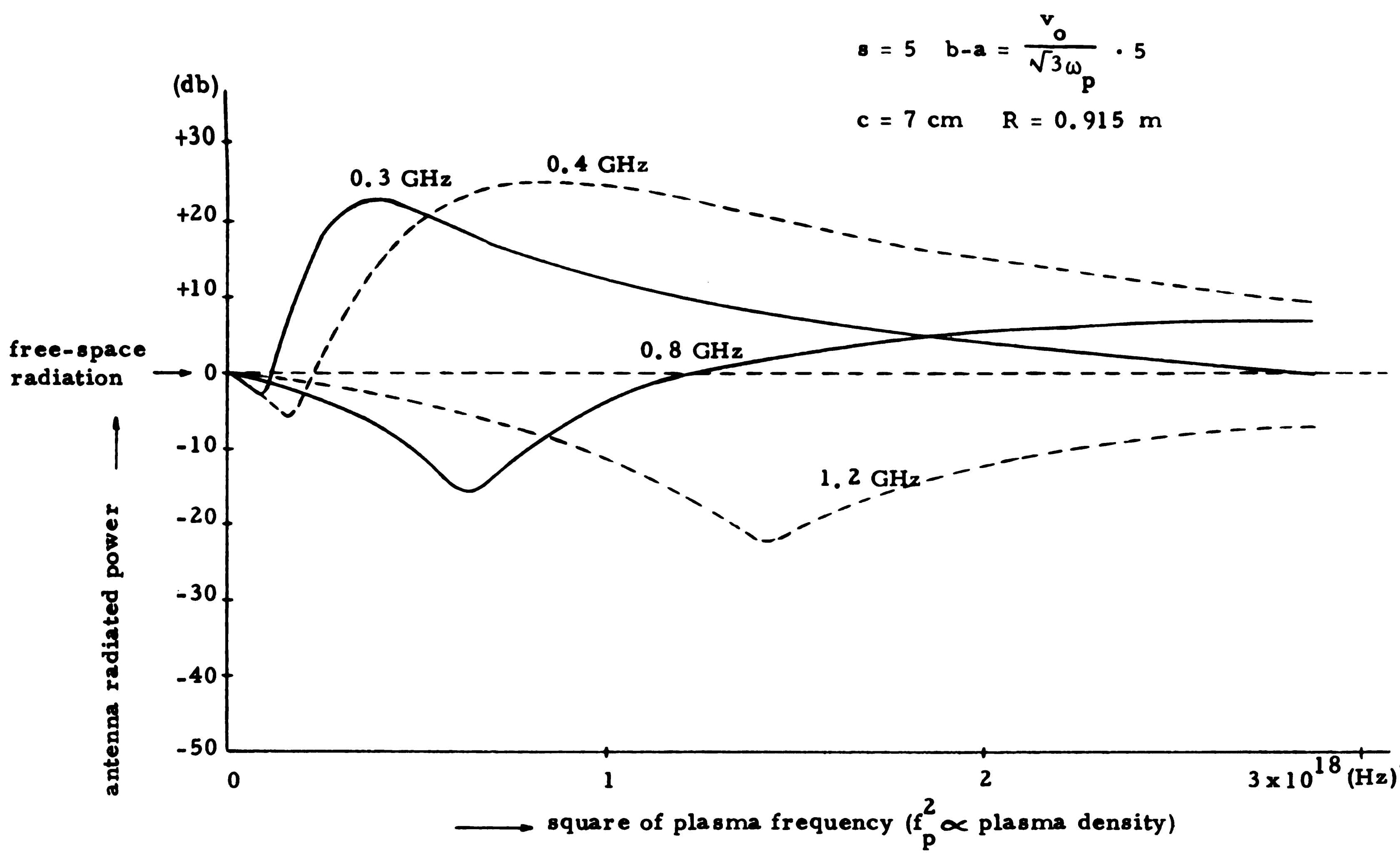

Fig. 3.6 Theoretical radiation of a spherical antenna (a = 1.27 cm) in a lossy, hot plasma ($\nu/2\pi$ = 0.12 GHz, v_o/c_o = 0.01) driven at various frequencies as a function of plasma density.

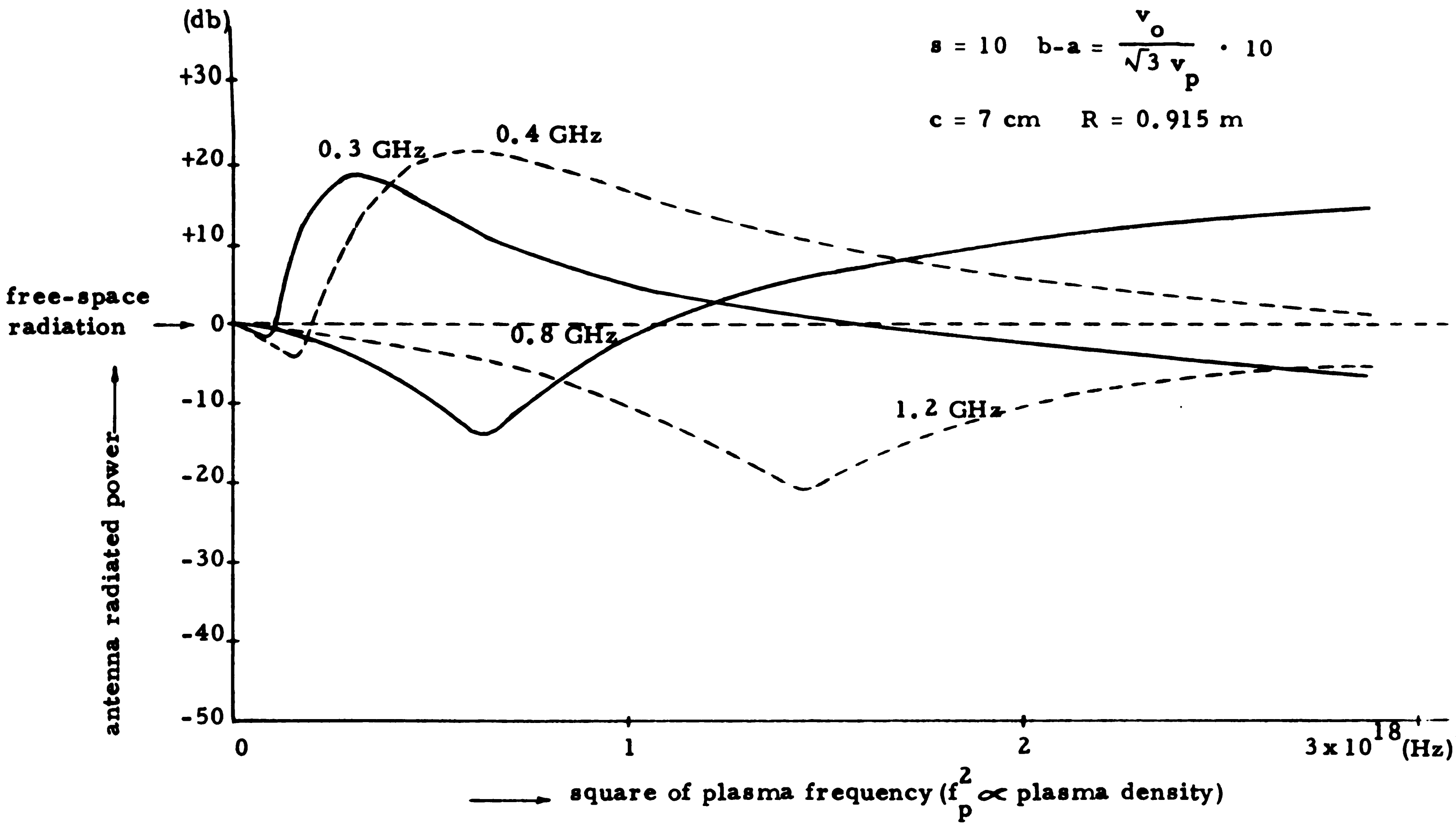

Fig. 3.7 Theoretical radiation of a spherical antenna ($a = 1.27$ cm) in a lossy, hot plasma ($\nu/2\pi = 0.12$ GHz, $v_o/c_o = 0.01$) driven at various frequencies as a function of plasma density.

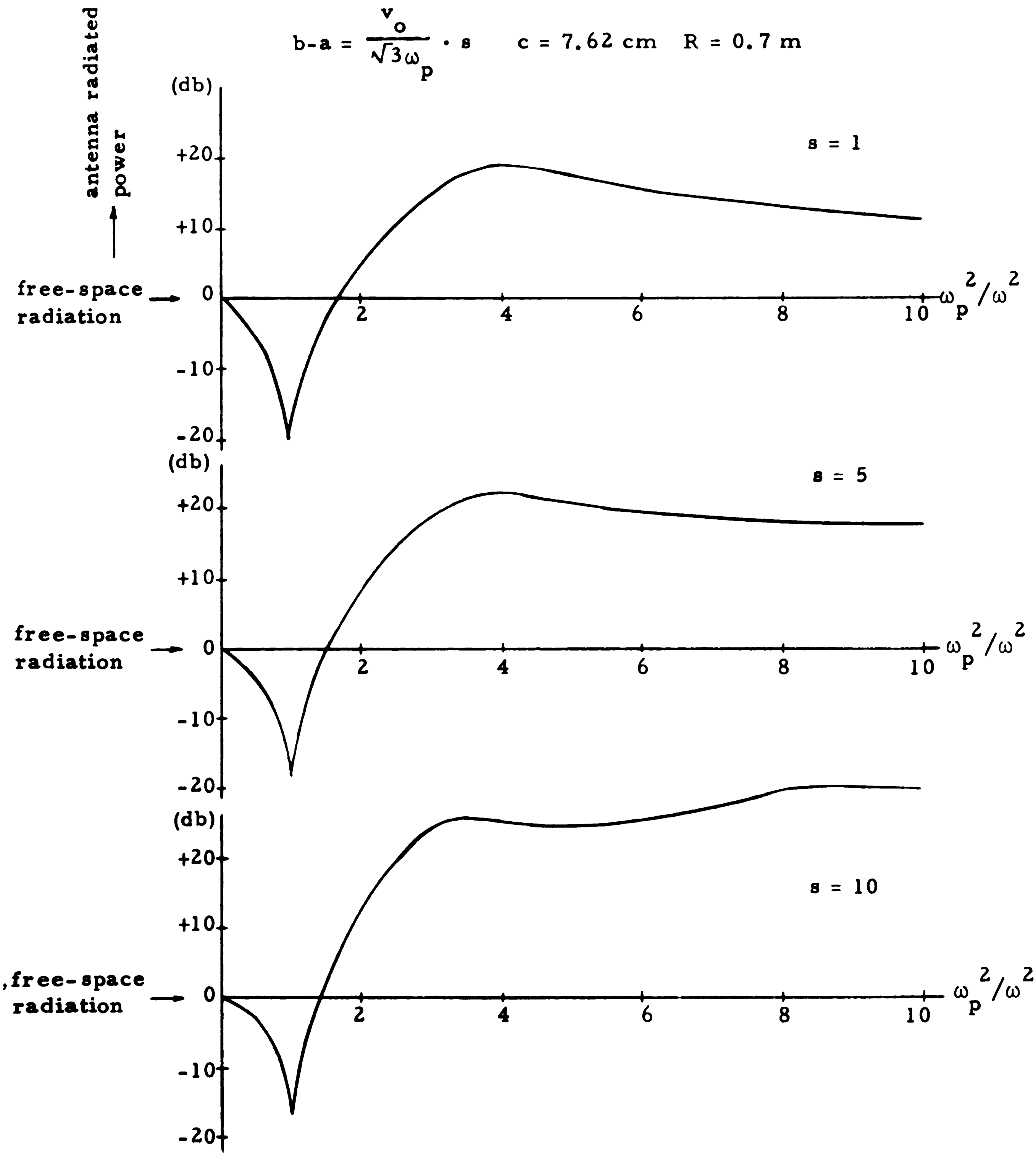

Fig. 3.8 Theoretical radiation of a spherical antenna (a = 2.54 cm) in a lossy, hot plasma ($\nu/2\pi$ = 0.03 GHz, v_o/c_o = 0.01) driven at 0.4 GHz as a function of plasma density.

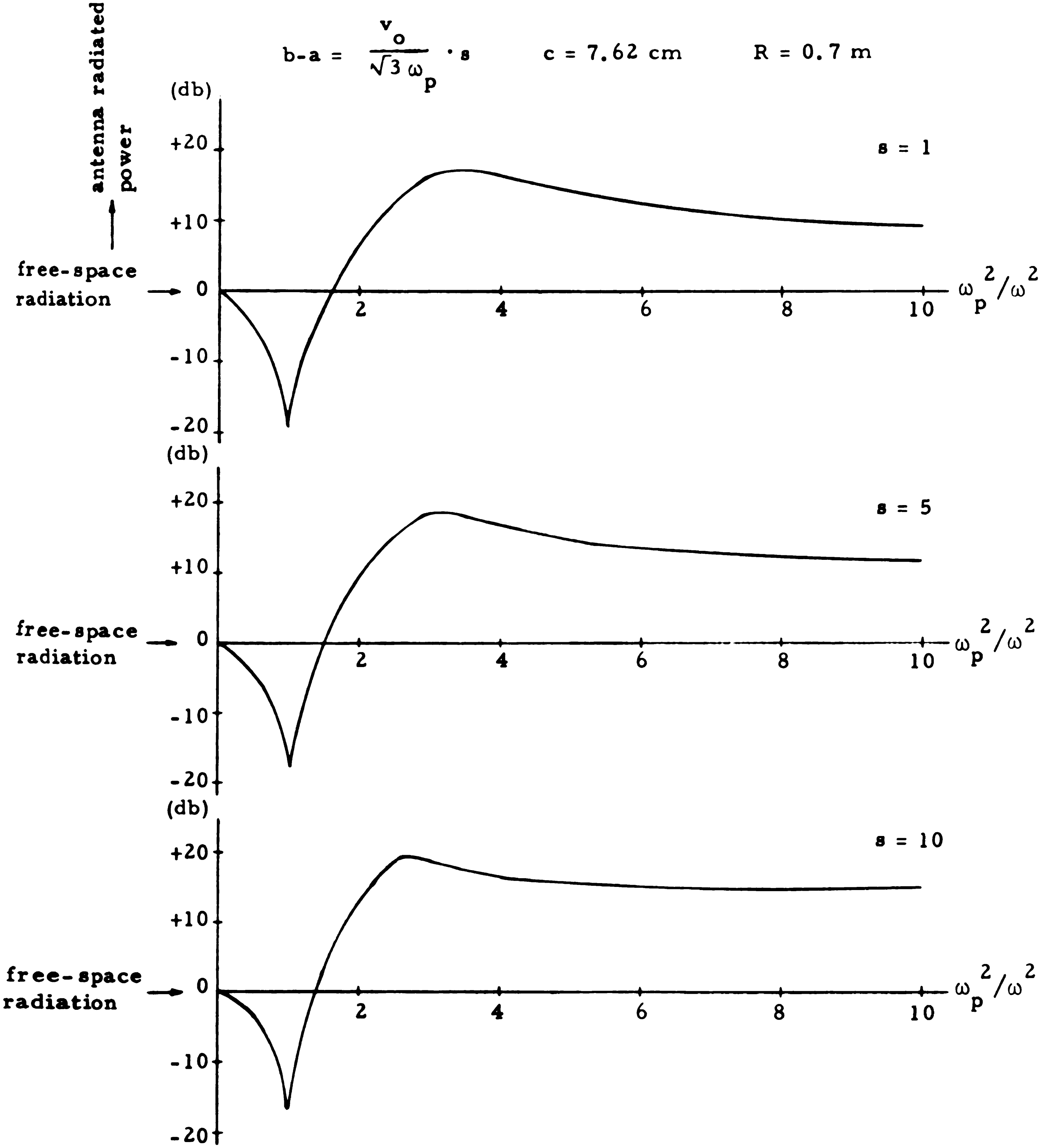

Fig. 3.9 **Theoretical radiation of a spherical antenna (a = 3.81 cm) in a lossy, hot plasma ($\nu/2\pi$ = 0.03 GHz, v_o/c_o = 0.01) driven at 0.4 GHz as a function of plasma density.**

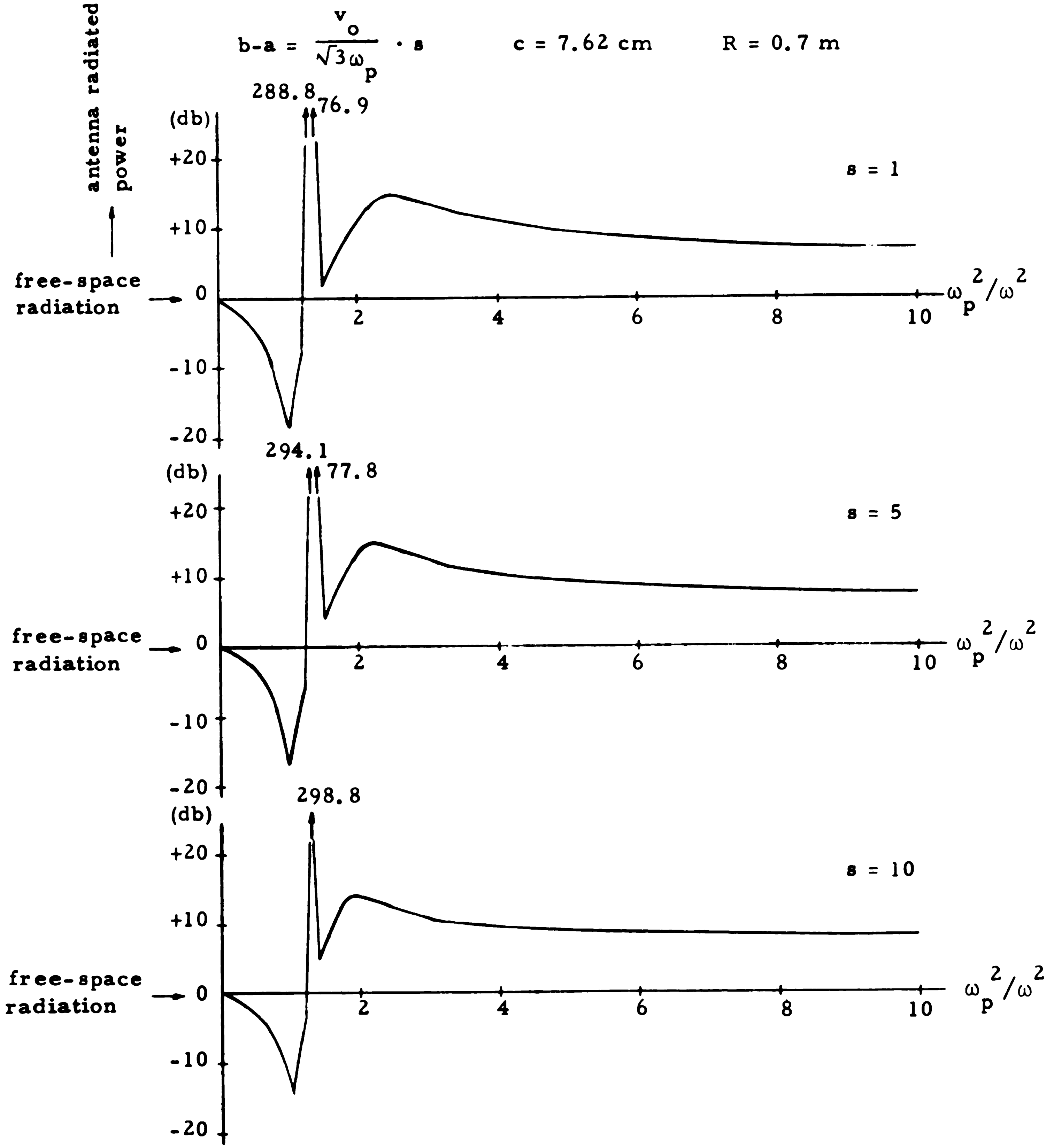

Fig. 3.10 **Theoretical radiation of a spherical antenna (a = 5.08 cm) in a lossy, hot plasma ($\nu/2\pi$ = 0.03 GHz, v_o/c_o = 0.01) driven at 0.4 GHz as a function of plasma density.**

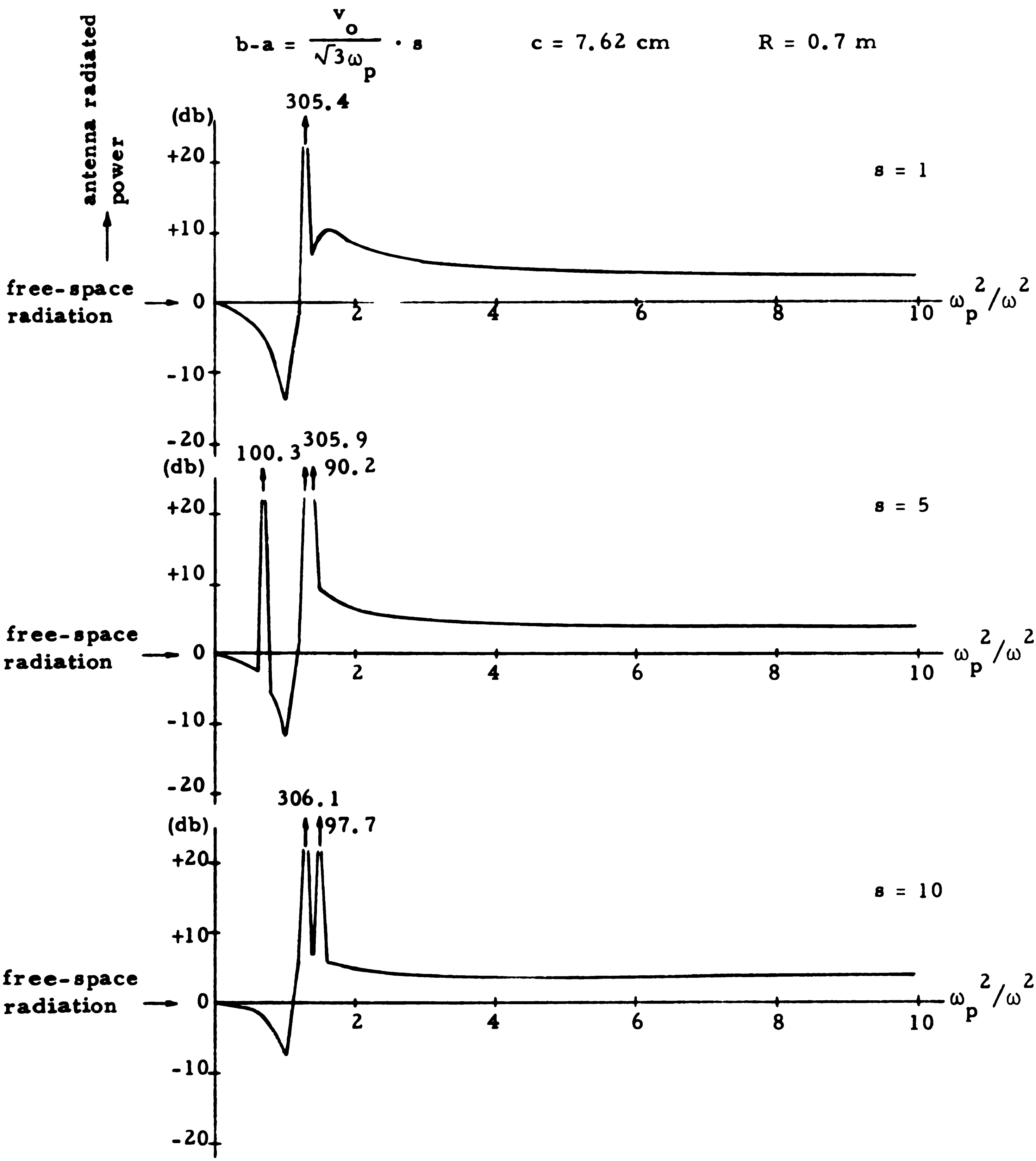

Fig. 3.11 Theoretical radiation of a spherical antenna (a = 6.35 cm) in a lossy, hot plasma ($\nu/2\pi$ = 0.03 GHz, v_o/c_o = 0.01) driven at 0.4 GHz as a function of plasma density.

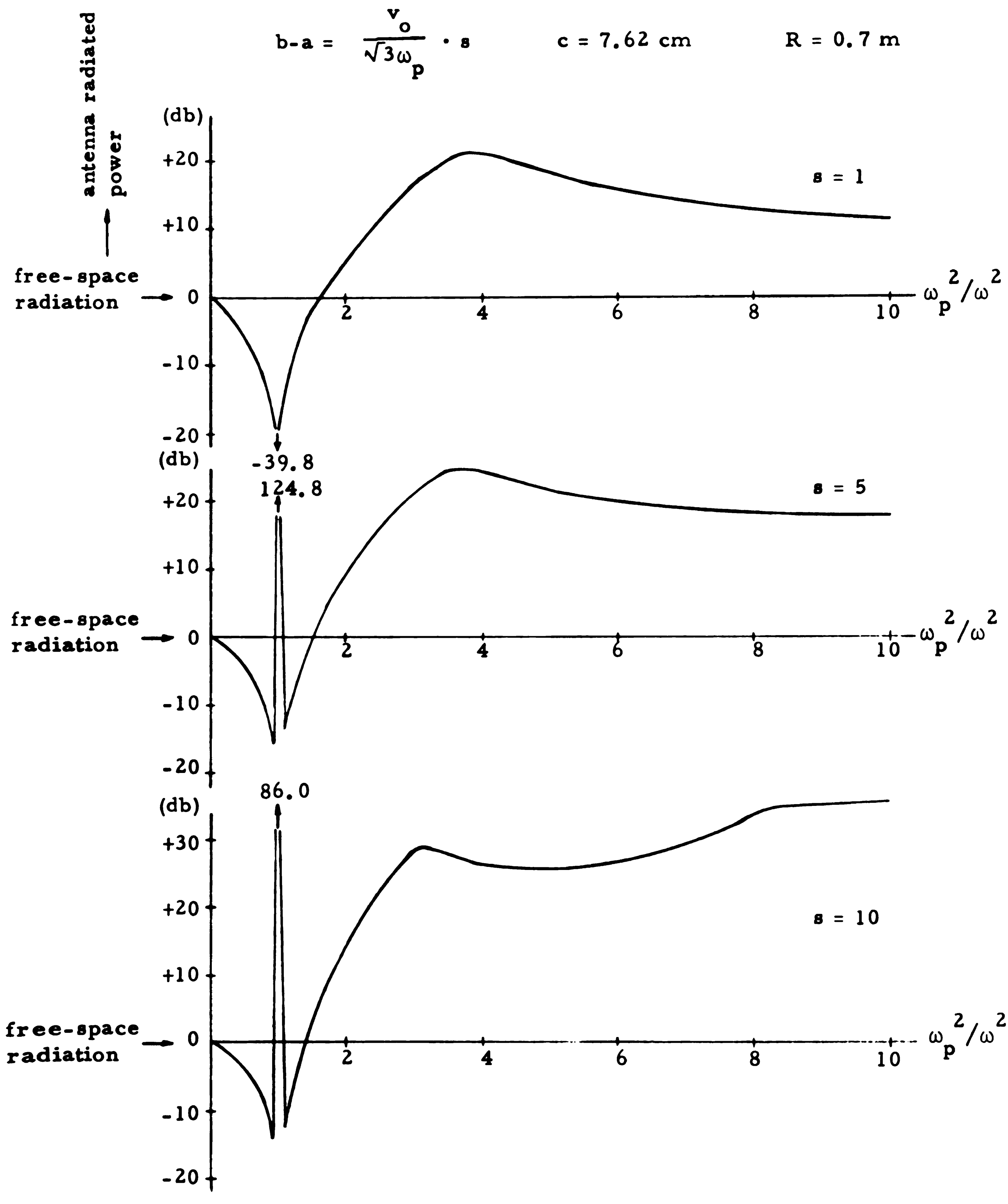

Fig. 3.12 Theoretical radiation of a spherical antenna (a = 2.54 cm) in a lossy, hot plasma ($\nu/2\pi$ = 0.003 GHz, v_o/c_o = 0.01) driven at 0.4 GHz as a function of plasma density.

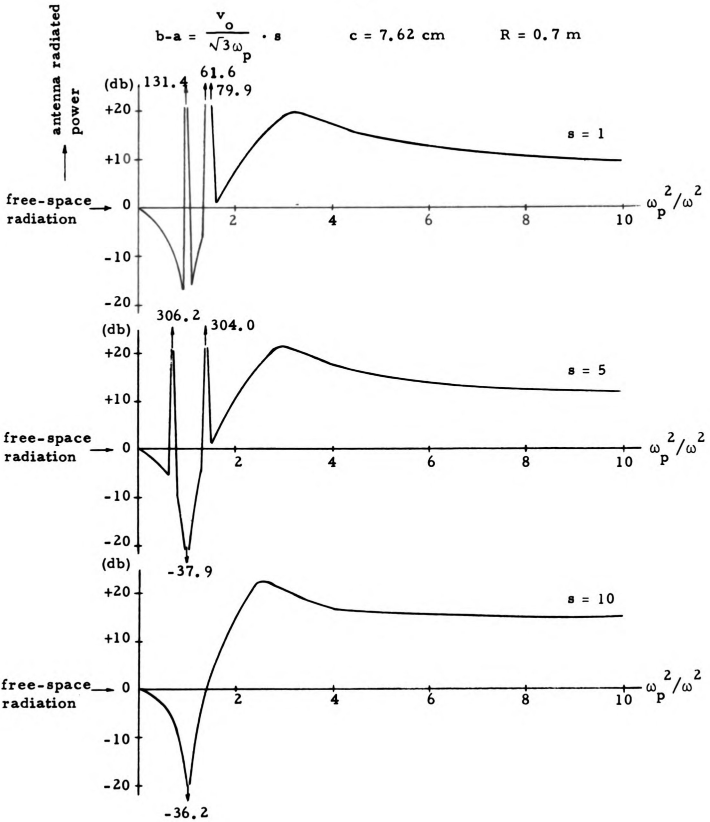

Fig. 3.13 Theoretical radiation of a spherical antenna (a = 3.81 cm) in a lossy, hot plasma ($\nu/2\pi$ = 0.003 GHz, v_o/c_o = 0.01) driven at 0.4 GHz as a function of plasma density.

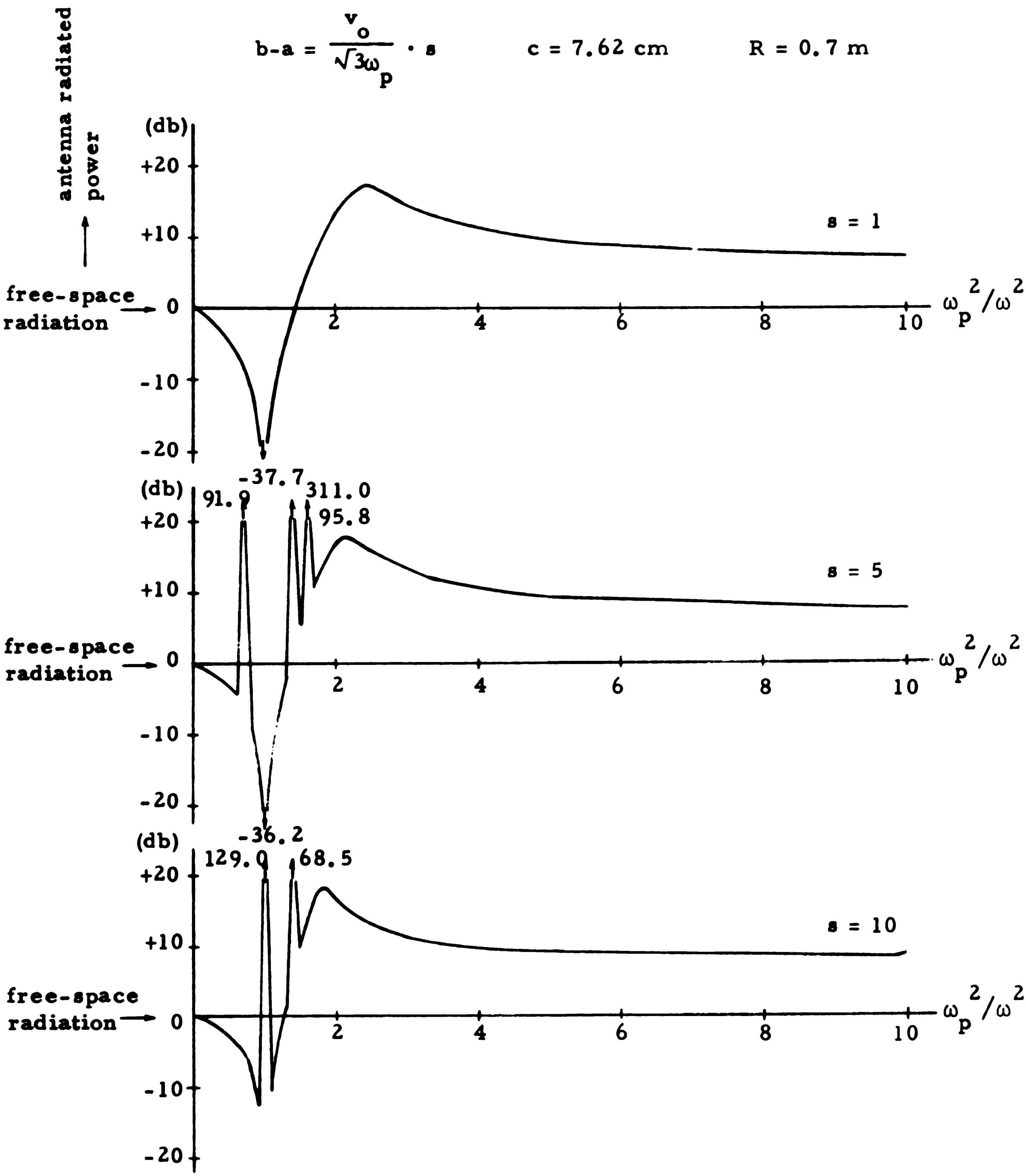

Fig. 3.14 Theoretical radiation of a spherical antenna (a = 5.08 cm) in a lossy, hot plasma ($\nu/2\pi$ = 0.003 GHz, v_o/c_o = 0.01) driven at 0.4 GHz as a function of plasma density.

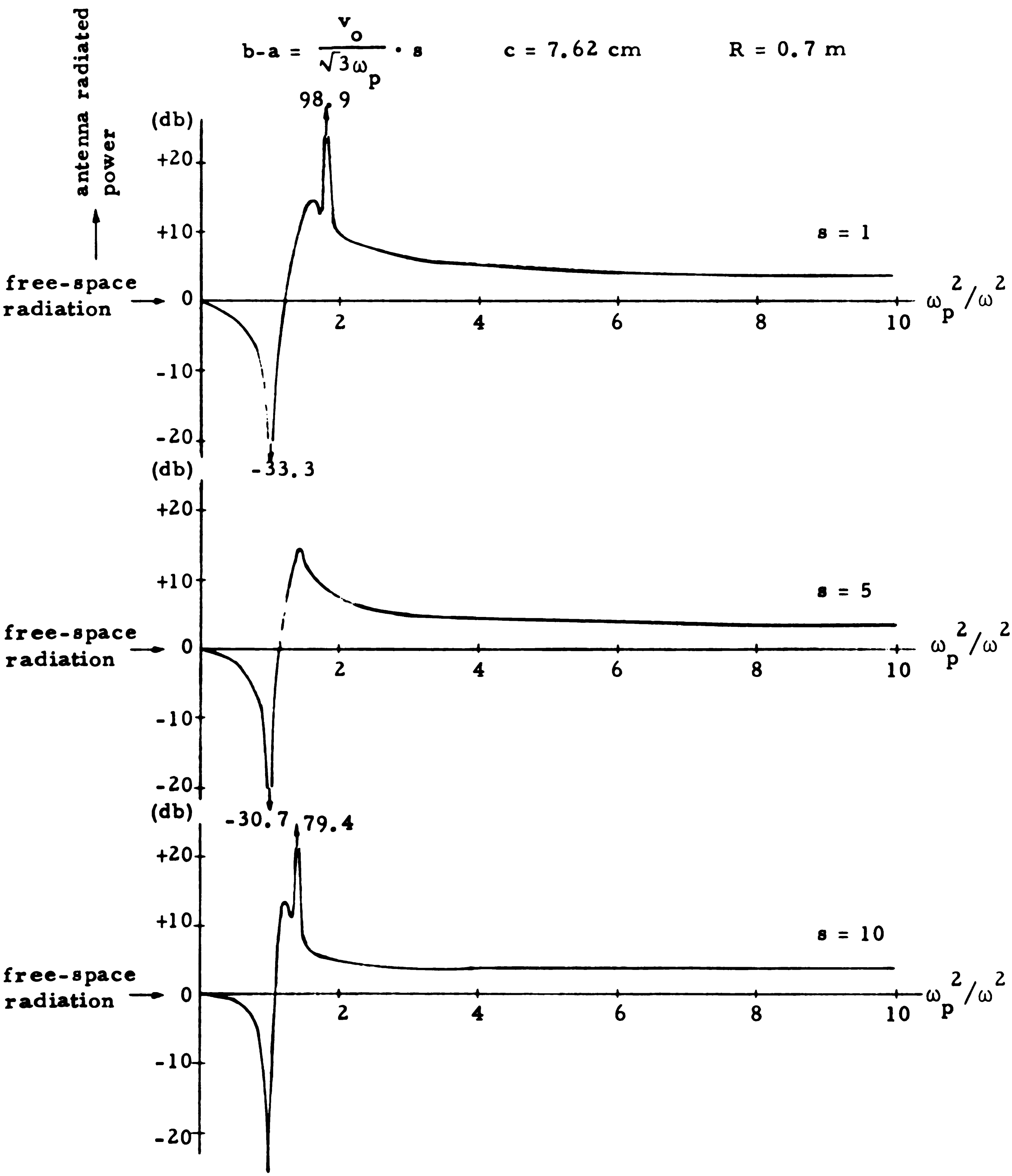

Fig. 3.15 **Theoretical radiation of a spherical antenna (a = 6.35 cm) in a lossy, hot plasma ($\nu/2\pi$ = 0.003 GHz, v_o/c_o = 0.01) driven at 0.4 GHz as a function of plasma density.**

CHAPTER 4

EXPERIMENTAL INVESTIGATION ON THE RADIATION FROM A SPHERICAL ANTENNA IN A HOT PLASMA

4.1 Introduction

The radiation from a spherical antenna imbedded in a finite, spherical plasma layer has been studied theoretically in Chapters 2 and 3. In order to confirm the theoretical results, an experimental investigation on the subject has been conducted.

The main purpose of this experimental investigation is to detect the strong enhancement on the antenna radiation over a wide band of antenna frequencies which are much lower than the plasma frequency of the plasma volume. This phenomenon has been predicted theoretically and it has also been confirmed in this experimental study.

In our experiment, the hot plasma was provided by a mercury arc discharge which was created in a hemi-spherical pyrex tube. Hemi-spherical antennas were used as the radiating sources and a large metal plane was used as an image plane.

4.2 Experimental Setup

The experimental setup for the antenna radiation measurement is schematically shown in Fig. 4.1. The plasma tube is made of a hemi-spherical pyrex glass tube with a radius of 3 inches. A small mercury pool with a floating spot fixer is located at one end of the tube. The open end of the tube is sucked to the ground plane when the tube is being pumped. With this arrangement the ground plane acts as the anode and the mercury pool as the cathode of the plasma tube and the discharge is maintained by a DC voltage. The discharge current can be varied from zero to about 8 amperes, corresponding to a plasma density of about $2 \times 10^{17} (m^3)^{-1}$. The electron temperature and the pressure of the plasma are about $20,000^{\circ}K$ and 3×10^{-3} mm Hg, respectively. A spherical monopole antenna is fed into the center of the plasma tube through the ground plane and is driven by a RF signal. The antenna is DC blocked from the rest of the system to insure a floating potential for the antenna. The radiation of the antenna through the plasma is measured by a fixed receiving antenna on the ground plane. The output of the receiving antenna is connected to a hetrodyne receiving system. The distance between the radiating and receiving antennas is 0.915 m. The radiating antenna with the plasma tube and the receiving antenna are all enclosed in a microwave anechoic chamber. Figure 4.2 shows the photograph of this plasma tube under operation inside of the microwave anechoic chamber. The photograph of the experimental setup outside of the microwave anechoic chamber is shown in Fig. 4.3.

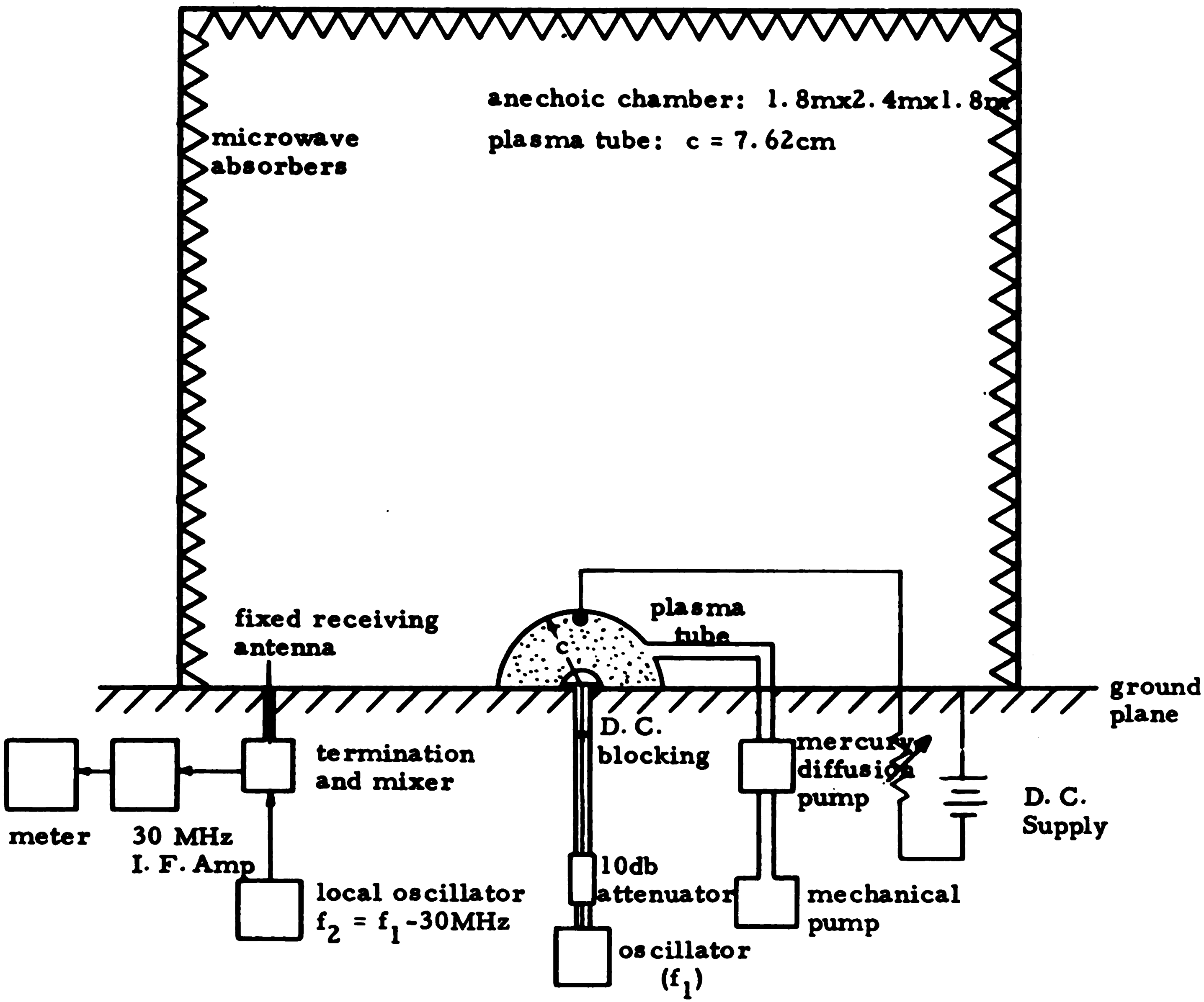

Fig. 4.1 Experimental setup for the radiation measurement of spherical antenna.

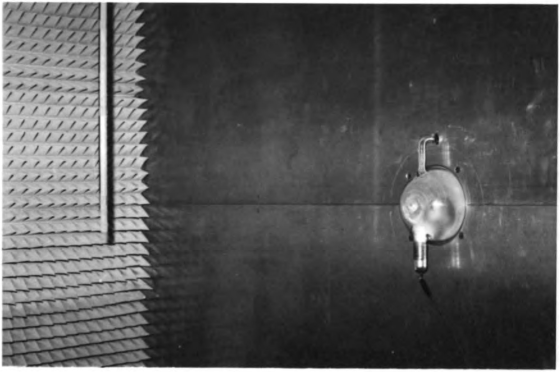

Fig. 4.2 A hemi-spherical plasma tube (3-inch radius) under operation inside of a microwave anechoic chamber.

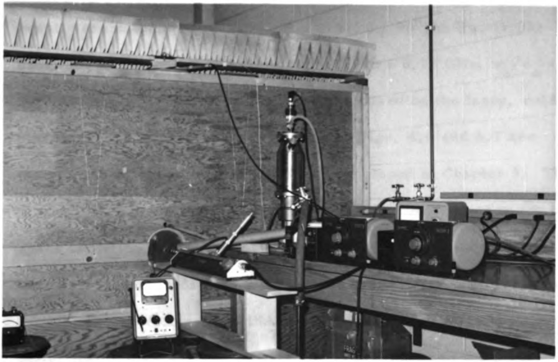

Fig. 4.3 Experimental setup outside of a microwave anechoic chamber.

4.3 Experimental Results and Comparison with Theories

The experimental results of the radiation from two spherical antennas of radii 2.54 cm and 1.27 cm driven by various frequencies are plotted in comparison with the corresponding theoretical results in Figs. 4.4 to 4.7. At each driven frequency the antenna radiation is measured as a function of the plasma density and the radiated power is normalized to the value when no plasma is present (free-space radiation). The antenna radiation is measured at R = 0.915 m and in the broadside direction of the radiating antenna.

In Figs. 4.4 and 4.5, the corresponding theoretical results are calculated from $E_{2\theta}(R = 0.915\,\mathrm{m},\ 90^{\circ})$ in Eq. (2.59) under the assumption of a cold plasma and an electron collision frequency of 0.12 GHz. In Figs. 4.6 and 4.7, the corresponding theoretical results are calculated from $E_{3\theta}(R = 0.915\,\mathrm{m},\ 90^{\circ})$ in Eq. (3.86) under the assumptions of a hot plasma, $\nu/2\pi = 0.12$ GHz, $v_o/c_o = 0.01$ and $s = 1$. Figures 4.4 and 4.5 are based on the lossy, cold-plasma theory studied in Chapter 2 while Figs. 4.6 and 4.7 are based on the lossy, hot-plasma theory developed in Chapter 3. The theoretical value of the radiated power is also normalized to the free-space radiation. The comparison of two theories (lines) with the experiment (dots) indicates a very close agreement. The agreement between the experiment and the lossy, hot-plasma theory is somewhat better than the agreement between the experiment and the lossy, cold-plasma theory. It should be noted that only four cases are considered in Figs. 4.6 and 4.7 because the numerical result obtained from the lossy, hot-plasma theory, require extensive computing time.

In the experiment, the antenna radiation was observed to be enhanced about 15 db over the free-space radiation when the antenna frequency was 0.3 or 0.4 GHz and the plasma frequency was at least twice higher than the antenna frequency. It was also observed in the experiment that when the antenna frequency was higher than 0.8 GHz no enhancement above the free-space radiation could be obtained after passing the cut-off point. All these phenomena are well predicted by the theory. Also in the experiment, the DC potential of the antenna was varied between $\pm$ 20 volts to see the effect of the plasma sheath on the phenomenon of enhanced radiation. Except for a slight effect due to the bias circuit, negligible effect by the plasma sheath had been observed. Furthermore, no resonance peaks was found in the experiment.

4.4 Discussion

In this study, the phenomenon of enhanced radiation from an antenna coated by a layer of plasma is confirmed theoretically and experimentally. It appears feasible to apply this phenomenon in overcoming the blackout problem of a reentry antenna or in providing a low-loss tuning for a small antenna.

There remains two facts which should be pointed out. The first is the appropriate size of plasma layer for a possible enhancement in radiation. In our experiments and most of numerical examples, the size of plasma layer was made bigger than the antenna size for structural convenience. This does not mean that a large volume of plasma is always needed for a possible enhancement in radiation. In fact, it has been shown in Fig. 2.6 that even for a plasma layer with a thickness equal to the antenna radius can lead to a 15 db enhancement. Furthermore, in Figs. 3.10 to 3.15 we observe resonance peaks when the thickness of the plasma layer is very thin.

The second is that antennas on a space vehicle are usually matched under free-space condition and in our study this fact was not taken into account. This is not very important because a more important fact is that even a matched antenna when covered by a plasma will suffer a blackout and after that the antenna radiation can not be recovered by any tuning or impedance matching. Thus, the method discussed in this paper may offer a possible solution to the blackout problem.

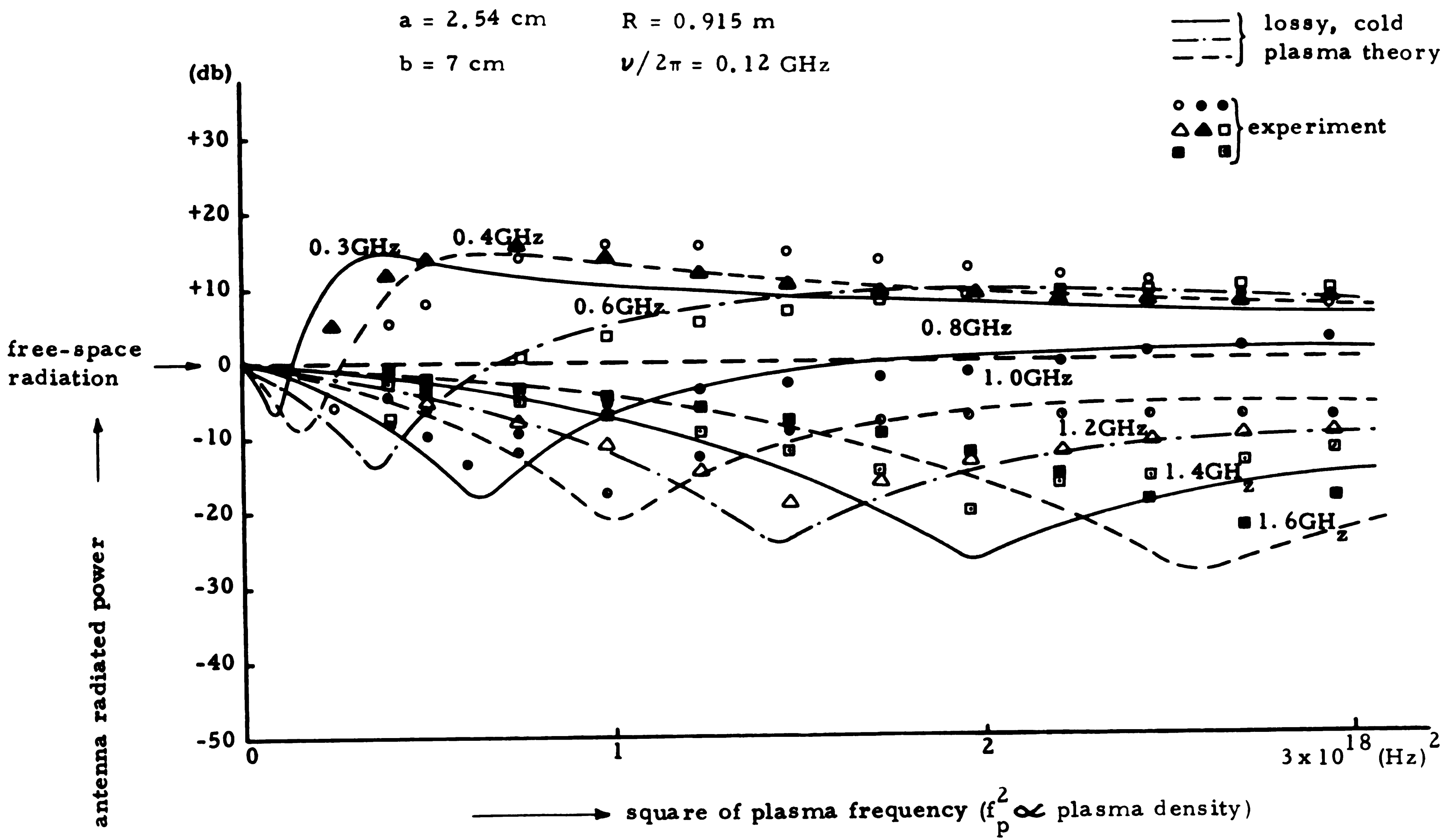

Fig. 4.4 Experimental and theoretical radiation of a spherical antenna (a = 2.54 cm) in a plasma driven at various frequencies as a function of plasma density.

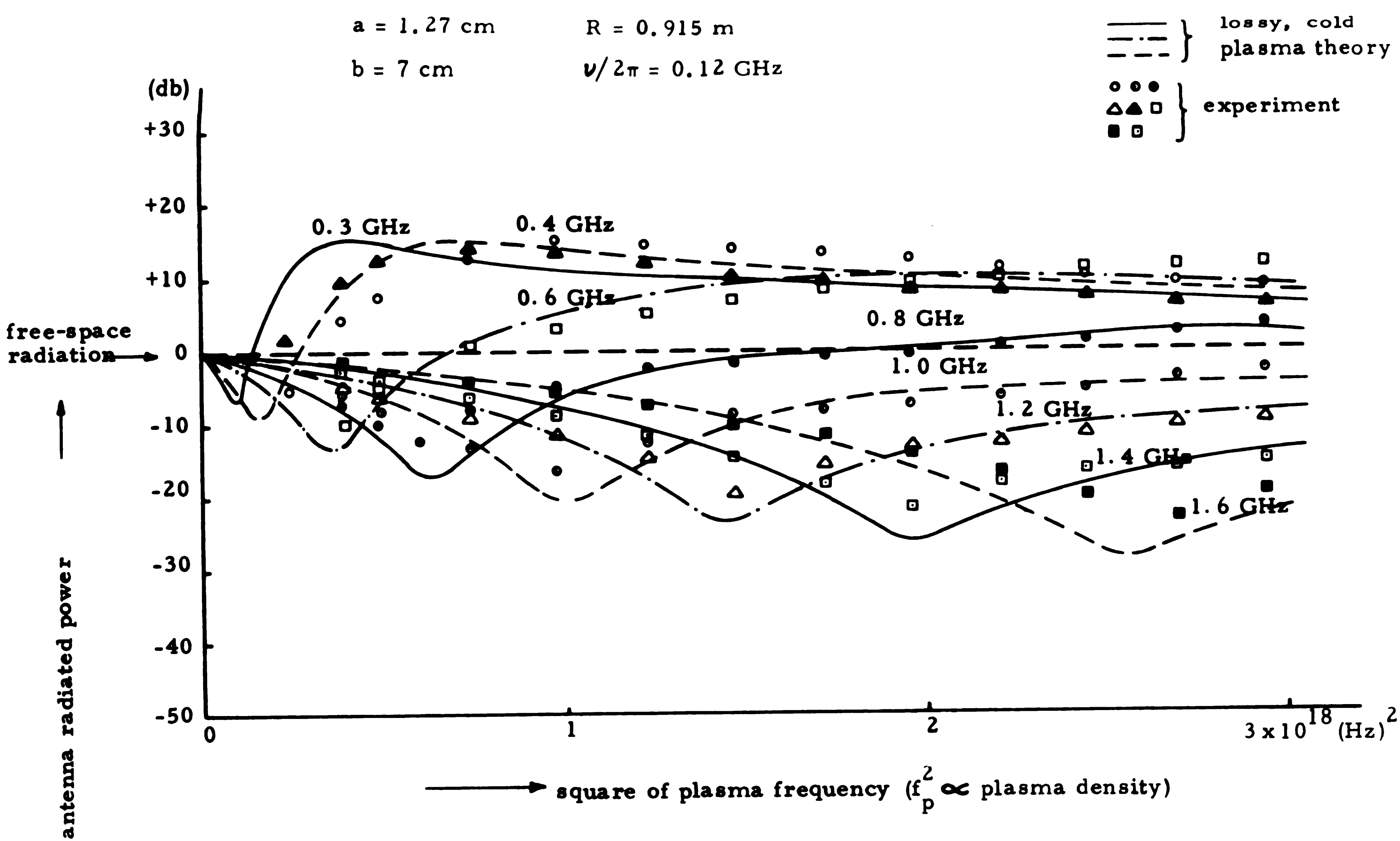

Fig. 4.5 Experimental and theoretical radiation of a spherical antenna (a = 1.27 cm) in a plasma driven at various frequencies as a function of plasma density.

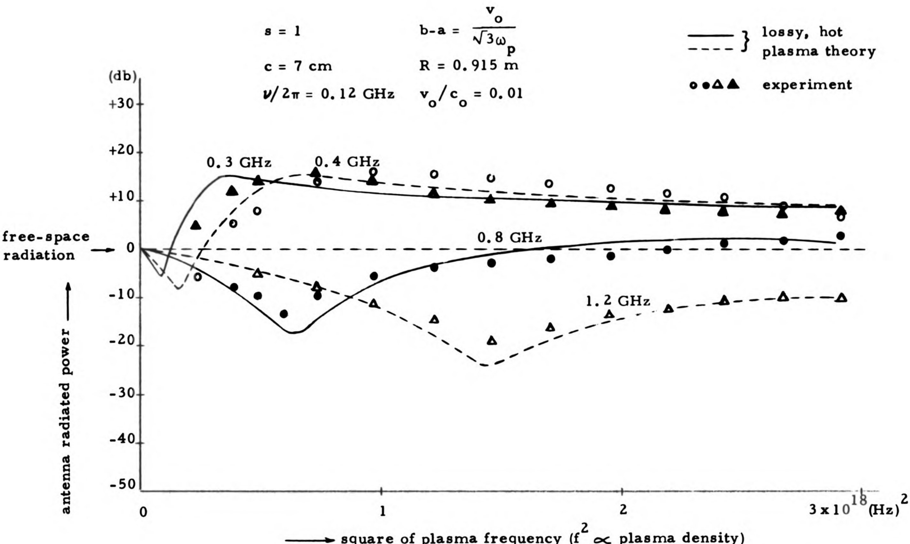

Fig. 4.6 Experimental and theoretical radiation of a spherical antenna (a = 2.54 cm) in a hot plasma driven at various frequencies as a function of plasma density.

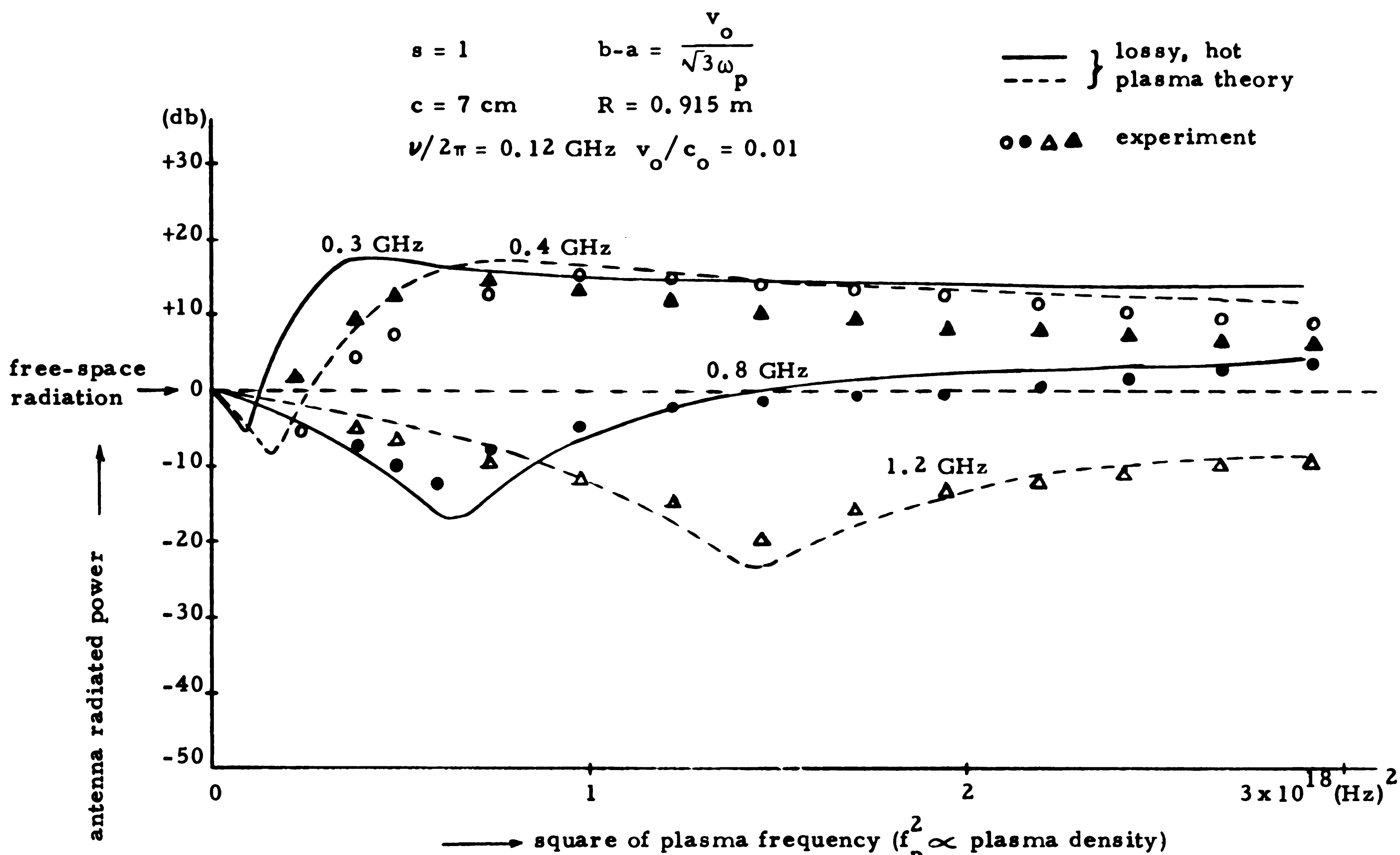

Fig. 4.7 Experimental and theoretical radiation of a spherical antenna (a = 1.27 cm) in a hot plasma driven at various frequencies as a function of plasma density.

CHAPTER 5

RADIATION OF A CYLINDRICAL ANTENNA IMMERSED IN A LOSSY, COLD PLASMA OF INFINITE EXTENT

5.1 Introduction

A cylindrical antenna is one of the most commonly used radiators. When it is used on a space vehicle, it is often operated in a plasma region. The electrical properties of a cylindrical antenna in a plasma medium thus become important in view of practical and academic reasons. In this chapter, the electrical properties of a cylindrical dipole antenna immersed in a lossy, cold plasma of infinite extent is studied.

Many workers have theoretically investigated the electrical characteristics of a cylindrical antenna immersed in a hot plasma of infinite extent. Chen[7] studied a thin cylindrical antenna of finite length with a sinusoidally distributed current in a hot plasma. Balmain[16] treated the problem of an electrically short antenna with a triangular current distribution immersed in a hot plasma. Their results gave the antenna resistance only valid for $\omega_p/\omega < 1$ where

ω_p and ω are the plasma and antenna frequencies. Kuehl[17,18,19] studied the same problem, but solved the Boltzmann equation instead of using the simpler hydrodynamic plasma equations. An interesting result of his work is the existence of the antenna resistance for $\omega_p/\omega > 1$. Since the Poynting-vector and induced-emf methods which require a certain prescribed current distribution have been adopted to calculate the impedance of the antenna in those papers, the antenna reactance was not determined. Meltz, Freyheit and Lustig[20] investigated an infinite cylindrical antenna covered by a set of coaxial plasma layers, based on a variational formulation. They were able to deduce both the antenna resistance and the antenna reactance for a wide range of ω_p/ω. There are many other theoretical papers which are not mentioned here.

To our best knowledge, there is no theoretical paper which accurately determines the complete impedance of a cylindrical antenna of finite length immersed in a hot plasma of finite or infinite extent. This problem is intractable both mathematically and physically. In this study a simpler cold-plasma model is chosen to make the analysis tractable.

Employing the King-Middleton theory[21] and King's modified method[22], the complete input impedance of a cylindrical antenna is determined as a function of antenna dimensions and plasma parameters. The effect of the collision frequency on the antenna impedance is carefully examined.

5.2 Geometry and Statement of the Problem

The geometry of the problem is shown in Fig. 3.1. A cylindrical dipole antenna of radius a and length 2h is center-driven at $z = 0$ by an idealized delta function generator with a voltage of V and an angular frequency of ω. The antenna surface is assumed to be perfectly conducting except at the small gap 2δ at the center of the antenna. The antenna is immersed in an infinite, homogeneous and cold plasma. The plasma is assumed to be a weakly ionized gas and can be characterized as a lossy medium with a permittivity of $\epsilon = \epsilon_o \left(1 - \frac{\omega_p^2}{\omega^2 + \nu^2}\right)$, a conductivity of $\sigma = \frac{n_o e^2}{m_e} \frac{\nu}{\omega^2 + \nu^2}$, and a permeability of $\mu = \mu_o$ where ω_p is the plasma frequency, n_o is the density of plasma, ν is the collision frequency of electrons with neutral particles, e and m_e are the charge and mass of electrons, and ϵ_o and μ_o are the permittivity and permeability of free space.

In order to employ the quasi-one-dimensional theory, the following dimensional restrictions on the antenna are made:

$$\begin{cases} h \gg a \\ \beta a = \dfrac{2\pi a}{\lambda} \ll 1 \end{cases} \tag{5.1}$$

where β is the wave number and λ is the wave length in this medium. Based on these thin-wire assumptions, the current can be considered[23] to be concentrated along the axis of the antenna when calculating the field or vector potential at a point in the medium. Even in the vicinity of the antenna surface, the error caused by this approximation is insignificant.

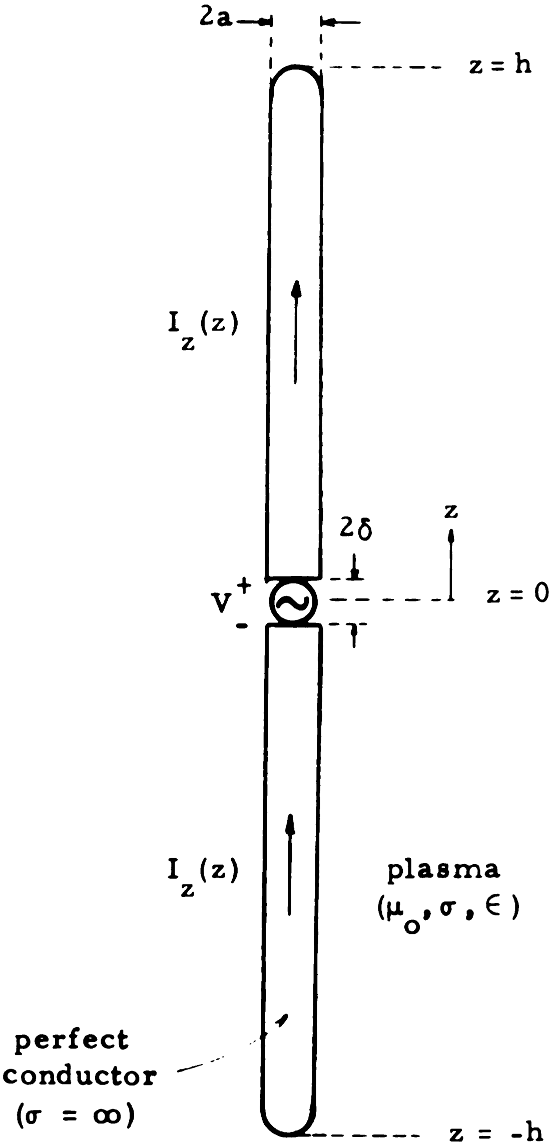

Fig. 5.1 A cylindrical antenna immersed in an infinite, lossy and cold plasma.

In this study rationalized MKS units are used. Cylindrical coordinates (r, θ, z) are adopted and the rotational symmetry is assumed. The time dependences for the radiating source and all the fields are assumed to be $\exp(j\omega t)$.

5.3 Basic Equations

The basic equations which govern the system are Maxwell's equations. For harmonic time dependence of $\exp(j\omega t)$, Maxwell's equations in this infinite, homogeneous and lossy medium can be written as

$$\left\{\begin{array}{ll} \nabla \cdot \vec{E} = \dfrac{\rho^s}{\xi} & (5.2) \\ \nabla \times \vec{E} = -j\omega\vec{B} & (5.3) \\ \nabla \times \vec{B} = \mu_o \vec{J}^s + j\omega\mu_o \xi \vec{E} & (5.4) \\ \nabla \cdot \vec{B} = 0 & (5.5) \end{array}\right.$$

where $\vec{E}$ and $\vec{B}$ are electric and magnetic fields, ξ is the complex permittivity given by

$$\xi = \epsilon\left(1 - j\frac{\sigma}{\omega\epsilon}\right), \qquad (5.6)$$

and $\vec{J}^s$ and ρ^s are the volume densities of the source current and charge which are related by the continuity equation,

$$\nabla \cdot \vec{J}^s + j\omega\rho^s = 0 . \qquad (5.7)$$

It is convenient for this case to solve the Maxwell's equations by introducing the vector potential $\vec{A}$ and the scalar potential Φ. From Eqs. (5.5) and (5.2) $\vec{B}$ and $\vec{E}$ can thus be defined in terms of these potential functions as

$$\vec{B} = \nabla \times \vec{A} \tag{5.8}$$

$$\vec{E} = -\nabla\Phi - j\omega\vec{A} \,. \tag{5.9}$$

The substitution of Eqs. (5.8) and (5.9) into Eqs. (5.4) and (5.3) leads to two inhomogeneous wave equations,

$$\nabla^2\vec{A} + k^2\vec{A} = -\mu_o\vec{J}^s \tag{5.10}$$

$$\nabla^2\Phi + k^2\Phi = -\frac{\rho^s}{\xi} \quad , \tag{5.11}$$

subject to the Lorentz condition of

$$\nabla\cdot\vec{A} + \frac{jk^2}{\omega}\Phi = 0 \tag{5.12}$$

where k is the complex propagation constant given by

$$k^2 = \omega^2\mu_o\xi \,. \tag{5.13}$$

If we write

$$k = \beta - j\alpha \,, \tag{5.14}$$

β and α can be expressed as

$$\beta = \frac{\beta_o}{\sqrt{2}}\left\{1 - \frac{\omega_p^2}{\omega^2+\nu^2} + \left[1 - \frac{2\omega_p^2}{\omega^2+\nu^2} + \frac{\omega_p^4}{\omega^2(\omega^2+\nu^2)}\right]^{\frac{1}{2}}\right\}^{\frac{1}{2}} \tag{5.15}$$

$$\alpha = \frac{\beta_o}{\sqrt{2}}\left\{-1 + \frac{\omega_p^2}{\omega^2+\nu^2} + \left[1 - \frac{2\omega_p^2}{\omega^2+\nu^2} + \frac{\omega_p^4}{\omega^2(\omega^2+\nu^2)}\right]^{\frac{1}{2}}\right\}^{\frac{1}{2}} \tag{5.16}$$

where β is the wave number in this lossy medium, α is the attenuation constant, and β_o is the wave number in free space defined as

$$\beta_o = \omega\sqrt{\mu_o\epsilon_o} \,. \tag{5.17}$$

Equations (5.10) and (5.11) are also called Helmholtz's equations.

The general solutions to Eqs. (5.10) and (5.11) are given by

$$\vec{A}(\vec{r}) = \frac{\mu_o}{4\pi}\left[\int_{V'} \vec{J}^s(\vec{r}\,')\frac{e^{-jkR}}{R}\,dV' + \int_{S'} \vec{K}^s(\vec{r}\,')\frac{e^{-jkR}}{R}\,dS'\right] \tag{5.18}$$

$$\Phi(\vec{r}) = \frac{1}{4\pi\xi}\left[\int_{V'} \rho^s(\vec{r}\,')\frac{e^{-jkR}}{R}\,dV' + \int_{S'} \eta^s(\vec{r}\,')\frac{e^{-jkR}}{R}\,dS'\right] \tag{5.19}$$

where $\vec{K}^s$ and η^s are the surface densities of the source current and charge, R is the distance between the observation point and the source point, and $e^{-jkR}/4\pi R$ is the Green's function.

For the case of a thin-wire linear antenna we have

$$\vec{J}^s(\vec{r}\,')dV' + \vec{K}^s(\vec{r}\,')dS' = \hat{z}\,I_z(z')dz' \tag{5.20}$$

$$\rho^s(\vec{r}\,')dV' + \eta^s(\vec{r}\,')dS' = q(z')dz', \tag{5.21}$$

since the antenna current flows primarily along the axial or z-direction.

Using Eqs. (5.20) and (5.21), Eqs. (5.18) and (5.19) can be reduced to

$$\vec{A}(\vec{r}) = \frac{\mu_o}{4\pi}\int_{-h}^{h} \hat{z}\,I_z(z')\frac{e^{-jkR}}{R}\,dz' \tag{5.22}$$

$$\Phi(\vec{r}) = \frac{1}{4\pi\xi}\int_{-h}^{h} q(z')\frac{e^{-jkR}}{R}\,dz' \tag{5.23}$$

where I_z and q are the source current and charge densities per unit length along the antenna.

Using the Lorentz condition Eq. (5.12), Eq. (5.9) becomes

$$\vec{E} = -\frac{j\omega}{k^2} \nabla(\nabla\cdot\vec{A}) - j\omega\vec{A} . \qquad (5.24)$$

Thus $\vec{E}$ and $\vec{B}$ fields are expressed in terms of $\vec{A}$ only. If we can determine $\vec{A}$ from Eq. (5.22), all the fields are then obtained from Eqs. (5.8) and (5.24).

5.4 Boundary Conditions

It is shown by King and Harrison[24] that the boundary conditions for an antenna immersed in a lossy medium are the same as for an antenna in free space. The King-Middleton's method is then adopted to solve the present problem.

Due to the symmetry about the origin and the end condition of the antenna, a pair of boundary conditions on the antenna current can be expressed as

$$\begin{cases} I_z(z) = I_z(-z) \\ I_z(\pm h) = 0 \end{cases} \qquad (5.25)$$

From the boundary condition that the tangential component of electric field should be continuous at the surface of the antenna, it follows

$$E_z^a(r = a^-) = E_z^i(r = a^+) \qquad (5.26)$$

where $E_z^i(r = a^+)$ is the induced electric field just outside of the antenna surface at $r = a^+$, which is maintained by the current and charge on the antenna, and $E_z^a(r = a^-)$ is the electric field just inside the antenna surface at $r = a^-$.

5.5 Integral Equation for the Current

Since the cylindrical antenna is assumed to be constructed of a perfect conductor, its internal impedance per unit length Z^i is equal to zero and the electric field inside the conductor surface at $r = a^-$ vanishes except at the small gap, i.e.,

$$E_z^a(z) = \begin{cases} 0 & \text{for } -h \leq z \leq -\delta \text{ and } \delta \leq z \leq h \\ -\dfrac{V}{2\delta} & \text{for } -\delta < z < \delta \end{cases} \qquad (5.27)$$

where V is the applied voltage and 2δ is the gap width.

The applied voltage across the gap at $z = 0$ is

$$V = -\int_{-\delta}^{\delta} E_z^a(z)\, dz \,. \qquad (5.28)$$

In the limit of a slice generator where $2\delta \rightarrow 0$, the tangential electric field on the antenna surface can be expressed as

$$\lim_{2\delta \rightarrow 0} E_z^a(z) = -V_o\, \delta(z) \qquad (5.29)$$

where $\delta(z)$ is the Dirac delta function.

Since the current flows only in the axial direction, from Eq. (5.22) the vector potential has only the z-component, i.e.,

$$\vec{A} = \hat{z} A_z \,. \qquad (5.30)$$

From Eqs. (5.30) and (5.24) we obtain the induced electric field on the antenna surface as

$$E_z^i(z) = -\frac{j\omega}{k^2}\left[\frac{\partial^2}{\partial z^2} + k^2\right] A_z(z) . \qquad (5.31)$$

In order to satisfy the boundary condition given by Eq. (5.26), Eqs. (5.29) and (5.31) are equated to yield a second-order inhomogeneous differential equation for the vector potential at the antenna surface as

$$\left[\frac{\partial^2}{\partial z^2} + k^2\right] A_z(z) = -\frac{jk^2}{\omega} V_o \delta(z) . \qquad (5.32)$$

The complementary solution of Eq. (5.32) is obtained easily as

$$A_z^c(z) = -\frac{jk}{\omega} (c_1 \cos kz + c_2 \sin kz) \qquad (5.33)$$

where c_1 and c_2 are arbitrary constants, and the parameter $(-\frac{jk}{\omega})$ is added merely for convenience.

Since the particular integral for an equation of the form

$$\frac{d^2y}{dx^2} + b^2 y = f(x)$$

is given by

$$y^p(x) = \frac{1}{b} \int_o^x f(s) \sin b(x-s) ds ,$$

the particular solution of Eq. (5.32) can be verified to be

$$A_z^p(z) = -\frac{jk}{2\omega} V_o \sin k|z| . \qquad (5.34)$$

The general solution to Eq. (5.32) is then

$$A_z(z) = A_z^c(z) + A_z^p(z)$$

$$= -\frac{jk}{\omega}\,[\,c_1 \cos kz + c_2 \sin kz + \frac{V}{2}\,\sin k|z|\,]. \tag{5.35}$$

From Eq. (5.22) we obtain the vector potential on the antenna surface as

$$A_z(z) = \frac{\mu_o}{4\pi}\int_{-h}^{h} I_z(z')\,K_a(z, z')\,dz' \tag{5.36}$$

where $K_a(z, z')$ is the kernel defined as

$$K_a(z, z') = \frac{e^{-jkR}}{R}$$

and

$$R = \sqrt{(z-z') + a^2}$$

By the summetry of the antenna current, $I_z(z) = I_z(-z)$, it can be shown from Eq. (5.36) that the vector potential is also symmetric about the origin, i.e., $A_z(z) = A_z(-z)$. It is obvious that the arbitrary constant c_2 should be equal to zero and Eq. (5.35) reduces to

$$A_z(z) = -\frac{jk}{\omega}\,[\,c_1 \cos kz + \frac{V}{2}\sin k|z|\,]. \tag{5.37}$$

By letting $z = h$ in Eq. (5.37), c_1 can be determined as

$$c_1 = \frac{1}{\cos kh}\,[\,\frac{j\omega}{k}\,A_z(h) - \frac{V}{2}\,\sin kh]\ . \tag{5.38}$$

Using Eqs. (5.36) and (5.37) we can write an equation such as,

$$\frac{4\pi}{\mu_o}[A_z(z) - A_z(h)] = \int_{-h}^{h} I_z(z')[K_a(z, z') - K_a(h, z')]$$

$$= -\frac{j4\pi k}{\omega\mu_o}[c_1(\cos kz - \cos kh) + \frac{V}{2}(\sin k|z| - \sin kh)]. \quad (5.39)$$

The substitution of Eq. (5.38) in Eq. (5.39) leads to

$$\int_{-h}^{h} I_z(z')K_d(z, z')dz' = \frac{j4\pi k}{\omega\mu_o \cos kh}[\frac{V}{2}\sin k(h - |z|)$$

$$- \frac{j\omega}{k} A_z(h)(\cos kz - \cos kh)] \quad (5.40)$$

where $K_d(z, z')$ is the difference kernel defined as

$$K_d(z, z') = K_a(z, z') - K_a(h, z')$$

$$= \frac{e^{-jkR}}{R} - \frac{e^{-jkR_h}}{R_h}$$

and

$$R_h = \sqrt{(h-z') + a^2} \; .$$

Equation (5.40) is an integral equation for the antenna current which is valid for $-h \leq z \leq h$ and convenient for the further development.

5.6 Approximate Solution of the Integral Equation

The current distribution on the antenna can be determined quite accurately by solving the integral equation (5.40) approximately following King's modified method[22]. In this method the antenna current is assumed to be proportional to the vector potential difference (the difference between the vector potential at a point on the antenna and that at the end of antenna). In other words, it is assumed that the ratio of the vector potential difference to the antenna current is relatively constant along the antenna. Since $A_z(z) - A_z(h)$ vanishes at $z = \pm h$, it is consistent with the end condition of $I_z(z = \pm h) = 0$.

By the peaking property of the kernels

$$K_a(z, z') \sim \delta(z-z')$$

$$K_a(h, z') \sim \delta(h-z')$$

and from Eq. (5.39) it follows that

$$\frac{4\pi}{\mu_o}[A_z(z) - A_z(h)] \sim I_z(z) - I_z(h).$$

Since $I_z(h) = 0$ as imposed in Eq. (5.25), then

$$I_z(z) \sim A_z(z) - A_z(h)$$

and the antenna current can be assumed to have the form

$$I_z(z) = A\, I_c(z) + B\, I_s(z) \tag{5.41}$$

where A and B are arbitrary constants and

$$I_c(z) = \cos kz - \cos kh$$

$$I_s(z) = \sin k(h - |z|).$$

Note that Eq. (5.41) satisfies the boundary conditions given by Eq. (5.25).

Since the difference kernel is a complex function, it can be separated into real and imaginary parts as

$$K_d(z, z') = K_{dr}(z, z') + j K_{di}(z, z') \tag{5.42}$$

where

$$K_{dr}(z, z') = \frac{e^{-\alpha R}}{R} \cos \beta R - \frac{e^{-\alpha R_h}}{R_h} \cos \beta R_h$$

$$K_{di}(z, z') = -\frac{e^{-\alpha R}}{R} \sin \beta R + \frac{e^{-\alpha R_h}}{R_h} \sin \beta R_h$$

Substituting Eqs. (5.41) and (5.42) into Eq. (5.40) we have

$$\int_{-h}^{h} [A I_c(z') + B I_s(z')][K_{dr}(z, z') + j K_{di}(z, z')] dz'$$

$$= \frac{j4\pi k}{\omega\mu_o \cos kh} \left[\frac{V}{2} \sin k(h - |z|) - \frac{j\omega}{k} A_z(h)(\cos kz - \cos kh) \right] \tag{5.43}$$

Since $K_{dr}(z, z')$ becomes very large when z' is near z, it follows that the principal contribution to the part of the integral that has $K_{dr}(z, z')$ as kernel comes from elements of current near $z' = z$. On the other hand, K_{di} remains very small when z' is near z. This suggests that the contribution to the part of the integral that has $K_{di}(z, z')$ as kernel comes from all the elements of current along the antenna. Due to this peaking property of kernel $K_{dr}(z, z')$ and non peaking property of kernel $K_{di}(z, z')$, various integrals on the left hand side of Eq. (5.43) can be equated to the functions on the right hand side of Eq. (5.43) in the following manner:

$$\int_{-h}^{h} (\cos kz' - \cos kh) K_{dr}(z, z')dz' \sim (\cos kz - \cos kh) \qquad (5.44a)$$

$$\int_{-h}^{h} (\cos kz' - \cos kh) K_{di}(z, z')dz' \sim (\cos kz - \cos kh) \qquad (5.44b)$$

$$\int_{-h}^{h} \sin k(h - |z'|) K_{dr}(z, z')dz' \sim \sin\beta_o(h - |z|) \qquad (5.44c)$$

$$\int_{-h}^{h} \sin k(h - |z'|) K_{di}(z, z')dz' \sim (\cos kz - \cos kh) \qquad (5.44d)$$

where Eqs. (5.44a) and (5.44c) are based on the characteristics of kernel $K_{dr}(z, z')$, and Eqs. (5.44b) and (5.44d) are justified from numerical calculation. Indeed, it can be shown numerically that the integrals on the left side of Eqs. (5.44b) and (5.44d) are roughly proportional to the shifted cosine function $(\cos kz - \cos kh)$.

These properties suggest that Eq. (5.43) can be split into two parts by equating the corresponding terms on the right and left hand sides of this equation as follows:

$$\int_{-h}^{h} [A I_c(z')K_d(z, z') + j B I_s(z')K_{di}(z, z')] dz' = \frac{4\pi}{\mu_o \cos kh} A_z(h)(\cos kz - \cos kh) \qquad (5.45)$$

$$\int_{-h}^{h} B I_s(z') K_{dr}(z, z')dz' = \frac{j\, 2\pi kV}{\omega \mu_o \cos kh} \sin k(h - |z|) \qquad (5.46)$$

Equations (5.45) and (5.46) can be rearranged as

$$\int_{-h}^{h} [A \frac{I_c(z')}{I_c(z)} K_d(z, z') + jB \frac{I_s(z')}{I_c(z)} K_{di}(z, z')] dz' = \frac{4\pi}{\mu_o \cos kh} A_z(h) \qquad (5.47)$$

$$\int_{-h}^{h} B \frac{I_s(z')}{I_s(z)} K_{dr}(z, z')\, dz' = \frac{j\, 2\pi k V}{\omega \mu_o \cos kh} \tag{5.48}$$

The current $I_z(z)$ can be expressed in terms of a reference current $I_z(z_o)$ and a distribution function $f(z)$ that is unknown. Let

$$I_z(z) = I_z(z_o) f(z) . \tag{5.49}$$

From Eq. (5.49) we have

$$I_z(z') = I_z(z_o) f(z') . \tag{5.50}$$

Then

$$I_z(z') = I_z(z) \frac{f(z')}{f(z)} = I_z(z)\, g(z, z')$$

and

$$g(z, z') = \frac{I_z(z')}{I_z(z)} \tag{5.51}$$

It has been shown by King[21] that a function $\psi(z)$ can be defined as

$$\psi(z) = \frac{4\pi}{\mu_o} \frac{A_z(z)}{I_z(z)} = \psi + \gamma(z) \tag{5.52}$$

where ψ is the constant part of $\psi(z)$ and is called as the expansion parameter. $\psi(z)$ is roughly constant in the central part of the antenna but increases rapidly at the ends of the antenna. Usually $\gamma(z)$ is chosen to be close to zero at the point of maximum current. It can be shown that $\gamma(z)$ remains very small over the central part of the antenna and has a large value only at the ends of the antenna. Therefore, we can let

$$\psi = \psi(z_1) = \frac{4\pi}{\mu} \frac{A_z(z_1)}{I_z(z_1)} \tag{5.53}$$

where z_1 is the point of maximum current on the antenna. It has been commonly assumed that $z_1 = 0$ when $h \leq \lambda/4$ and $z_1 = h - \lambda/4$ when $h > \lambda/4$. Using Eqs. (5.52), (5.36) and (5.51) we can express $\psi(z)$ in another form as

$$\psi(z) = \int_{-h}^{h} g(z, z') K(z, z') dz' \tag{5.54}$$

where $K(z, z')$ stands for an arbitrary kernel. Thus from Eqs. (5.53) and (5.54) we obtain an expression for the expansion parameter,

$$\psi = \psi(z_1) = \int_{-h}^{h} [g(z, z')K(z, z')]_{z=z_1} dz' . \tag{5.55}$$

Using Eq. (5.55), Eqs. (5.47) and (5.48) can be reduced to

$$A\,\psi_{d1} + j\,B\,\psi_{d2} = \frac{4\pi}{\mu_o \cos kh} A_z(h) \tag{5.56}$$

$$B\,\psi_{d3} = \frac{j\,2\pi k V}{\omega\,\mu_o \cos kh} \tag{5.57}$$

where

$$\psi_{d1} = \int_{-h}^{h} [g_{d1}(z, z')K_d(z, z')]_{z=z_1} dz'$$

$$\psi_{d2} = \int_{-h}^{h} [g_{d2}(z, z')K_{di}(z, z')]_{z=z_1} dz'$$

$$\psi_{d3} = \int_{-h}^{h} [\, g_{d3}(z, z')\, K_{dr}(z, z')]_{z=z_1} \, dz'$$

and

$$g_{d1}(z, z') = \frac{I_c(z')}{I_c(z)} = \frac{\cos kz' - \cos kh}{\cos kz - \cos kh}$$

$$g_{d2}(z, z') = \frac{I_s(z')}{I_c(z)} = \frac{\sin k(h - |z'|)}{\cos kz - \cos kh}$$

$$g_{d3}(z, z') = \frac{I_s(z')}{I_s(z')} = \frac{\sin k(h - |z'|)}{\sin k(h - |z|)} \; .$$

From Eq. (5.36) we have

$$\frac{4\pi}{\mu_o} A_z(h) = \int_{-h}^{h} I_z(z') K_a(h, z') dz' \tag{5.58}$$

The substitution of Eq. (5.41) into Eq. (5.58) gives

$$\frac{4\pi}{\mu_o} A_z(h) = A\, T_c + B\, T_s \tag{5.58}$$

where

$$T_c = \int_{-h}^{h} I_c(z')\, K_a(h, z') dz'$$

$$T_s = \int_{-h}^{h} I_s(z') K_a(h, z') dz' \; .$$

Substituting Eq. (5.58) into Eq. (5.56), an expression is obtained as

$$A = B\, T(h) \tag{5.59}$$

where

$$T(h) = \frac{T_s - j\psi_{d2}\cos kh}{\psi_{d1}\cos kh - T_c}$$

From Eq. (5.57) we obtain

$$B = \frac{j\,2\pi k V}{\psi_{d3}\omega\mu_o \cos kh} \tag{5.60}$$

The combination of Eqs. (5.41), (5.59) and (5.60) leads to the current distribution along the cylindrical antenna as

$$I_z(z) = \frac{j\,2\pi kV}{\psi_{d3}\omega\mu_o\cos kh}\left[\sin k(h - |z|) + T(h)(\cos kz - \cos kh)\right] \tag{5.61}$$

Equation (5.61) is the final expression for the antenna current.

5.7 Input Impedance of the Cylindrical Antenna

The input impedance of the cylindrical dipole antenna is defined as

$$Z_{in} = \frac{V}{I_z(z=0)} = R_{in} + jX_{in}$$

where R_{in} is the input resistance and X_{in} is the input reactance of the antenna.

From Eq. (5.61), this impedance can be obtained as

$$Z_{in} = \frac{\psi_{d3}\omega\mu_o\cos kh}{j2\pi k[\sin kh + T(h)(1 - \cos kh)]} \tag{5.62}$$

where the symbols can be expressed more explicitly as follows:

$$T(h) = \frac{T_s - j\psi_{d2}\cos kh}{\psi_{d1}\cos kh - T_c}$$

$$T_c = \int_{-h}^{h} (\cos kz' - \cos kh)\, \frac{\exp(-jk\sqrt{(h-z')^2 + a^2})}{\sqrt{(h-z')^2 + a^2}}\, dz'$$

$$T_s = \int_{-h}^{h} \sin k(h - |z'|)\, \frac{\exp(-jk\sqrt{(h-z')^2 + a^2})}{\sqrt{(h-z')^2 + a^2}}\, dz'$$

$$\psi_{d1} = \frac{1}{\cos kz_1 - \cos kh} \int_{-h}^{h} (\cos kz' - \cos kh) \left[\frac{\exp(-jk\sqrt{(z_1-z')^2 + a^2})}{\sqrt{(z_1 - z')^2 + a^2}} - \frac{\exp(-jk\sqrt{(h-z')^2 + a^2})}{\sqrt{(h-z')^2 + a^2}} \right] dz'$$

$$\psi_{d2} = \frac{-1}{\cos kz_1 - \cos kh} \int_{-h}^{h} \sin k(h - |z'|) \left[\frac{\exp(-\alpha\sqrt{(z_1-z')^2 + a^2}}{\sqrt{(z_1 - z')^2 + a^2}} \sin\beta\sqrt{(z_1-z')^2 + a^2} - \frac{\exp(-\alpha\sqrt{(h-z')^2 + a^2})}{\sqrt{(h-z')^2 + a^2}} \sin\beta\sqrt{(h-z')^2 + a^2} \right] dz'$$

$$\psi_{d3} = \frac{1}{\sin k(h - |z_1|)} \int_{-h}^{h} \sin k(h - |z'|) \left[\frac{\exp(-\alpha\sqrt{(z_1-z)^2 + a^2})}{\sqrt{(z_1-z')^2 + a^2}} \cos\beta\sqrt{(z_1-z') + a^2} - \frac{\exp(-\alpha\sqrt{(h-z')^2 + a^2})}{\sqrt{(h-z')^2 + a^2}} \cos\beta\sqrt{(h-z')^2 + a^2} \right] dz'$$

$$z_1 = 0 \qquad \text{when} \qquad h \le \frac{\lambda}{4}$$

$$z_1 = h - \frac{\lambda}{4} \qquad \text{when} \qquad h > \frac{\lambda}{4}\,.$$

5.8 Numerical Results

The input impedance of a cylindrical dipole antenna as expressed in Eq. (5.62) has been numerically calculated as a function of the antenna dimensions and plasma parameters. All the integrals given in Eq. (5.62) are numerically evaluated by the Simpson's rule using a CDC 3600 computer. The theoretical results on the input impedances of cylindrical monopole antennas of various lengths are then calculated from $Z_{in}/2$ where Z_{in} is given by Eq. (5.62), and graphically shown in Figs. 5.2 to 5.5. The input impedance is plotted as a function of ω_p^2/ω^2 with ν/ω as the running parameter. The value of ω_p^2/ω^2 is directly proportional to the plasma density when the antenna frequency is kept constant, and ν/ω is the ratio between the collision frequency and the antenna frequency. The antenna is assumed to be driven at the frequencies of 1.8 and 2.0 GHz.

In Figs. 5.2 to 5.5, the solid lines represent the antenna input resistances while the dotted lines stand for the antenna input reactances. Observing from these figures, the effects of the collision frequency on the antenna input impedance can be summarized as follows:

(1) For low plasma density ($\omega_p^2/\omega^2 < 0.4$) and low collision frequency ($\nu/\omega < 0.01$), as the plasma density is increased the antenna resistance decreases and the antenna reactance becomes more negative in such a way that the antenna behaves

progressively shorter electrically. The collision frequency has almost no effect on the antenna impedance.

(2) For low plasma density ($\omega_p^2/\omega^2 < 0.4$) and high collision frequency ($\nu/\omega > 0.01$), the antenna still behaves progressively shorter electrically as the plasma density is increased. The collision frequency has small effect on the antenna resistance but still no significant effect on the antenna reactance.

(3) For $0.4 < \omega_p^2/\omega^2 < 0.85$ and $\nu/\omega < 0.01$, the antenna behaves as the same in case (1).

(4) For $0.4 < \omega_p^2/\omega^2 < 0.85$ and $\nu/\omega > 0.01$, as the plasma density is increased the antenna resistance tends to increase monotonically and the antenna reactance behaves in an opposite way. The effect of the collision frequency on the antenna impedance becomes more obvious over this range. The increase of the collision frequency causes the increase of the antenna resistance and makes the antenna reactance less negative. This implies that over this range there is more energy transferred from the electromagnetic wave to the electron gas of plasma.

(5) In the range of $0.85 < \omega_p^2/\omega^2 < 1.15$, there are sharp peaks of antenna resistance and a sharp change from capacitive to inductive for the antenna reactance when the plasma frequency approaches the antenna frequency. Over this range, there is

tremendous energy transferred from the electromagnetic wave to the electron gas of plasma.

(6) When $\omega_p^2/\omega^2 > 1.15$, both antenna resistance and reactance decrease rapidly as the plasma density is increased.

The significant findings of this study are: (1) the peaking of antenna resistance at $\omega \sim \omega_p$ due to the collision, and (2) the change of sign for the antenna reactance at $\omega \sim \omega_p$.

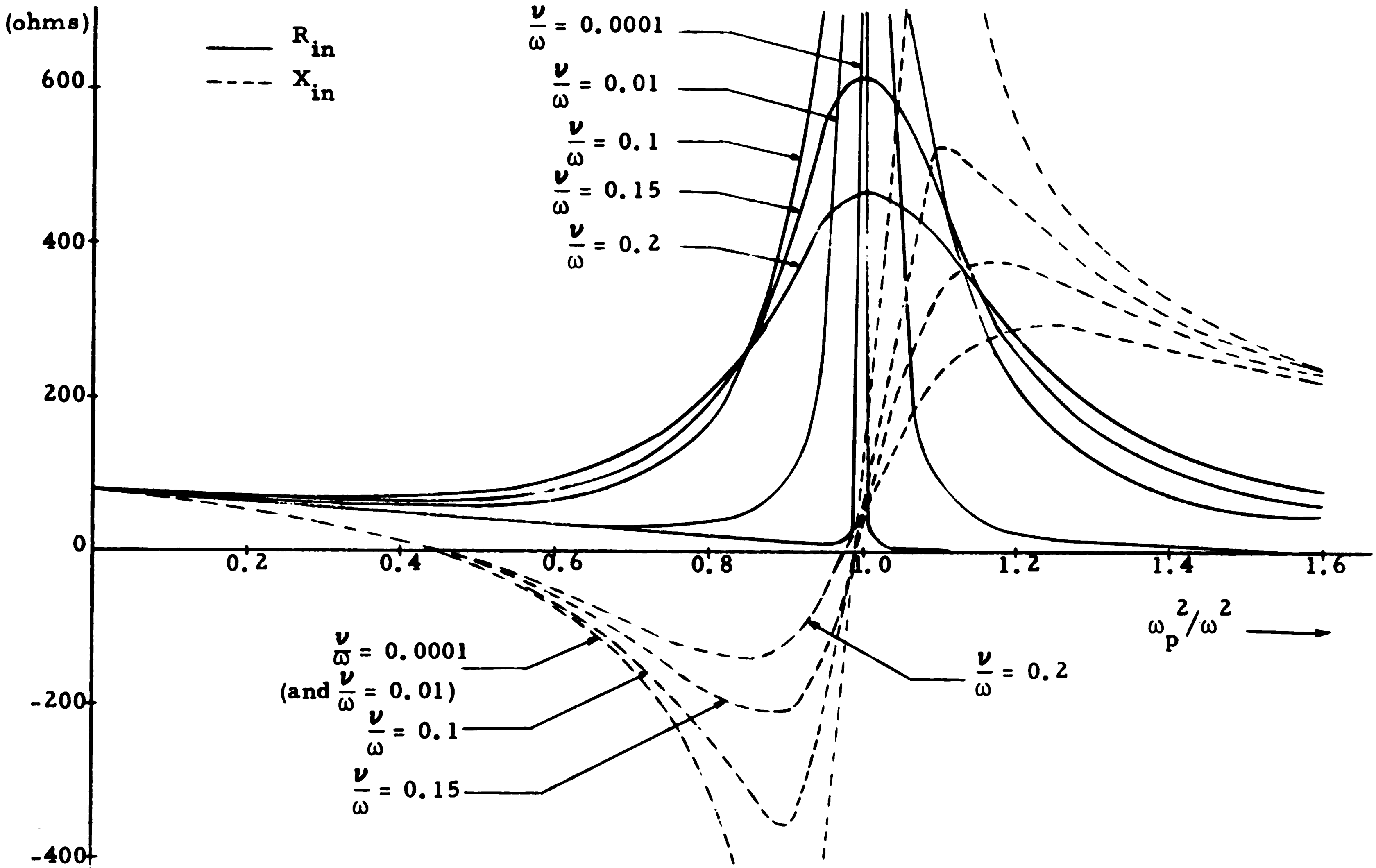

Fig. 5.2 Theoretical input impedance of a monopole ($h/\lambda_o = 0.313$, $a/\lambda_o = 0.008$) in a cold plasma as a function of plasma density.

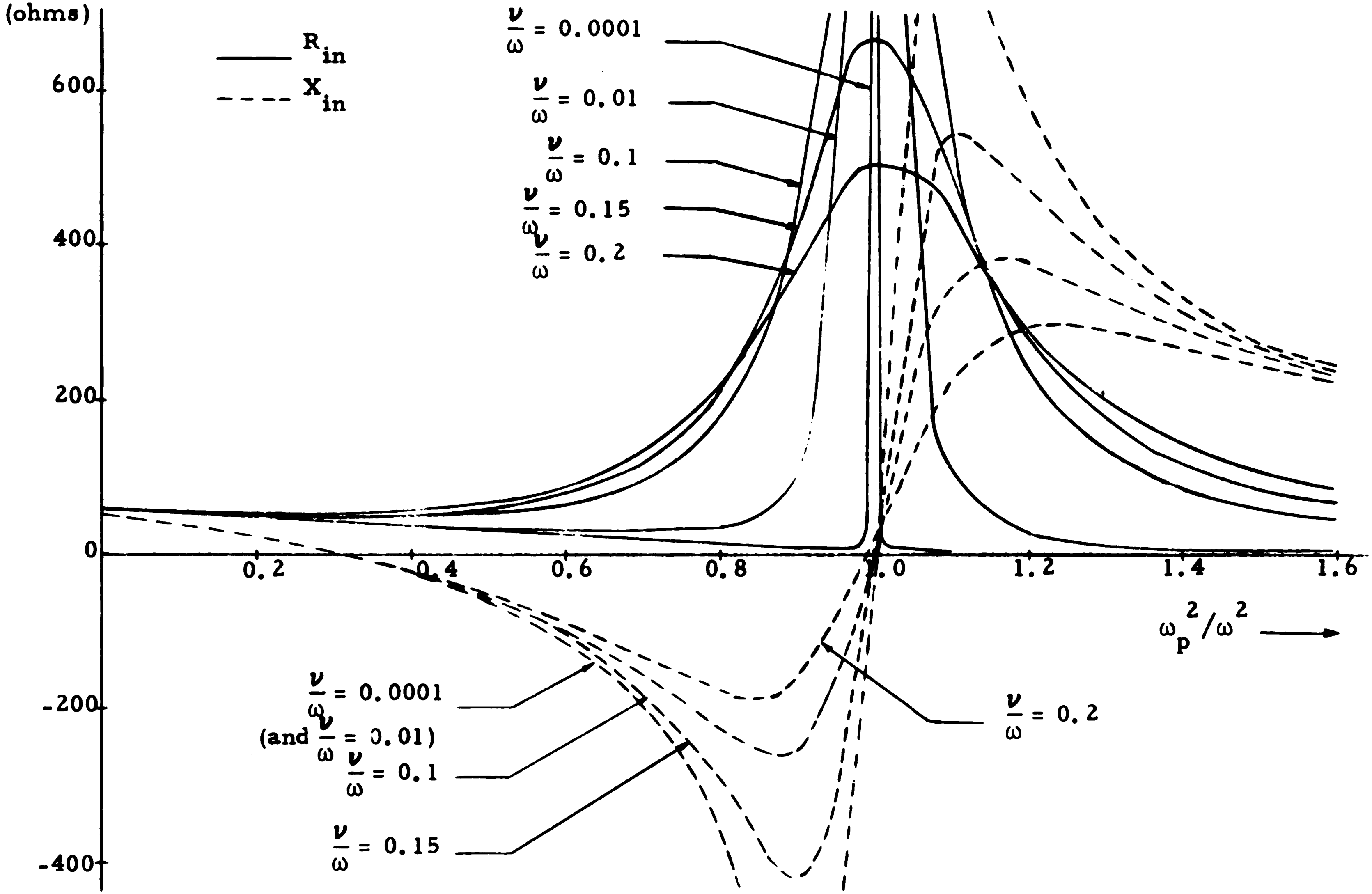

Fig. 5.3 Theoretical input impedance of a monopole (h/λ_o = 0.282, a/λ_o = 0.0072) in a cold plasma as a function of plasma density.

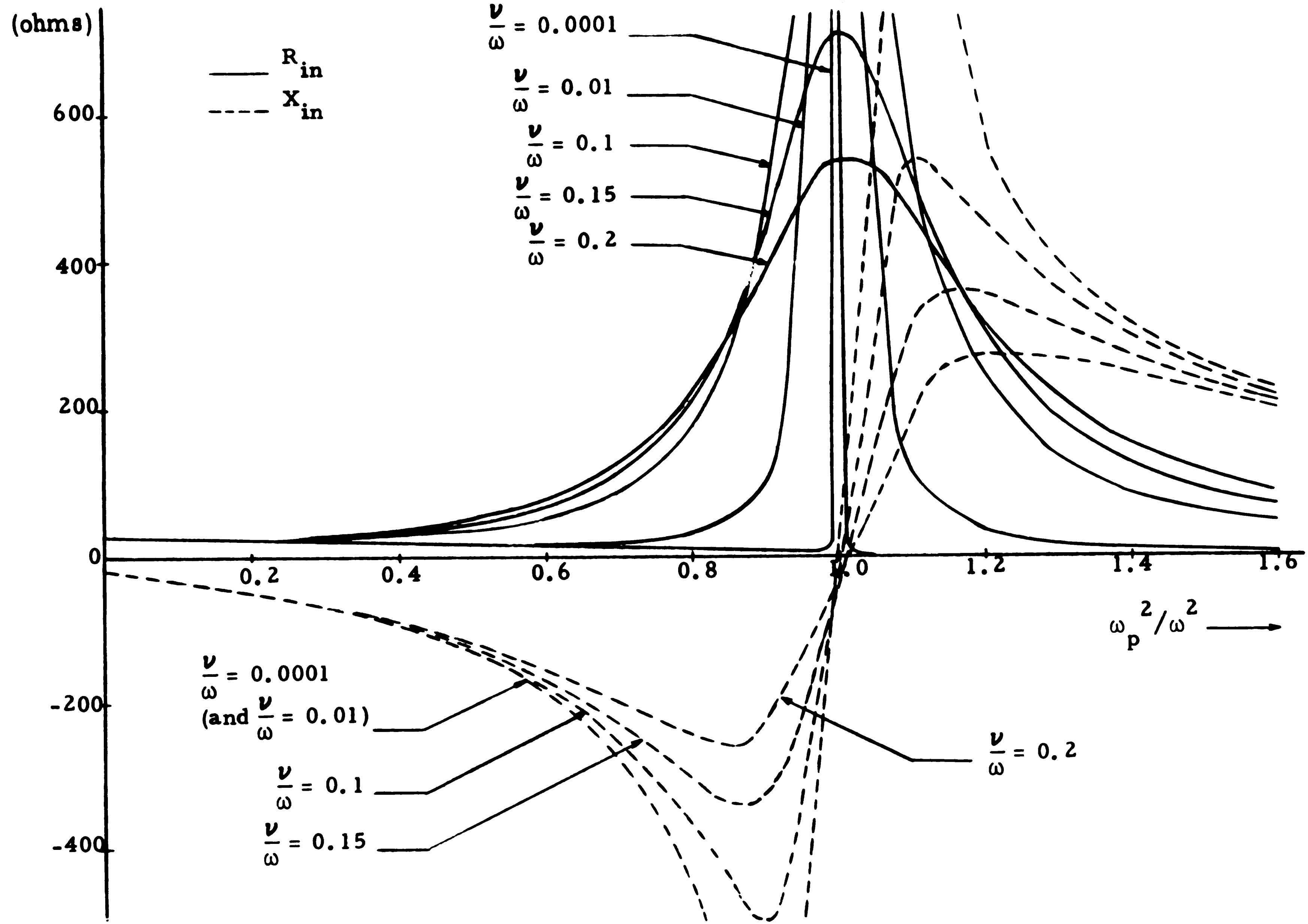

Fig. 5.4 Theoretical input impedance of a monopole ($h/\lambda_o = 0.213$, $a/\lambda_o = 0.008$) in a cold plasma as a function of plasma density.

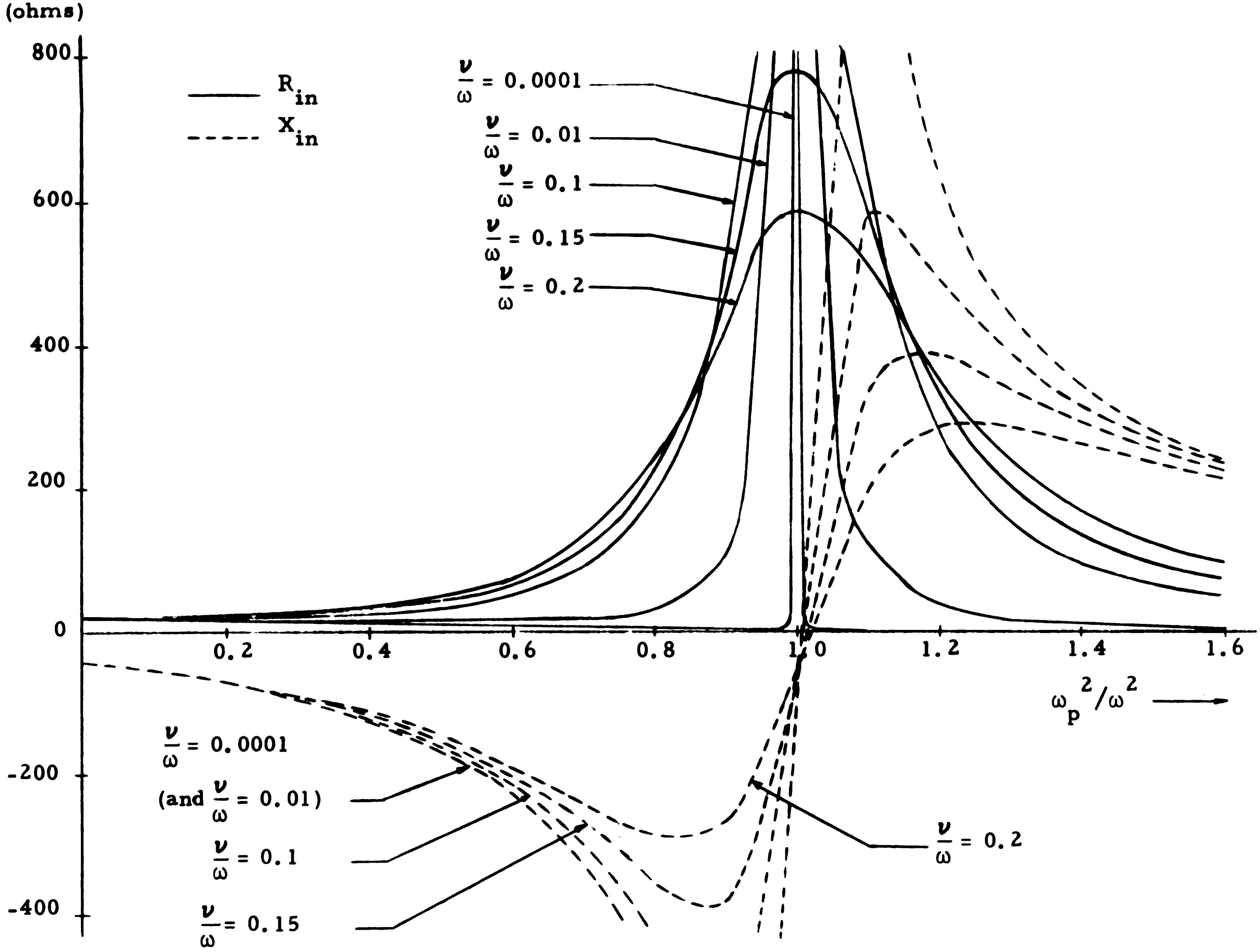

Fig. 5.5 Theoretical input impedance of a monopole ($h/\lambda_o = 0.192$, $a/\lambda_o = 0.0072$) in a cold plasma as a function of plasma density.

CHAPTER 6

EXPERIMENTAL INVESTIGATION ON THE RADIATION OF A CYLINDRICAL ANTENNA IN A HOT PLASMA

6.1 Introduction

The radiation of a cylindrical antenna in a hot plasma has been studied theoretically by many researchers as mentioned before. In contrast with the abundance of theoretical papers, extremely few experimental studies have been published. The relevant experimental studies were the observation of electroacoustic wave by Whale[9] in a rocket flight, Schmitt's[10] observation of Tanks-Dattner's resonance excited by an antenna, and the experiments on the antenna in a hot plasma conducted by Jassby and Bachyski[11] and by Chen, Jackson and Lin[12, 13]. Nevertheless, to our best knowledge, no extensive experimental study has been conducted to study the electroacoustic wave excited by an antenna in a hot plasma.

The purposes of this experimental investigation are to (1) detect the existence of an electroacoustic wave excited by an antenna in a hot plasma, and (2) study the effect of this electroacoustic wave on the circuit and the radiation properties of an antenna. Two approaches, (1) to measure the antenna input impedance as a function of plasma parameters, and (2) to measure the antenna radiation field as a function of plasma parameters, have been used to detect the electroacoustic wave.

In order to conduct an accurate experiment on the interaction of an antenna with a hot plasma, a great deal of time and effort was exerted to produce a large volume of stable, high-density plasma. In our experiment, the hot plasma was the mercury arc discharge which was created in two plasma tubes. The cylindrical monopole antennas were used as the radiating source.

6.2 Experimental Setups

Two experimental setups have been used in the present investigation. One setup consisting of a large plasma tube with the dimensions of 14-inch diameter by 18-inch length was designed primarily for the antenna impedance measurement. The other setup using a smaller plasma tube of 6-inch diameter by 12-inch length was designed for the purpose of the antenna radiation measurement. The construction of the plasma tubes and the details of these two setups are described below.

6.2.1 Construction of a Large Volume of Stable, High-Density Plasma

To conduct an accurate experiment on the interaction of an electric source with a plasma at a convenient frequency range, a large volume of stable, high-density plasma is required. Conventional laboratory-produced plasma are either a gas afterglow discharge or a mercury glow discharge. A gas afterglow discharge is not a continuous plasma and it is usually of low density. A mercury glow discharge can only give a small volume of high-density plasma. In the present investigation, a mercury arc discharge was employed. A mercury arc discharge can give a large volume of high-density plasma. However, it is inherently unstable due to its moving hot spots on the mercury pool. A novel method of placing a spot fixer on the mercury pool of the plasma tube was used to stabilize the plasma. Using this device, a stable plasma with the plasma frequency of 1 to 5 GHz can be obtained and the plasma tube can be operated continuously for many hours.

6.2.2 Experimental Setup for the Measurement of Antenna Impedance in a Hot Plasma

The schematic diagram of the experimental setup for the antenna impedance measurement is shown in Fig. 6.1. The plasma tube is made of an open-end pyrex bell jar with the dimensions of 14-inch diameter and 18-inch length. The upper end of the tube is the anode with a cylindrical monopole antenna feeding through its center. The lower end of the tube is the cathode which consists of a mercury pool. A floating metallic ring is placed at the middle of the mercury pool to fix the moving hot spots of the mercury arc. An ignition circuit is installed in the mercury pool for the purpose of starting the plasma. Between the anode and the cathode a DC

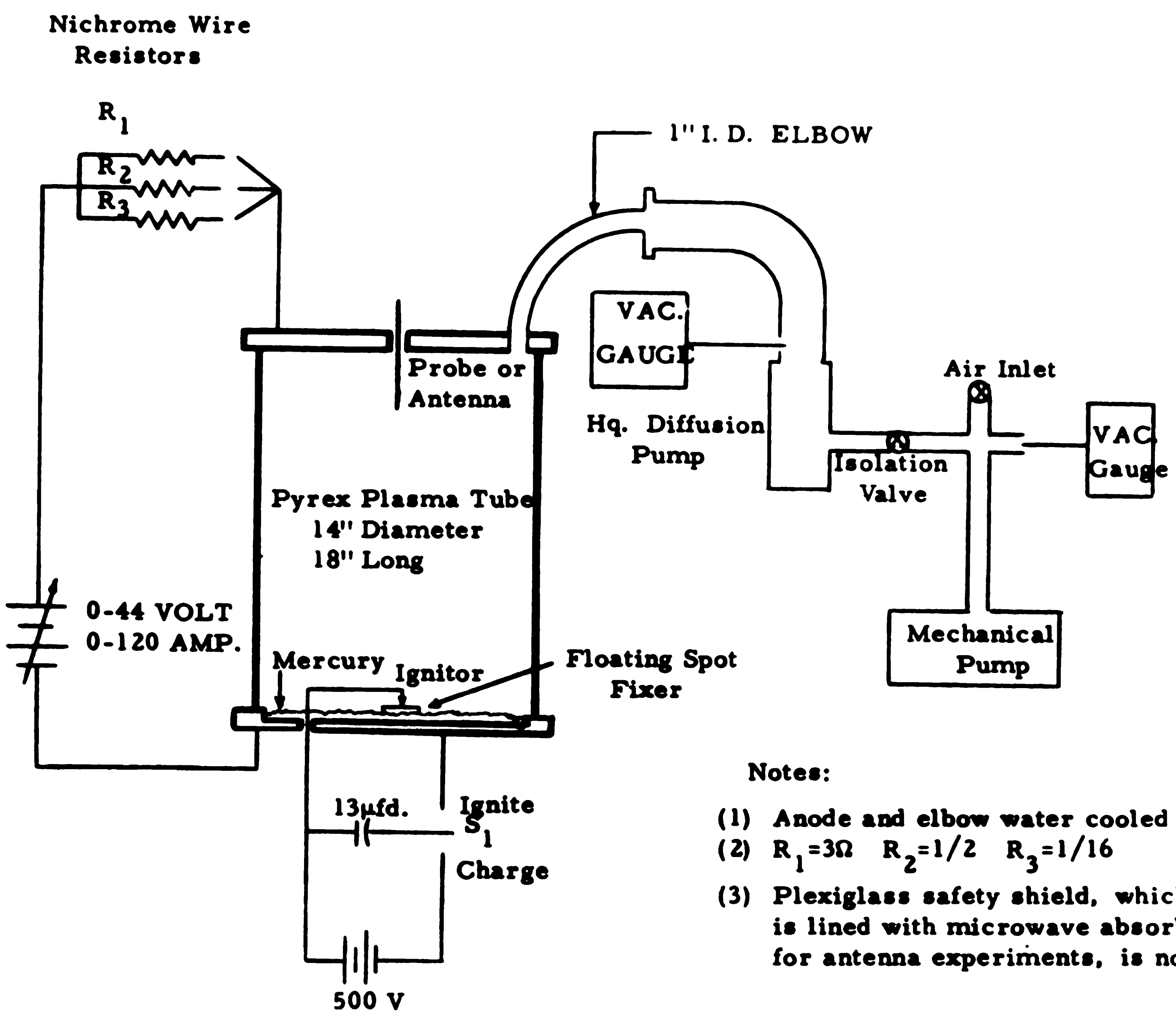

Notes:

(1) Anode and elbow water cooled

(2) $R_1 = 3\Omega$ $R_2 = 1/2$ $R_3 = 1/16$

(3) Plexiglass safety shield, which is lined with microwave absorber for antenna experiments, is not shown.

Fig. 6.1 Experimental setup for the impedance measurement of cylindrical antenna.

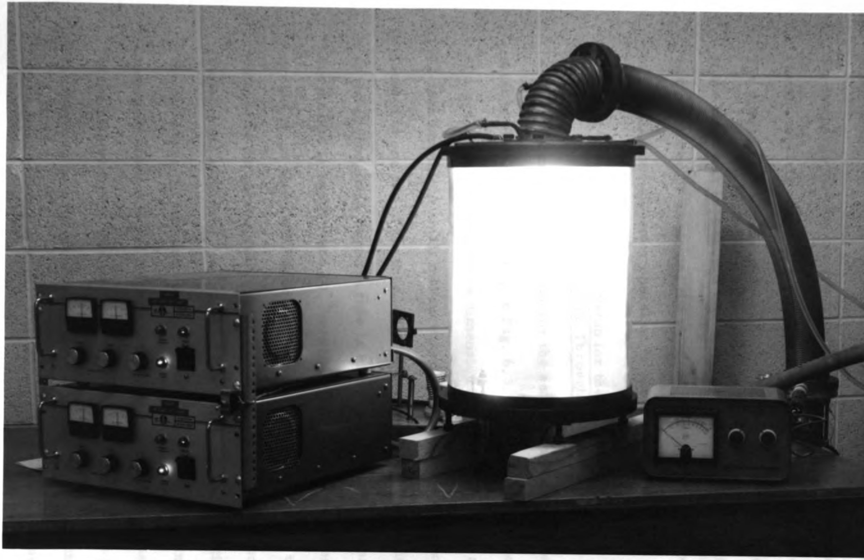

Fig. 6.2 A cylindrical plasma tube (14-inch diameter by 18-inch length) under operation and the surrounding experimental setup.

power supply circuit is connected. Under the normal operation the discharge current can run from 0 to 120 amperes. The pumping system consists of a mechanical pump and a mercury diffusion pump. The tube is continuously pumped during the experiment and the pressure of the plasma is kept around 10^{-3} mm Hg. The antenna input impedance was measured by employing the standard SWR method. A photograph of this plasma tube under operation is shown in Fig. 6.2.

6.2.3 Experimental Setup for the Measurement of Antenna Radiation Through a Hot Plasma

The experimental setup for the antenna radiation measurement is shown schematically in Fig. 6.3. The plasma tube is made of a pyrex glass tube with the dimensions of 6-inch diameter and 12-inch length. A small mercury pool with a floating spot fixer is located at one end of the tube. The open end of the tube is sucked to the ground plane when the tube is being pumped. The pressure of the plasma is kept around 10^{-3} mm Hg. With this arrangement the ground plane acts as the anode and the mercury pool acts as the cathode of the plasma tube. A DC power supply circuit is connected between the anode and the cathode. Under the normal operation the discharge current can run from 0 to 10 amperes. A cylindrical monopole antenna is fed through the ground plane and into the center of the plasma tube. The radiation of the antenna through the plasma is measured by a movable receiving antenna which is connected to a hetrodyne receiving system. The distance between the radiating and

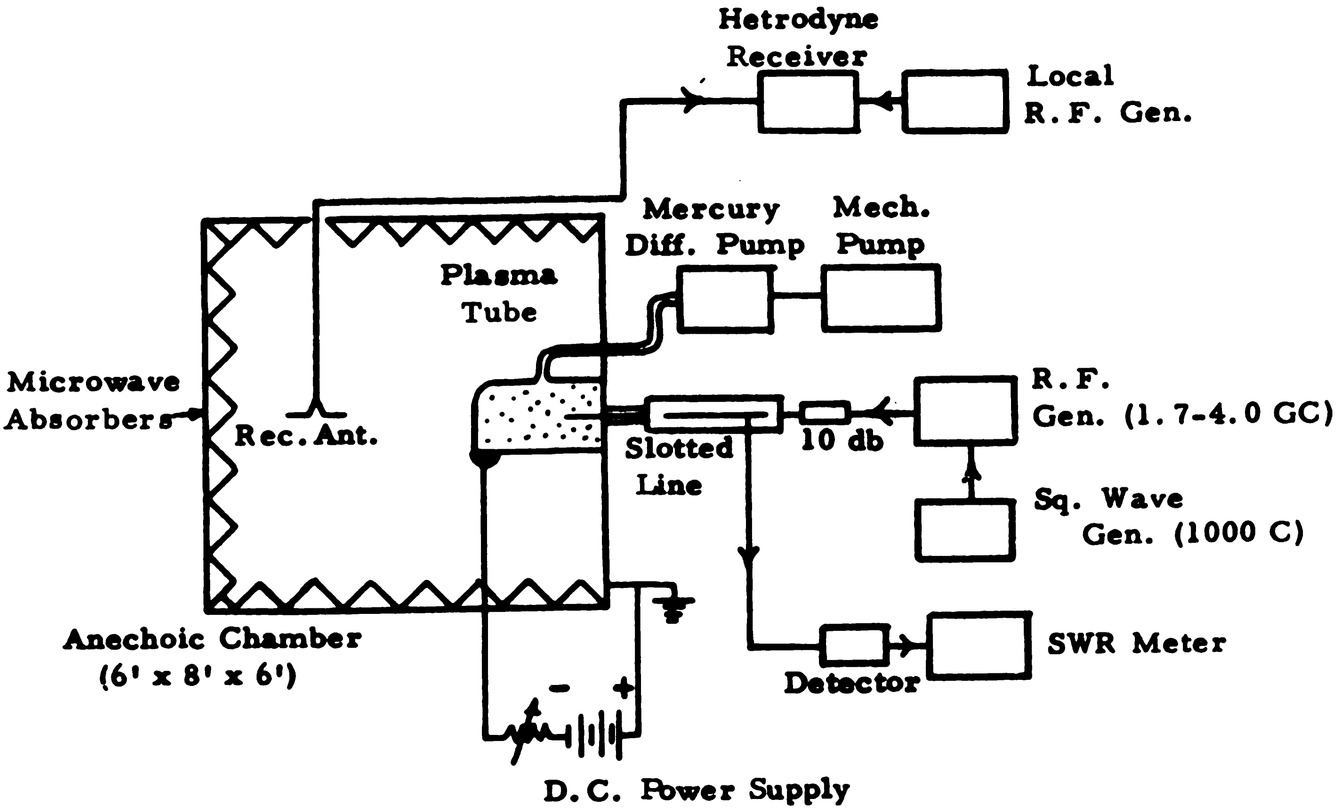

Fig. 6.3 Experimental setup for the radiation measurement of cylindrical antenna.

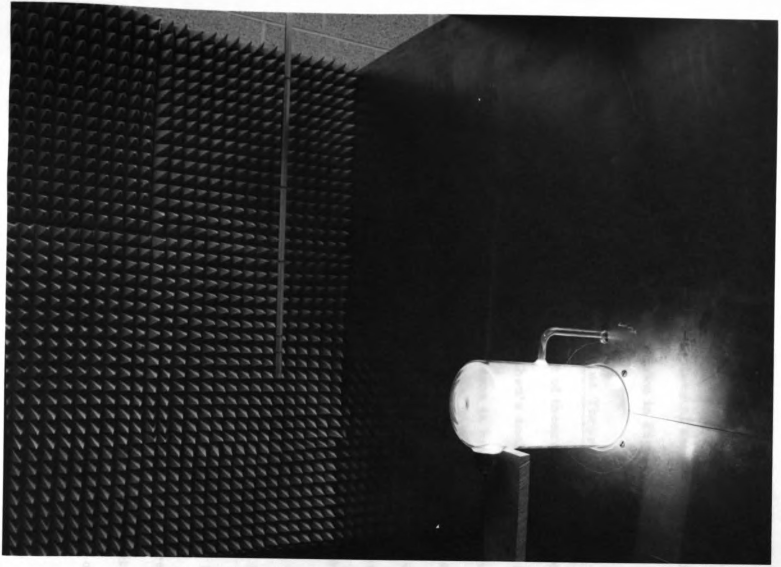

Fig. 6.4 A cylindrical plasma tube (6-inch diameter by 12-inch length) under operation inside of a microwave anechoic chamber.

receiving antennas is 0.7 m. The plasma tube, the radiating and the receiving antennas are all enclosed in an anechoic chamber. Figure 6.4 shows the photograph of this plasma tube under operation inside of the anechoic chamber. The experimental setup outside of the anechoic chamber is the same as that shown in Fig. 4.3.

6.3 Review of a Lossless, Hot-Plasma Theory

In order to provide another set of theoretical results for comparison with the experimental data, Chen's analysis[7] on the interaction of a radiating source with a plasma is briefly outlined here.

In Chen's analysis, the radiating source is a cylindrical antenna with a length of 2h and a radius of a. The antenna is center-driven by a delta-function generator and immersed in a lossless, hot plasma of infinite extent. The current and charge distributions of the antenna are assumed to be

$$\vec{I}^{s} = I_m \sin[k_e(h - |z|)]\, e^{j\omega t}\, \hat{z} \tag{6.1}$$

$$q^{s} = \pm j \sqrt{\mu_o \epsilon_o (1 - \omega_p^2/\omega^2)}\, I_m \cos[k_e(h - |z|)]\, e^{j\omega t} \tag{6.2}$$

where I_m is the maximum current on the antenna, ω and ω_p are the antenna and plasma frequencies, μ_o and ϵ_o are the permeability and permittivity in free space, and k_e is the propagation constant of the electromagnetic wave given by

$$k_e = \frac{1}{c}\sqrt{\omega^2 - \omega_p^2} \tag{6.3}$$

where c is the velocity of light in free space. In Eqs. (6.1) and (6.2) the distributions of antenna current and charge are assumed to be entirely controlled by the electromagnetic mode. This approximation is necessary since the effect of the electroacoustic wave on the antenna current and charge is still not well known.

Based on Eqs. (6.1) and (6.2), the power density of the electromagnetic wave can be derived to be

$$\vec{p}_e = \frac{15 I_m^2}{\pi\sqrt{1 - \omega_p^2/\omega^2}\; r_o^2}\left[\frac{\cos(k_e h\cos\theta) - \cos(k_e h)}{\sin\theta}\right]\hat{r} \tag{6.4}$$

where r_o is the distance between the observation point and the center of antenna, θ is the polar angle and $\hat{r}$ is the unit radial vector in the spherical coordinates.

The total power radiated as an electromagnetic wave can be calculated by integrating $\vec{p}_e$ over a large sphere. The result is

$$P_e = \frac{15 I_m^2}{\sqrt{1-\omega_p^2/\omega^2}}\{-\cos(2k_e h)\mathrm{Cin}(4k_e h) + 2[1+\cos(2k_e h)]\,\mathrm{Cin}(2k_e h) + \sin(2k_e h)[\,\mathrm{Si}(4k_e h) - 2\,\mathrm{Si}(2k_e h)]\} \tag{6.5}$$

where Si(x) and Cin(x) are the sine and cosine integrals. The electromagnetic component of the antenna input resistance is obtained by dividing P_e with $1/2\, I_o^2$ where I_o is the antenna input current and related to I_m by $I_o = I_m \sin(k_e h)$. This gives

$$R_e = \frac{30}{\sin^2(k_e h)\sqrt{1-\omega_p^2/\omega^2}} \{-\cos(2k_e h)\mathrm{Cin}(4k_e h)$$

$$+ 2[1+\cos(2k_e h)]\,\mathrm{Cin}(2k_e h)$$

$$+ \sin(2k_e h)[\mathrm{Si}(4k_e h) - 2\,\mathrm{Si}(2k_e h)]\} \qquad (6.6)$$

which is valid for $\omega > \omega_p$.

The power density of the electroacoustic wave can be obtained as

$$\vec{p}_p = \frac{15}{\pi}\left(\frac{c}{v_o}\right)^3 \frac{\omega_p^2}{\omega^2}\,\frac{I_m^2}{r_o^2}\,\frac{1}{\sqrt{1-\omega_p^2/\omega^2}}$$

$$\cdot \left[\frac{\cos\theta[\cos(k_p h\cos\theta) - \cos(k_e h)]}{1-(c/v_o)^2\cos^2\theta}\right]^2 \hat{r} \qquad (6.7)$$

where v_o is r.m.s. velocity of electrons and k_p is the propagation constant of the electroacoustic wave given by

$$k_p = \frac{1}{v_o}\sqrt{\omega^2 - \omega_p^2}\ . \qquad (6.8)$$

The total power radiated as an electroacoustic wave can be obtained by integrating $\vec{p}_p$ over a large sphere. This gives

$$P_p = \frac{15\pi}{2} \frac{\omega_p^2/\omega^2}{\sqrt{1-\omega_p^2/\omega^2}} \left[2k_e h + \sin(2k_e h)\right] I_m^2 \qquad (6.9)$$

under the condition of $c >> v_o$ and $\omega > \omega_p$. The electroacoustic component of the antenna input resistance can be determined by dividing P_p with $1/2\, I_o^2$. The result is

$$R_p = \frac{15\pi}{\sin^2(k_e h)} \frac{\omega_p^2/\omega^2}{\sqrt{1-\omega_p^2/\omega^2}} \left[2k_e h + \sin(2k_e h)\right]. \qquad (6.10)$$

Equation (6.10) is valid if $c >> v_o$ and $\omega > \omega_p$.

The total input resistance of the cylindrical dipole antenna is

$$R_{in} = R_e + R_p \,. \qquad (6.11)$$

For a monopole antenna the input resistance is $R_{in}/2$. R_e and R_p were numerically calculated to compare the experimental antenna resistance.

The antenna input reactance should also consist of both electromagnetic and electroacoustic components. The elctromagnetic component can be theoretically determined from King-Middleton's theory(25) once the electrical dimensions of antenna, $k_e h$ and $k_e a$, are known. The electroacoustic component of the antenna reactance is neglected in this study due to the lack of knowledge on the effect of the electroacoustic wave on the reactive power of an antenna. Due to this reason only the electromagnetic component of the antenna reactance was used in comparison with the experimental results in a later section.

The radiation field of an antenna in a hot plasma consists of the fields of electromagnetic and electroacoustic radiations. The radiation pattern of the electromagnetic wave is completely determined by the factor $k_e h$ as expressed in Eq. (6.4). The electromagnetic radiation has a characteristic of zero radiation in the axial direction ($\theta = 0^{\circ}$) of antenna. The radiation pattern of the electroacoustic wave is determined by Eq. (6.7). The special nature of the electroacoustic radiation is to have peak radiation in the direction near the axial direction of antenna. If an antenna is surrounded by a finite plasma, the electroacoustic wave may convert part of its energy to create an electromagnetic wave at the plasma discontinuity. This electromagnetic wave may, in turn, be detected outside of the plasma region.

6.4 Experimental Results and Comparison with Theories

Since the purposes of this investigation are to detect the excitation of an electroacoustic wave by an antenna and to examine the effect of this electroacoustic wave on the circuit and the radiation properties of an antenna, the antenna input impedance and the antenna radiation field are measured as functions of the plasma density. The experimental results on the antenna input impedance and the antenna radiation field are carefully studied and compared with two theories. The two theories are: (1) a lossless, hot-plasma theory reviewed in the preceding section, and (2) a lossy, cold-plasma theory developed in Chapter 5.

6.4.1 Comparison of Experiment With a Lossless, Hot-Plasma Theory on Antenna Input Impedance

The experimental results on the input impedances of cylindrical monopole antennas of various lengths are graphically shown in Figs. 6.5 to 6.8. The input impedance of the antenna is plotted as a function of ω_p^2/ω^2 where ω_p is the average local plasma frequency in the antenna vicinity and ω is the antenna frequency. The average local plasma density is used here because the plasma density in the antenna vicinity is not uniform due to the plasma sheath on the antenna surface. Furthermore, it was found that the circuit property of an antenna is primarily controlled by the plasma condition in the antenna vicinity. Experimentally this average local plasma frequency was found to be about 20% lower than the maximum plasma frequency in the plasma tube. The value of ω_p^2/ω^2 is directly proportional to the plasma density when the antenna frequency is kept constant throughout the experiment. The antenna input impedance was measured in the large plasma tube (14-inch diameter by 18-inch length) and at the frequencies of 1.8 and 2.0 GHz.

In Figs. 6.5 to 6.8, the solid line with solid dots is the measured antenna input resistance and the dotted line with solid dots is the measured antenna input reactance. The theoretical values are represented by circled dots. The experimental results on the antenna input impedance can be summarized as follows:

(1) For the case of low plasma density or $\omega_p^2/\omega^2 < 0.6$, as the plasma density is increased the antenna resistance decreases and the antenna reactance becomes more negative. This phenomenon indicates that the antenna behaves progressively shorter electrically and also implies that no electroacoustic wave or only an electromagnetic wave is excited over this range. Theoretical impedance was calculated over this range by assuming the existence of electromagnetic mode only. The agreement between experiment and theory is very good. The assumption of no electroacoustic wave over this range may be feasible since a longitudinal plasma wave will suffer a tremendous Landau damping in this range.

(2) For the range of $0.6 < \omega_p^2/\omega^2 < 1.0$, the antenna resistance monotonically increases and finally reaches a peak at $\omega_p = \omega$. The antenna reactance goes to a large negative value and then sharply changes its sign at $\omega_p = \omega$. The large antenna resistance over this range may be identified as being due to the excitation of an electroacoustic wave. The theoretical resistance of the monopole over this range was calculated from $R_{in} = \frac{1}{2}(R_e + R_p)$ where R_e and R_p are given by Eqs. (6.6) and (6.10). Excellent agreement between theoretical and experimental antenna resistances tends to confirm the excitation of an electroacoustic wave over this range. For the antenna reactance the large deviation between theory and experiment over this range is probably due to the fact that the electroacoustic component of antenna reactance was not taken into account. The assumption of the existence

of an electroacoustic wave over this range is justified since the Landau damping is small when ω_p is close to ω.

(3) For the case of $\omega_p^2/\omega^2 > 1.0$, both the electromagnetic and the electroacoustic waves are essentially cut off. If no loss mechanism is present in the plasma, the antenna resistance should drop sharply to zero. Experimental results, however, show that the antenna resistance decreases rather gradually in this range. The possible loss mechanisms are the finite collision loss of the mercury plasma and the possible excitation of Tanks-Dattner's resonance on the antenna surface and on the tube wall.

The weakness of this lossless, hot-plasma theory is its inadequacy of providing a theoretical prediction for the range of $\omega < \omega_p$.

6.4.2 Comparison of Experiment With a Lossy, Cold-Plasma Theory on Antenna Input Impedance

In Sec. 6.4.1 it is indicated that the experimental antenna input impedance can only be compared with a lossless, hot-plasma theory for the range of $\omega_p^2/\omega^2 < 1$. In order to have a comparison of experiment and theory for a wide range of ω_p^2/ω^2, the same experimental results of the antenna input impedance are compared with the theoretical results obtained from a lossy, cold-plasma theory developed in Chapter 5. These comparisons are shown in Figs. 6.9 to 6.12. The effect of the collision frequency on the antenna input impedance has been carefully studied in Chapter 5.

The theoretical input impedance of a monopole was calculated from $Z_{in}/2$ where Z_{in} is given by Eq. (5.62). The ratio between the collision frequency and the antenna frequency, ν/ω, was assumed to be 0.15 in the numerical calculation.

In Figs. 6.9 to 6.12, the solid lines with solid dots are the measured input resistance and ractance. The theoretical values are represented by the dotted lines. The comparison between experiment and theory can be summarized as follows:

(1) For the case of low plasma density or $\omega_p^2/\omega^2 < 0.4$, as the plasma density is increased both experimental and theoretical results indicate that the antenna behaves gradually shorter electrically.

(2) For the range of $0.4 < \omega_p^2/\omega^2 < 0.85$, the antenna resistance starts to increase and the antenna reactance continues to be more capactivie as predicted by the theory.

(3) For the range of $0.85 < \omega_p^2/\omega^2 < 1.15$, a sharp peak of antenna resistance and a change of antenna reactance from capacitive to inductive at $\omega_p = \omega$ have been observed both experimentally and theoretically.

(4) For the case of $\omega_p^2/\omega^2 > 1.15$, as the plasma density is increased the antenna resistance and reactance decrease gradually.

The agreement between the experimental results and the lossy, cold-plasma theory appears to be quite satisfactory over a very wide range of ω_p^2/ω^2. However, there is still a critical weakness in this lossy, cold-plasma theory. Because the temperature effect and the electroacoustic mode are completely ignored.

6.4.3 Experimental Results on Antenna Radiation Fields

The radiation field pattern of a cylindrical monopole antenna placed in the middle of the smaller plasma tube (6-inch diameter by 12-inch length) was measured under various plasma densities. The measured radiation patterns for three monopoles of different lengths are shown in Figs. 6.13 to 6.15. For each antenna the change in the radiation pattern was observed as the plasma density was varied. The main points of the observation can be summarized as follows:

(1) For the low plasma density case or $\omega_p^2/\omega^2 < 0.6$, the radiation field is primarily electromagnetic, since no radiation is observed in the axial direction of the antenna and the measured pattern resembles with that of antenna with the electrical length of $k_e h$ radiated in free space.

(2) For the case of $0.6 < \omega_p^2/\omega^2 < 1.0$, a peak of radiation starts to show in the axial direction of antenna. This radiation may be identified as due to the electroacoustic wave, since the radiation of an electroacoustic wave in the axial direction of antenna will create an electromagnetic wave at the plasma discontinuity which exists at the tube wall.

(3) For the case of $\omega_p^2/\omega^2 > 1.0$, the radiation peak in the axial direction of antenna disappears and the measured pattern is

again mainly of electromagnetic nature. The reason why only the electroacoustic wave is cut off in this range is that the plasma dimension is large in terms of electroacoustic wavelength but rather small compared with an electromagnetic wavelength. Thus an electromagnetic wave can still be detected outside of the plasma tube after suffering a relatively smaller attenuation.

To compare these experimental results more accurately, a theory dealing with the radiation from a cylindrical antenna through a finite volume of plasma is needed. Such a theory is unfortunately intractable.

6.5 Discussion

Extensive experimental study has been conducted to investigate the interaction of a cylindrical antenna with a hot plasma. Based on the comparison with the lossless, hot-plasma theory, the experimental results tend to indicate that an electroacoustic wave can be excited when the average local plasma frequency in the antenna vicinity is near the antenna frequency ($0.6 < \omega_p^2/\omega^2 < 1.0$). No electroacoustic wave can be excited if the plasma frequency is sufficiently lower than the antenna frequency ($\omega_p^2/\omega^2 < 0.6$). Based on the comparison with the lossy, cold-plasma theory, it appears that experimental results agree quite satisfactorily with the theoretical results if a suitable collision frequency is assigned to the plasma. The effects of the electroacoustic wave and the collision in the plasma on the antenna input impedance are quite simlar. While the effect of an electroacoustic wave on the radiation field is much more important than that due to the collision in the plasma.

Since the laboratory-produced plasma is hot, lossy and finite, the two theories used to compare with the experiment seem to be inadequate. If an accurate comparison is needed for the experimental results, a more complete theory of a plasma-imbedded cylindrical antenna which takes into account of the plasma temperature, collision and dimensions should be developed. It is unfortunate that such a theory has been proved to be quite intractable.

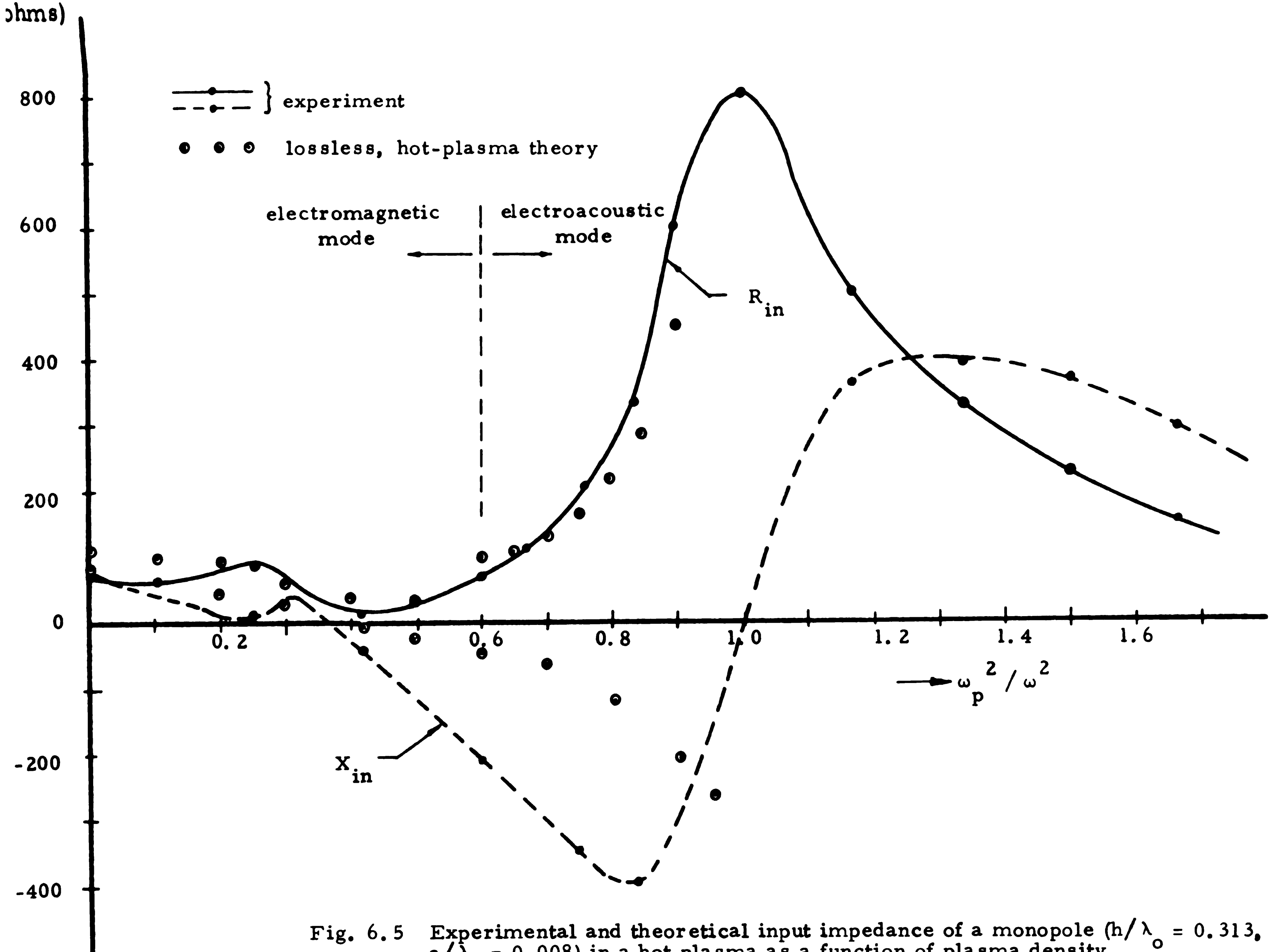

Fig. 6.5 Experimental and theoretical input impedance of a monopole ($h/\lambda_o = 0.313$, $a/\lambda_o = 0.008$) in a hot plasma as a function of plasma density.

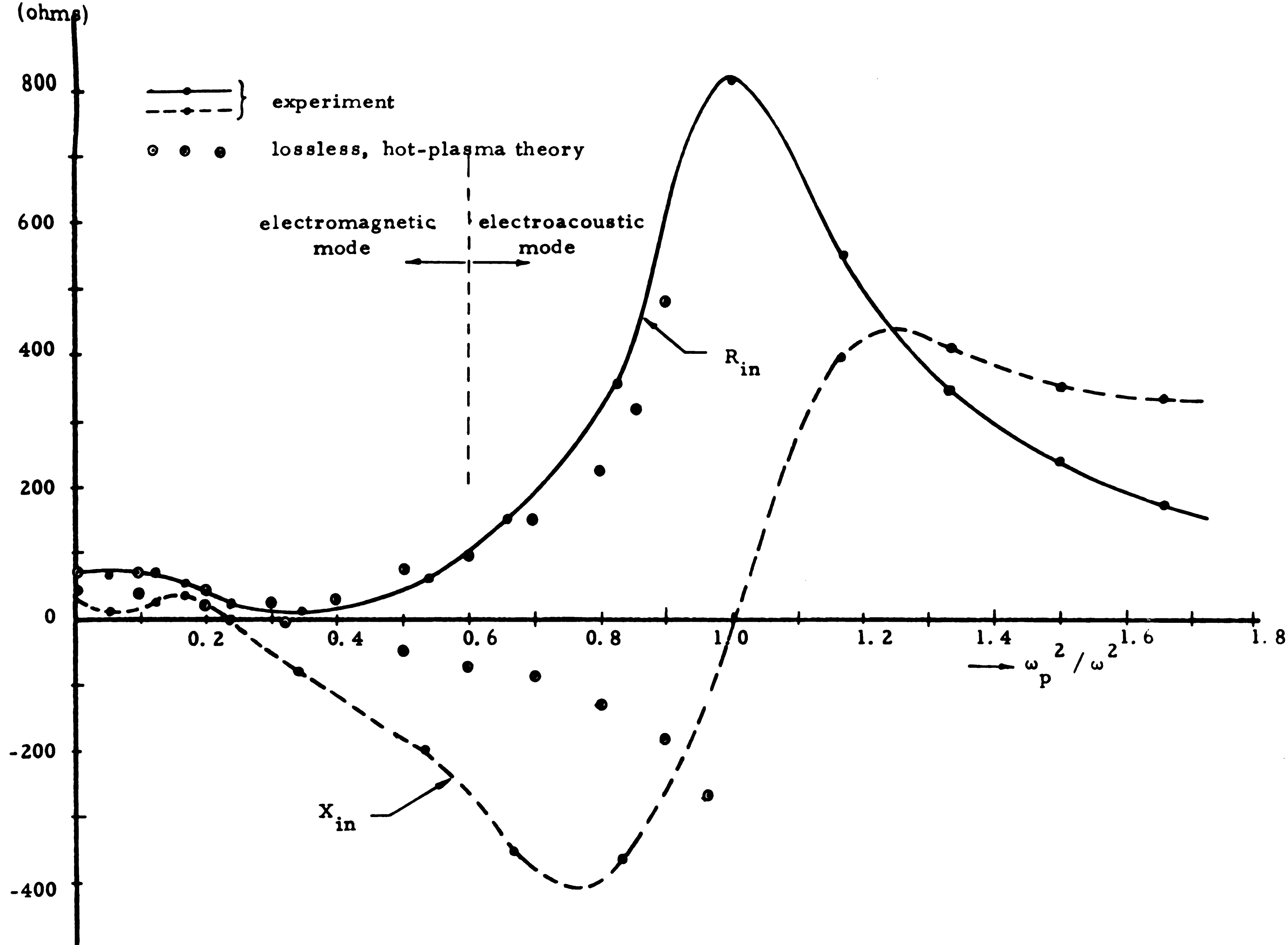

Fig. 6.6 **Experimental and theoretical input impedance of a monopole (h/λ_o = 0.282, a/λ_o = 0.0072) in a hot plasma as a function of plasma density.**

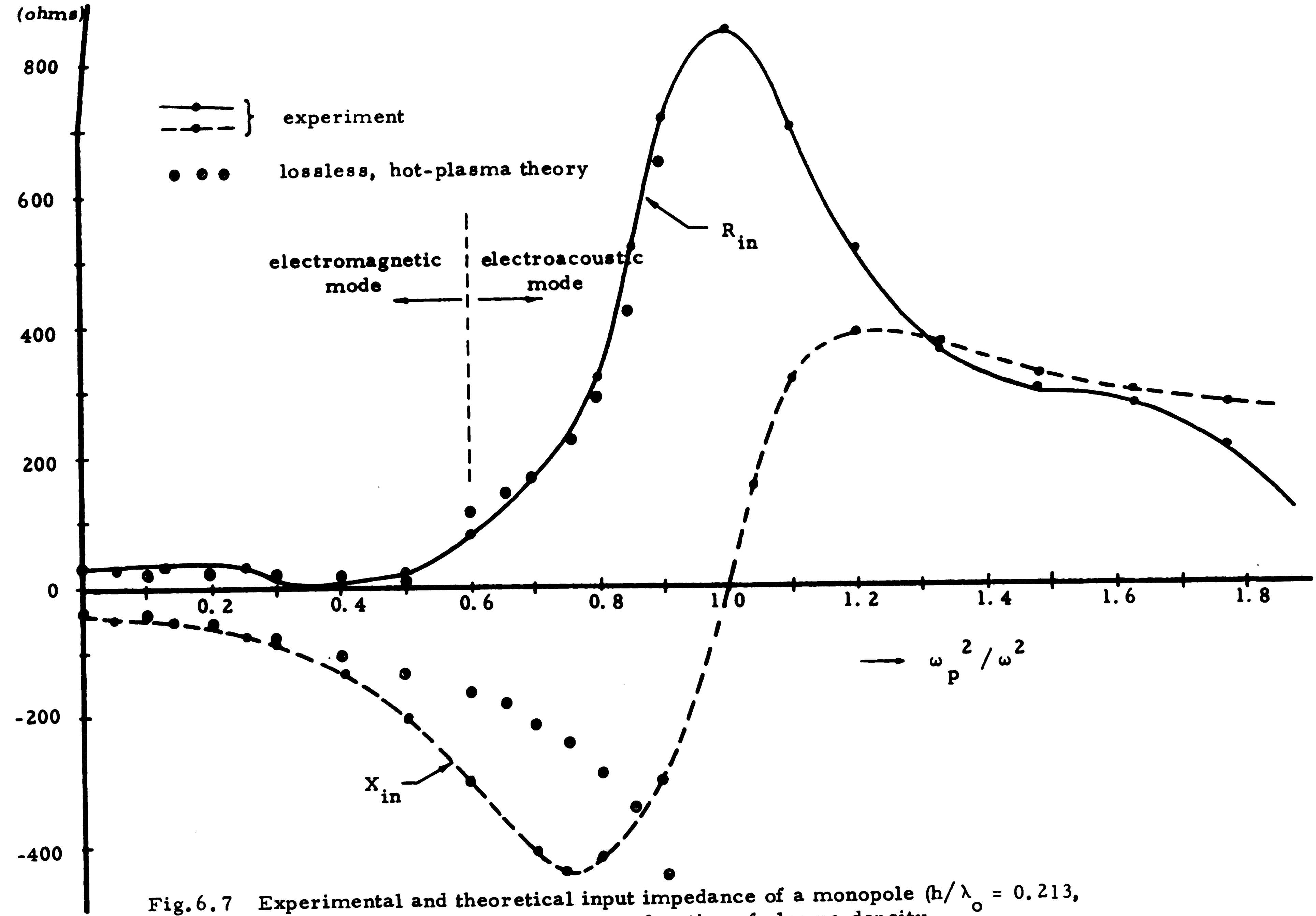

Fig.6.7 Experimental and theoretical input impedance of a monopole ($h/\lambda_o = 0.213$, $a/\lambda_o = 0.008$) in a hot plasma as a function of plasma density.

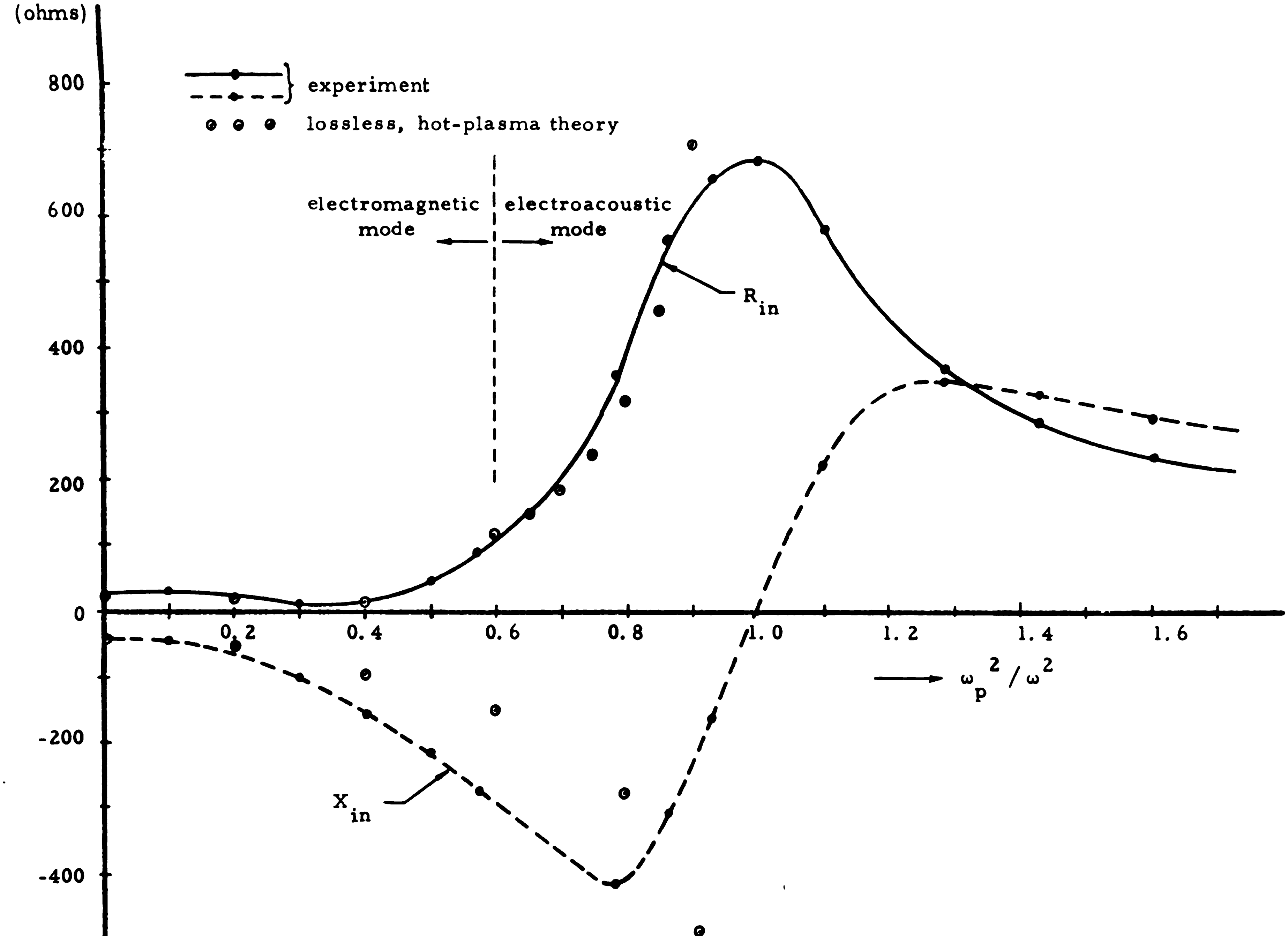

Fig. 6.8 Experimental and theoretical input impedance of a monopole ($h/\lambda_o = 0.192$, $a/\lambda_o = 0.0072$) in a hot plasma as a function of plasma density.

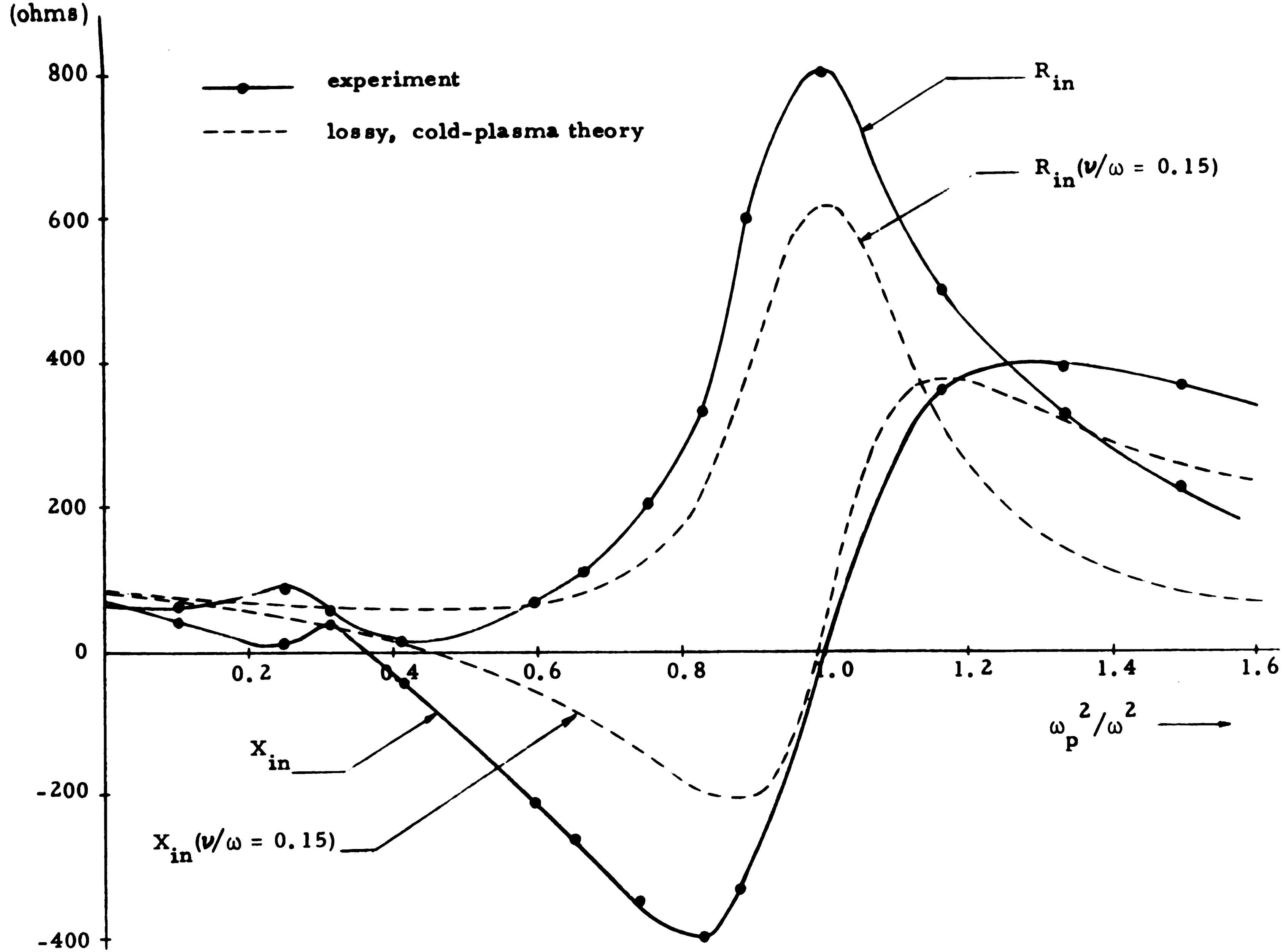

Fig. 6.9 Experimental and theoretical input impedance of a monopole ($h/\lambda_o = 0.313$, $a/\lambda_o = 0.008$) in a plasma as a function of plasma density.

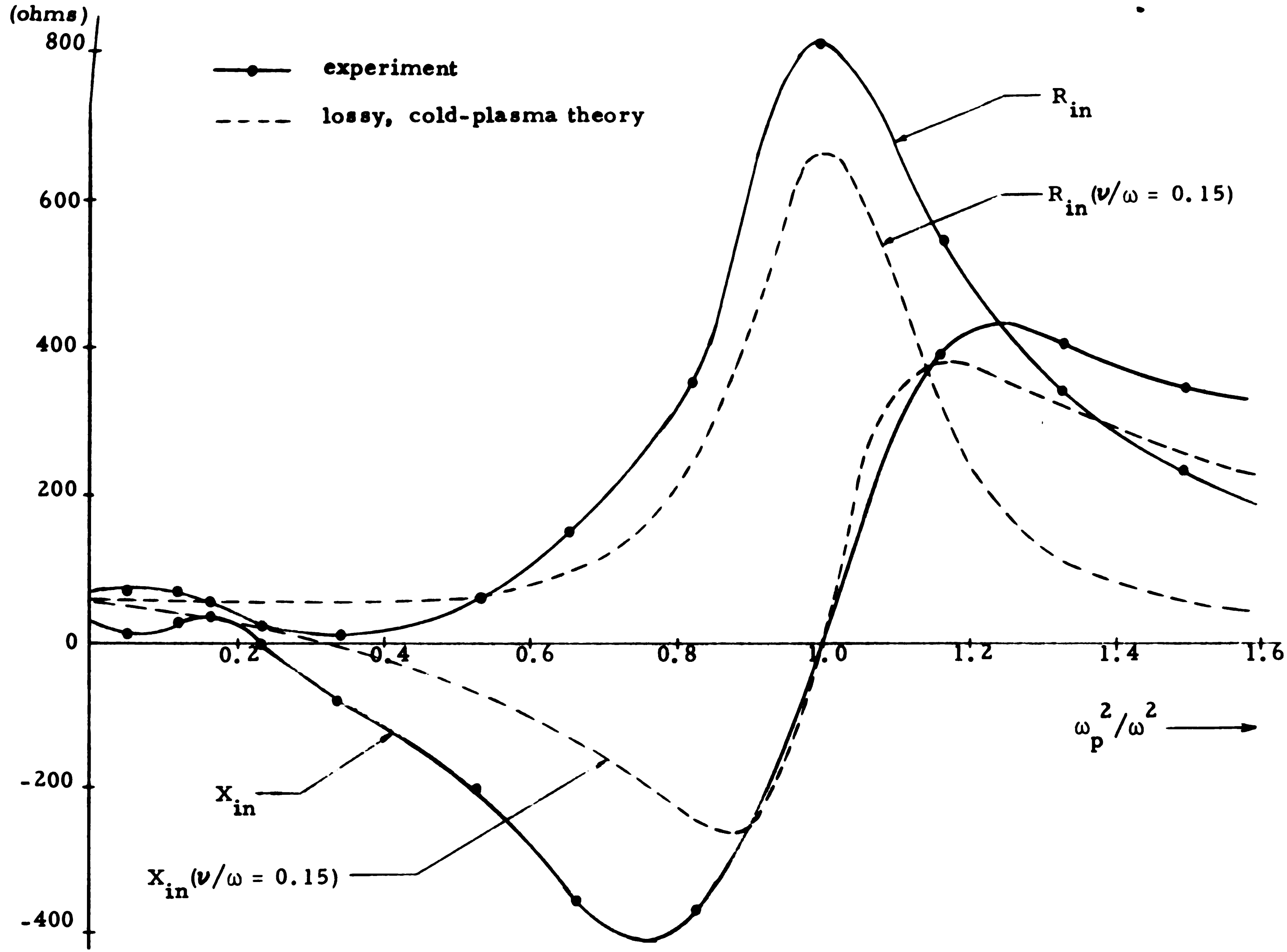

Fig. 6.10 Experimental and theoretical input impedance of a monopole ($h/\lambda_o = 0.282$, $a/\lambda_o = 0.0072$) in a plasma as a function of plasma density.

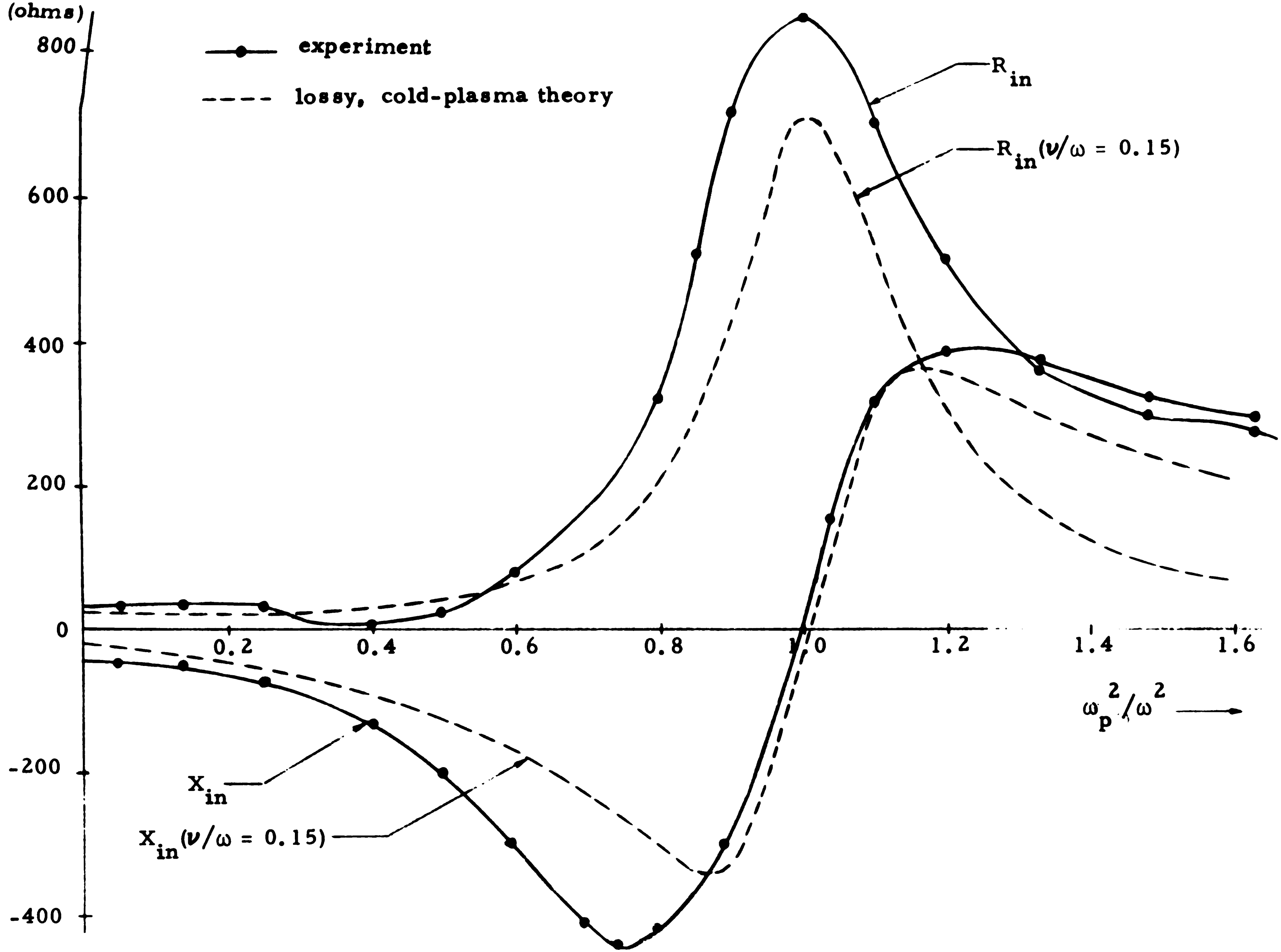

Fig. 6.11 Experimental and theoretical input impedance of a monopole ($h/\lambda_o = 0.213$, $a/\lambda_o = 0.008$) in a plasma as a function of plasma density.

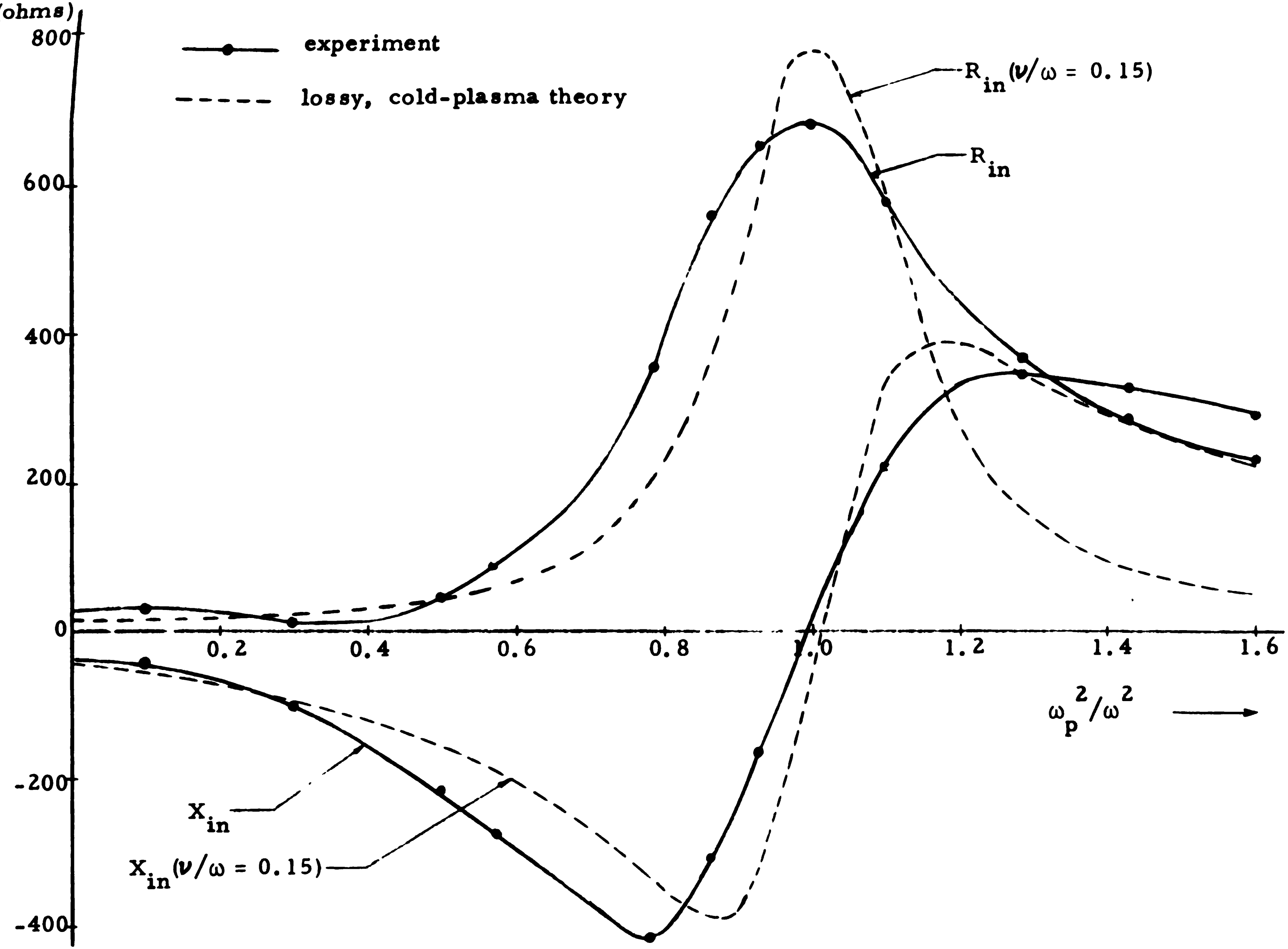

Fig. 6.12 Experimental and theoretical input impedance of a monopole ($h/\lambda_o = 0.192$, $a/\lambda_o = 0.0072$) in a plasma as a function of plasma density.

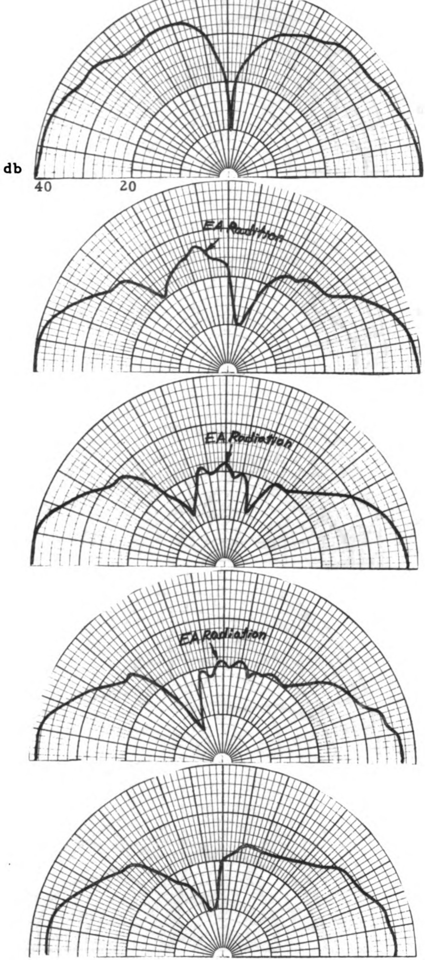

$\omega_p^2/\omega^2 = 0$

$\omega_p^2/\omega^2 = 0.6$

$\omega_p^2/\omega^2 = 0.8$

$\omega_p^2/\omega^2 = 0.9$

$\omega_p^2/\omega^2 = 1.0$

Fig. 6.13 Experimental radiation patterns of a monopole ($h/\lambda_o = 0.6$, $a/\lambda_o = 0.008$) surrounded by a hot plasma of various densities.

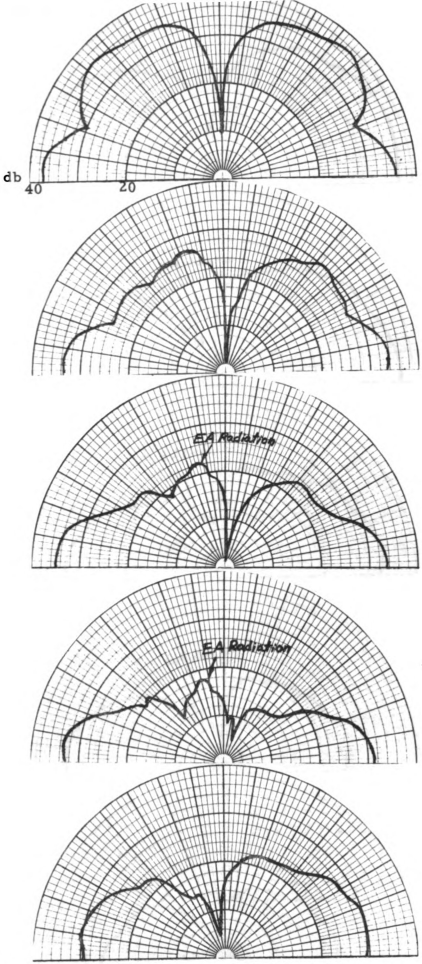

$\omega_p^2/\omega^2 = 0$

$\omega_p^2/\omega^2 = 0.6$

$\omega_p^2/\omega^2 = 0.8$

$\omega_p^2/\omega^2 = 0.9$

$\omega_p^2/\omega^2 = 1.0$

Fig. 6.14 Experimental radiation patterns of a monopoles ($h/\lambda_o = 0.66$, $a/\lambda_o = 0.008$) surrounded by a hot plasma of various densities.

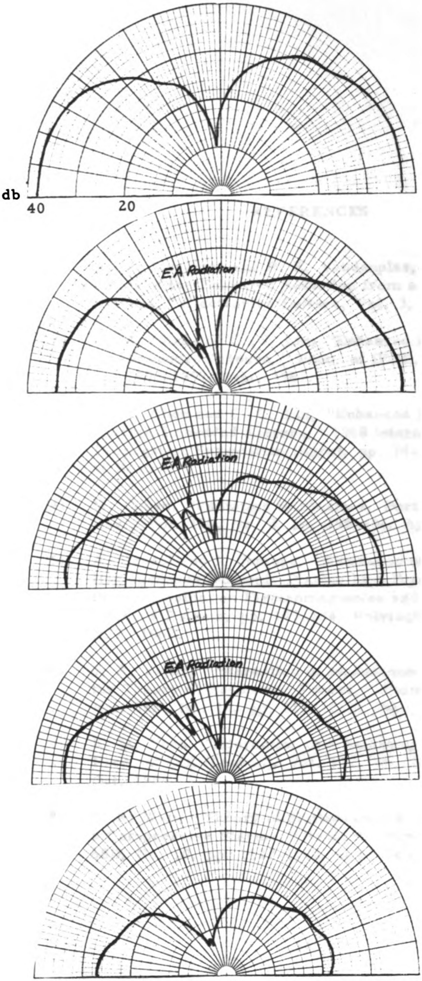

$\omega_p^2/\omega^2 = 0$

$\omega_p^2/\omega^2 = 0.6$

$\omega_p^2/\omega^2 = 0.8$

$\omega_p^2/\omega^2 = 0.9$

$\omega_p^2/\omega^2 = 1.0$

Fig. 6.15 Experimental radiation patterns of a monopole ($h/\lambda_o = 0.233$,

REFERENCES

(1) A. M. Messiaen and P. E. Vandenplas, "Theory and Experiments of the Enhanced Radiation from a Plasma-Coated Antenna," Electronics Letters, Vol. 3, pp. 26-27, Jan. 1967.

(2) K. M. Chen and C. C. Lin, "Enhanced Radiation from a Plasma-Imbedded Antenna," Proc. of IEEE, Vol. 56, No. 9, pp. 1595-1597, Sept. 1967.

(3) K. M. Chen and C. C. Lin, "Enhanced Radiation from a Plasma-Imbedded Antenna," 1968 International Antenna and Propagation Symposium Digest, pp. 74-78, Sept. 9-11, 1968 at Boston.

(4) M. Cohen, "Radiation in Plasmas, Parts II and III," Phys. Rev., Vol. 126, No. 2, pp. 398-404, April 1962.

(5) A. Hessel and J. Shmoys, "Excitation of Plasma Waves in a Homogeneous Isotropic Plasma by a Dipole," Proceedings of the Symposium on Electromagnetics and Fluid Dynamics of Gaseous Plasma, pp. 173-184, Polytechnic Press, Brooklyn, N.Y. 1962.

(6) J. A. Fejer, "Interaction of an Antenna with a Hot Plasma and the Theory of Resonance Probes," Radio Science J. Res. NBS, Vol. 68D, No. 11, pp. 1171-1176, Nov. 1964.

(7) K. M. Chen, "Interaction of a Radiating Source with a Plasma," Proc. of IEE (London), Vol. 111, No. 10, pp. 1668-1678, Oct. 1964.

(8) J. R. Wait, "Theory of Slotted-Sphere Antenna Immersed in a Compressive Plasma," Radio Science J. Res. NBS, Vol. 68D, No. 10, pp. 1127-1143, Oct. 1964.

(9) H. Whale, "The Excitation of Electroacoustic Wave by Antenna in the Ionosphere," J. Geophys. Res., Vol. 68, No. 2, pp. 415-422, Jan. 1963.

(10) H. Schmitt, "Plasma Resonances Excited by Antennas," Proc. of IEEE, p. 622, May 1964.

(11) D. L. Jassby and M. P. Bachynski, "Measurement of the Impedance and Radiation Pattern of a Quarter-Wave Monopole in an Isotropic Plasma," presented at URSI Meeting, Canada, May 1967.

(12) K. M. Chen, H. Judson and C. C. Lin, "Experimental Study of an Electroacoustic Wave Excited by an Antenna in a Hot Plasma," Proc. of IEEE, Vol. 55, No. 9, Sept. 1967.

(13) K M. Chen, H Judson and C. C. Lin, "Experimenta. Study on the Input Impedance and the Radiation Field of Cylindrical Antennas in a Compressive Plasma--Search for Electro-acoustic Wave," 1967 International Antenna and Propagation Symposium Digest, pp. 148-156, Oct. 17-19, 1967 at Ann Arbor.

(14) L. Spitzer, "Physics of Fully-Ionized Gases," Interscience, 1956.

(15) S. Ramo, J. R. Whinnery and T. Van Duzer, "Fields and Waves in Communication Electronics," John Wiley and Sons, Inc., 1965.

(16) K. G. Balmain, "Impedance of a Short Dipole in a Compressible Plasma," Radio Science J. Res. NBS, Vol. 69D, No. 4, pp. 559-566, April 1965.

(17) H. H. Kuehl, "The Kinetic Theory of Waves in a Warm Plasma Excited by a Current Source," J. Math. Phys., Vol. 43, pp. 218-226, Feb. 1964.

(18) H. H. Kuehl, "Resistance of a Short Antenna in a Warm Plasma," Radio Science (New Series), Vol. 1, No. 8, pp. 971-976, Feb. 1966.

(19) H. H. Kuehl, "Computation of the Resistance of a Short Antenna in a Warm Plasma," Radio Science (New Series), Vol. 2, No. 1, pp. 73-76, Jan. 1967.

(20) G. Meltz, P. J. Freyheit and C. D. Lustig, "Admittance of a Plasma-Covered Cylindrical Antenna," Radio Science (New Series), Vol. 2, No. 2, pp. 203-224, August 1966.

(21) R. W. P. King, "Theory of Linear Antennas," Harvard University Press, p. 81, 1956.

(22) R W. P. King, "Linear Arrays: Currents, Impedances and Fields," IRE Trans. on A & P, pp. 440-457, Dec. 1959.

(23) R. W. P. King, "Fundamental Electromagnetic Theory," Second Edition, Dover Publication, Inc., 1963.

(24) R. W. P. King and C. W. Harrison, "Half-Wave Cylindrical Antenna in a Dissipative Medium: Current and Impedance," J. Res. NBS, Vol. 64D, No. 4, pp. 365-380, 1960.

(25) R. W. P. King, "Theory of Linear Antennas," Harvard University Press, p. 169, 1956.